1-1-2006

# Development of a Seismic Design Methodology for Precast Diaphragms - PHASE 1 SUMMARY REPORT

Clay Naito

Wesley Peter

Liling Cao

*PCI / NSF Project*

# Development of a Seismic Design Methodology for Precast Diaphragms

# PHASE 1 SUMMARY REPORT

By

Clay Naito, Ph.D., P.E. - Principal Investigator
Wesley Peter - Graduate Student Researcher
Liling Cao – Graduate Student Researcher

January 2006

ATLSS REPORT NO. 06-03

**ATLSS is a National Center for Engineering Research on Advanced Technology for Large Structural Systems**

117 ATLSS Drive

Bethlehem, PA 18015-4729

Phone: (610)758-3525

Fax: (610)758-5902

www.atlss.lehigh.edu

Email: inatl@lehigh.edu

## ACKNOWLEDGEMENTS

This research is part of the PCI/NSF collaborative research project "Development of A Seismic Design Methodology for Floor Diaphragms" organized by Robert Fleischman at the University of Arizona, Clay Naito and Richard Sause at Lehigh University, and Jose Restrepo at the University of California San Diego . This project was financed in part by a grant from the Commonwealth of Pennsylvania, Department of Community and Economic development, through the Pennsylvania Infrastructure Technology Alliance (PITA), and through support from the Precast and Prestressed Concrete Institute (PCI) and the US National Science Foundation. The authors would also like to thank Dr. Richard Sause for guidance and consultation and the DSDM advisory board for development of the testing program and review of this document.

## TABLE OF CONTENTS

## LIST OF TABLES

## LIST OF FIGURES

## ABSTRACT

As part of the University of Arizona, Lehigh University, and University of California San Diego collaboratory research project Development of a Seismic Design Methodology for Pre-cast Diaphragms a first phase of experimental research was conducted at Lehigh University (LU). This first phase examines the local performance of various diaphragm connection details. Based on a review of the previous research and a survey of connection details used in practice, six pre-cast diaphragm connections were selected for experimental review. The connections represent both diaphragm panel to panel connections and panel to wall connections. A series of tests on each connection detail are conducted to investigate the behavior under in-plane shear, tension, and compression load combinations and compare them to accepted design formulation. It was found that in general all connectors displayed acceptable behavior under shear deformation with load capacities above design and deformations in excess of 1/2-in. before complete strength loss. The shear strength of field topped systems was sensitive to the level of joint opening. For the case of no opening, high shear strengths were maintained. For large joint openings the strength was controlled by the capacity of the connector bridging the joint. In tension, a variety of responses were observed. The splayed leg connectors did not achieve their design strength. This was often attributed to premature weld failures. The straight leg connectors exhibited tension capacities in accordance with their design. Also under tensile loading it was observed that the splayed leg connectors and the pour strip connector were ductile with moderate capacities being maintained under deformations higher than 1-in., whereas the remaining straight leg connectors all displayed limited ductility with failure at less than 1-in of deformation. Investigation of the cast-in-place topping revealed that the WWR mesh achieved its intended shear and tension force capacities. Due to the cold-working fabrication technique used for WWR the wires have limited deformation capacity. Wires reached fracture at joint openings between 0.1 and 0.2 inches. Details of the tests and the conclusions are presented within this report.

## PHASE 1 RESEARCH PROGRAM

### BACKGROUND

As a means of assessing the displacement and force capacity and structural stiffness of pre-cast diaphragm connections, an experimental research program was conducted. A subassembly consisting of the connector and a portion of the surrounding diaphragm was developed. The subassemblies include two connectors embedded in a standard 2-in. or 4-in. pre-cast section. All specimens were fabricated at full-scale and tested in combinations of horizontal shear and/or axial displacement.

### TEST SETUP

The subassembly was developed assuming that the connectors are spaced at 4 feet and embedded in a double tee panel with a 2ft distance from the DT web to the free flange face. The subassembly represents a 4-ft region around a flange to flange diaphragm connection. The specimens are fabricated from two panels 2ft wide and 4ft long. The panels are connected to form a 4ft square subassembly.

The panels were loaded in-plane using a multi-directional loading fixture (Figure 1). One edge of the panel is bolted onto the flange of a fixed restraining beam. The beam is welded to a base plate which is keyed into the lab floor. The other edge is attached to a low friction loading beam. The beam bears on Teflon sheets to reduce friction and is free to move in the horizontal plane. Control of the beam is made with a shear actuator and two tension-compression actuators. To provide vertical support to the test panels, two Teflon covered support beams are provided underneath the specimen.

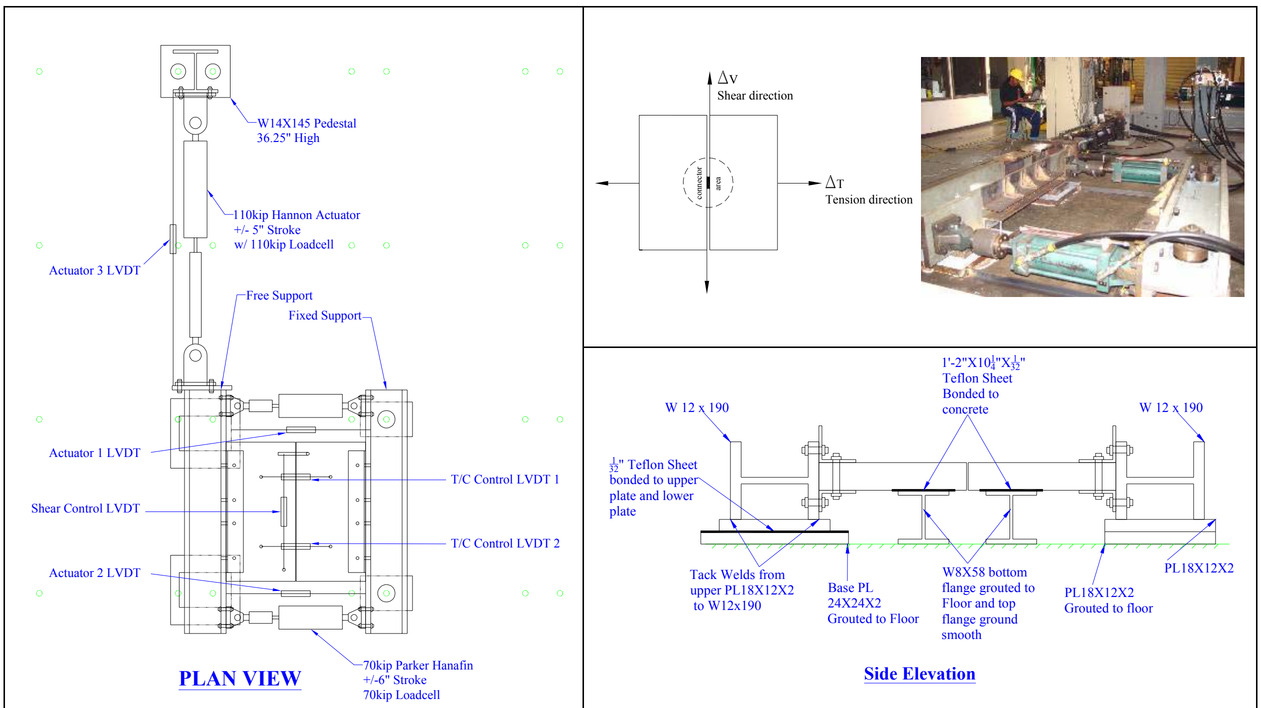


Figure 1: Test fixture and control

Tension and compression are applied to the connector through two 70 kip actuators, which are joined to the free-end load beam flange on both sides of the panel. Shear is applied with a 110 kip actuator attached to the movable load beam. Shear, tension, and compression loads are measured by load cells attached between the hydraulic jack and free-end load beam. External LVDT's are used between each beam to control the applied deformation. The LVDT's are centered pin to pin of each actuator (Figure 1).

In a diaphragm subject to lateral loads the panels will deform in shear and flexure along the joint. Local rotation at a connector will be small relative to the shear and tension deformations. To ensure that rotation is minimized all tests were conducted under deformation control. To achieve pure shear deformation at the specimen joint, the tension / compression actuators provide Kinematic compensation. For example, as shear deformation is applied, the tension and compression actuators are extended at a rate proportional to the shear deformation to maintain a constant joint separation. Likewise, during pure joint opening and closing the shear actuator is displaced proportionately to maintain zero shear deformation.

## DEFORMATION PROTOCOLS

The panels were tested under pure shear, pure tension, and combined shear with tension. All tests were conducted under quasi-static displacement control at a rate less than 0.05in/sec. The tests were continued until failure. Failure is defined as the point where the specimen capacity drops below 25% of the measured ultimate. Five displacement protocols have been developed to represent the spectrum of demands a local diaphragm connector could experience under lateral loading. Six deformation protocols are used:

1. Monotonic Shear
2. Cyclic Shear
3. Monotonic Tension
4. Cyclic Tension and Compression
5. Monotonic Shear with Proportional Tension
6. Cyclic Combined Shear with Proportional Tension

### *Monotonic Shear*

The monotonic shear tests were conducted to evaluate the connector response under pure shear deformation. The original panel separation of 1/4-in. will be maintained through the test. The test represents the joint condition where the panels are shearing without any flexural opening or closing. The test thus provides an estimate of average connector yield, peak strength, and the deformation capacity. Monotonic shear protocol consists of three cycles to 0.01-in. to estimate initial stiffness and verify equipment operation. Afterwards, the specimens were loaded monotonically to failure (Figure 2).

### *Cyclic Shear*

Cyclic shear tests provide insight on the degradation of shear properties (i.e., stiffness and ultimate strength) under loading reversals. The loading protocol is based on the PRESSS program [Priestley 1992]. Three preliminary cycles to 0.01-in. are conducted to evaluate control and acquisition accuracy. The remaining protocol consisted of groups of three symmetric shear cycles at increasing deformation levels. Each level is based on a percentage of a reference deformation computed from the preceding monotonic test. The reference deformation represents the effective yield deformation of the connector. It is computed by taking the intercept of a horizontal line at the max load and a secant stiffness line at 75% of the max load (Figure 2 inset). Three elastic levels of 0.25⊿, 0.50⊿ and 0.75⊿ followed by inelastic cycles to 1.0⊿, 1.5⊿, 2.0⊿, 3.0⊿, 4.0⊿, 6.0⊿, 8.0⊿, *etc*... will be conducted. The loading protocol is illustrated in Figure 2.

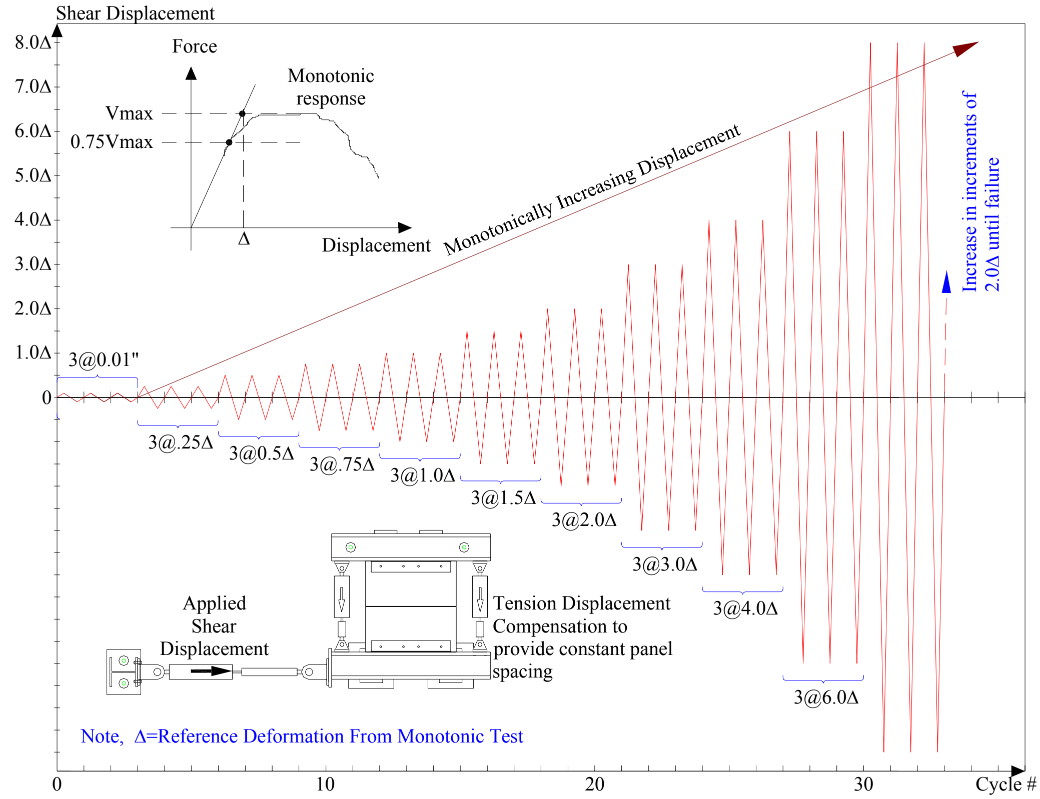


Figure 2: Shear loading protocol

***Monotonic Tension***

In current diaphragm design, the flexural diaphragm tensile forces are assumed to be resisted by the chord reinforcement. The contribution of shear connectors to flexural resistance is commonly neglected. Previous research has shown that in many cases web connectors provide high tension stiffness (i.e., connector D). To quantify the relative tensile contribution of the web connectors and chord connectors, a monotonic tension tests were conducted. The loading protocol consists of three tension/compression deformations to 0.01-in. followed by a monotonically increasing tension deformation to failure (Figure 3). The test was paused at each 0.1-in. for observations.

***Cyclic Tension / Compression***

Previous research indicates that connector compression stiffness can be in excess of ten times the tension stiffness. In order to make a comprehensive evaluation of the difference between tension and compression behavior of chord connectors, a cyclic tension/compression loading will be applied. The PRESSS cyclic loading protocol will again be used with a modification of the compression cycle. The first compression half cycle will be conducted by deforming the panel until the compression force equals the tension force measured in the first tension half cycle. The second and third compression half cycles will be taken to the compression deformation of the 1st half cycle. The loading protocol is illustrated in Figure 3.

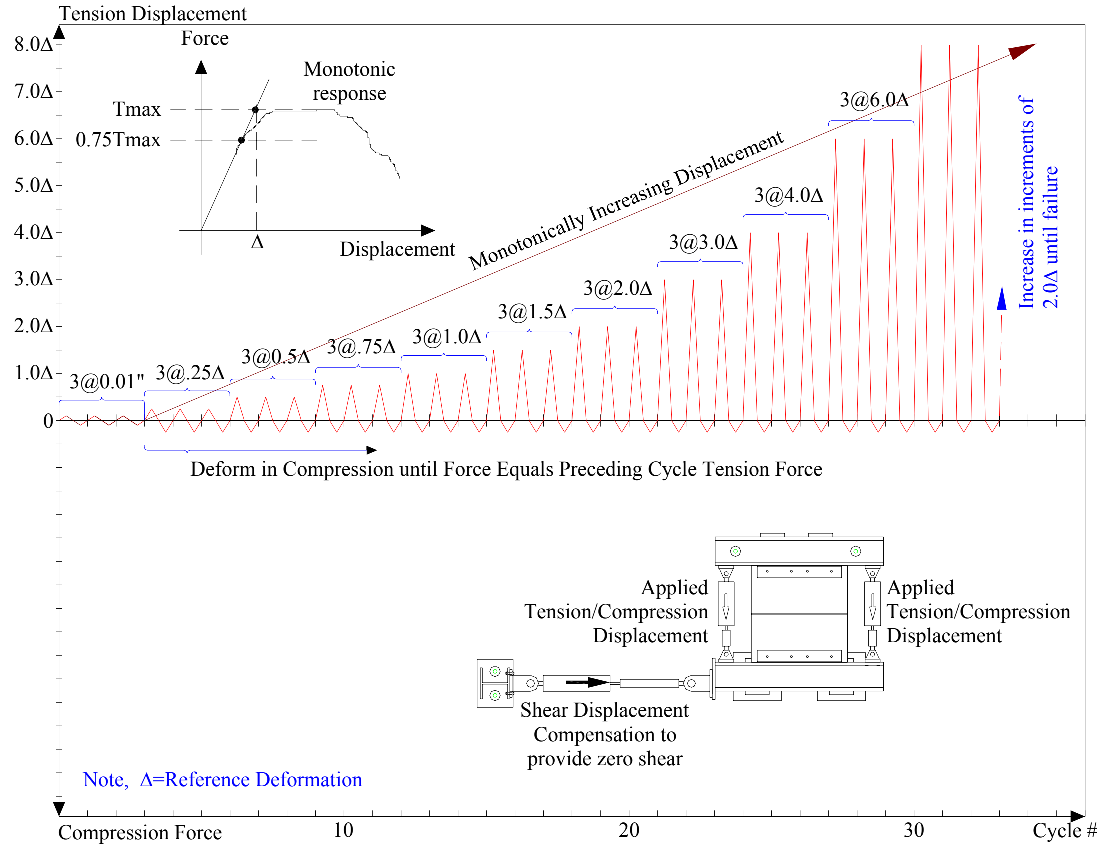

Figure 3: Tension/Compression protocol

### Monotonic Shear with Proportional Tension:

The monotonic shear with tension test consists of three cycles of 0.01-in. in shear and a proportional tension/compression deformation (Figure 4). The shear and tension deformations will be increased proportionally using the chosen constant shear-to-tension deformation ratio (Table 1). The test will be paused at each 0.1–in of shear deformation for observations. The test is performed with either zero joint opening or with an initial opening of 0.10-in. and kept constant through the test.

### Cyclic Shear with Proportional Tension/Compression:

The test initiates with three cycles of 0.01-in. of shear and a proportional tension/compression deformation. The remaining demands consist of three symmetric cycles of shear deformation. For the positive shear half cycle a proportional tension deformation is applied. For the negative shear half cycle the panel separation is kept constant at the original spacing. Following these three cycles a half cycle of compression deformation is applied with no shear. The compression half cycle will be conducted by deforming the panel until the compression force is on the order of the tension force measured in the first tension half cycle. This history will be repeated for increasing percentages of the reference shear deformation computed from the preceding monotonic results. The load increments are based on the PRESSS loading protocol. The shear-to-tension deformation ratio will be based on the chosen ratio for the connector summarized in Table 1. The loading protocol is illustrated in Figure 4. The test is performed with either zero joint opening or with an initial opening of 0.10-in. and kept constant through the test.

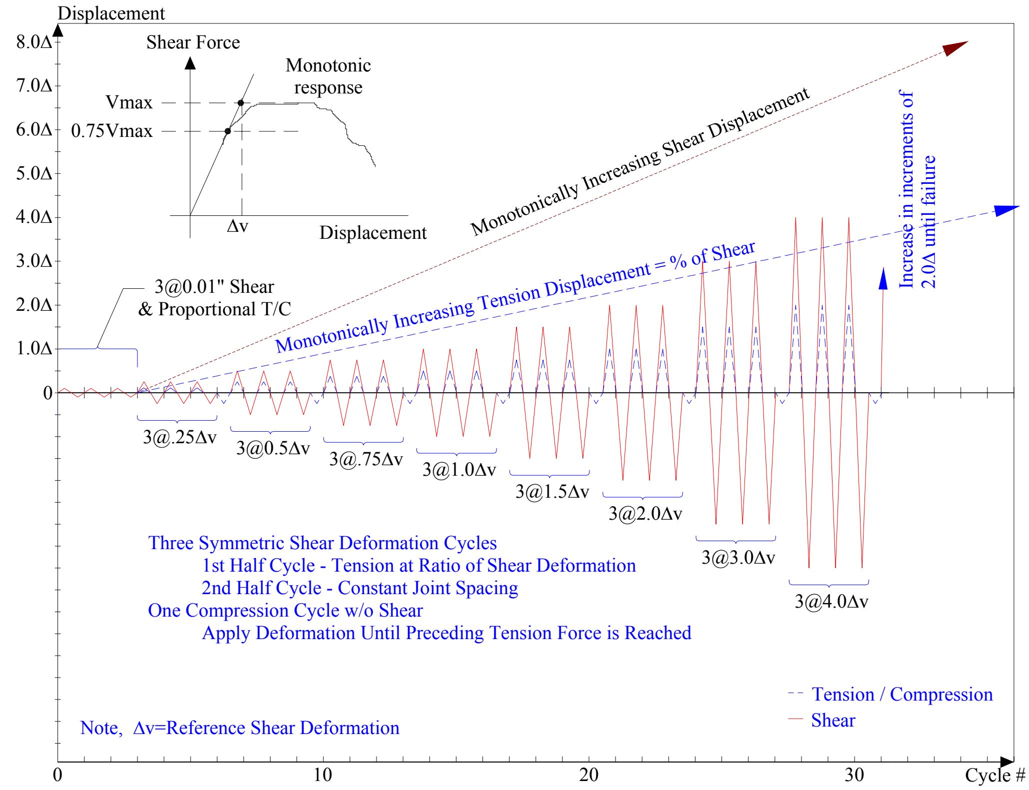


Figure 4: Combined Tension/Compression Shear protocol

## TEST MATRIX

The performance of seven connection details is included phase 1 research. A list of the tests conducted on each connector is presented in Table 1. The results are presented in the report as sequenced in the table. Each connector type is discussed separately with information provided on the specimen configuration, the test specific material properties and the observed and measured response. The force-deformation and a simplified backbone curve are provided. A simplified 10 point backbone curve is chosen to match the measured force-displacement curve at regions where significant events or changes in the load capacity was observed.

Table 1: Test matrix

| Test Specimen | Identification | Loading Protocol |
|---|---|---|
| JVI Vector | A-1 | Monotonic Tension with ΔV=0 |
| | A-2 | Monotonic Shear with ΔT=0 |
| | A-3 | Monotonic Tension & Shear ΔT/ΔV = 0.5 |
| | A-4 | Cyclic Tension & Compression with ΔV=0 |
| Pre-topped Chord | B-1 | Monotonic Tension with ΔV=0 |
| | B-2 | Monotonic Shear with ΔT=0 |
| | B-3 | Monotonic Tension & Shear ΔT/ΔV = 0.5 |
| | B-4 | Cyclic Shear with ΔT=0 |
| Un-topped Hairpin | C-1 | Monotonic Tension with ΔV=0 |
| | C-2 | Monotonic Shear (1) with ΔT=0 |
| | C-3 | Monotonic Shear (2) with ΔT=0 |
| Topped Hairpin | D-1 | Monotonic Tension with Fv=0 |
| | D-2 | Monotonic Shear (1) with ΔT=0.1-in. |
| | D-3 | Monotonic Shear (2) with ΔT=0.1-in. |
| | D-4 | Monotonic Tension & Shear ΔT/ΔV = 0.5 |
| | D-5 | Cyclic Shear with ΔT=0.1-in. |
| Topped Cover Plate | E-1 | Monotonic Tension with Fv=0 |
| | E-2 | Monotonic Shear with ΔT=0.1-in. |
| | E-3 | Monotonic Tension & Shear ΔT/ΔV = 0.5 |
| | E-4 | Cyclic Shear with ΔT=0.1-in. |
| Pour Strip | F-1 | Monotonic Tension with Fv=0 |
| | F-2 | Monotonic Shear with ΔT=0.1-in. |
| | F-3 | Monotonic Tension & Shear ΔT/ΔV = 2.0 |
| | F-4 | Cyclic Shear with ΔT=0.1-in. |
| | F-5 | Cyclic Tension & Compression with Fv=0 |
| Topping | G-1 | Monotonic Tension with Fv=0 |
| | G-2 | Monotonic Shear (1) with ΔT=0.1-in. |
| | G-3 | Monotonic Shear (2) with ΔT=0 |
| | G-4 | Monotonic Tension & Shear ΔT/ΔV = 0.5 |
| | G-5 | Cyclic Shear with ΔT=0 |
| Note: Fv – Shear force, ΔT – Tension deformation, ΔV – Shear deformation | | |

## SUPPLEMENTAL REINFORCEMENT

To provide integrity at the boundary of the panels during testing, additional reinforcement was included (Figure 5). The reinforcement was placed at the edge of the panel to minimize conflict with the connector under examination. This reinforcement is included in all test panels.

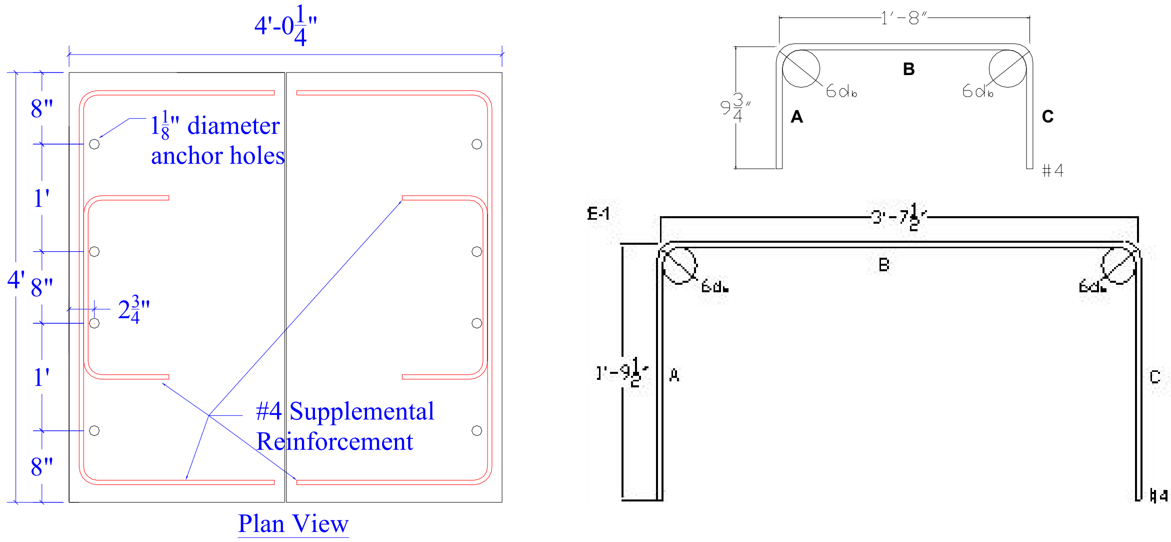


Figure 5: Supplemental reinforcement layout and details

## CONCRETE MIX DESIGN

The pre-cast base panels and cast-in-place topping were designed to match common construction materials. The pre-cast panel was fabricated from a self consolidating early strength concrete with compressive design strength of 7 ksi. The cast-in-place topping had a design compressive strength of 3.5 to 4 ksi. The panels were fabricated in a number of batches. The mix proportions are presented in Table 2. Due to the number of specimens that had to be fabricated, the panels were cast in a total of 13 different batches from three different mix designs P1, P2 & P3. These panels were built at High Concrete pre-cast facility under typical construction conditions. The topping was cast separately in two batches with two different mix designs T1 & T2. The topping was placed in the lab after the panels were connected to simulate on-site placement conditions. The average 28 day compressive strengths for each batch were determined from a series of 4-in. x 8-in. cylinder compressive tests conducted in accordance with ASTM C39. The average strength and standard deviation for each concrete element are presented along with each test description in subsequent sections (Tables A through G).

## CONNECTOR PROPERTIES

The material properties vary from connector to connector. The material properties used for each panel is described in line with each test summary.

| Table 2: Concrete proportions [per cubic yard] | | | | | |
|---|---|---|---|---|---|
| Batch # | P1 | P2 | P3 | T1 | T2 |
| Design Strength [ksi] | 7 | 7 | 7 | 4 | 3.5 |
| Air [%] | 6 | 6.5 | 5 | 1.5 | 1.5 |
| Spread [in] | 5 | 22 | 22 | 4 | 4 |
| Cement Type 1 (C-150) [lb] | 400 | 600 | 600 | 470 | 429 |
| Slag (C-989) [lb] | 400 | 200 | 200 | - | - |
| Slag (C-618) [lb] | - | - | - | 118 | 107 |
| C. Agg Martin #67 SSD [lb] | 1450 | 1050 | 1400 | - | - |
| C. Agg Martin #8 SSD [lb] | - | 350 | - | - | - |
| C. Agg Crushed Stone #57 SSD [lb] | - | - | - | 1575 | 1475 |
| C. Agg Crushed Stone #467 SSD [lb] | - | - | - | 500 | - |
| C. Agg Keystone #8 SSD [lb] | - | - | - | - | 545 |
| F. Agg Orange Sand SSD [lb] | 1267 | 1397 | 1374 | - | - |
| F. Agg Sand SSD [lb] | - | - | - | 1108 | 1205 |
| Water [lb] | 280 | 304 | 304 | 306 | 306 |
| VR AEA (C-260) [oz] | 16 | 7 | 16 | - | - |
| Plastiment Retarder [oz] | 24 | 24 | 24 | - | - |
| Daratard Retarder [oz] | - | - | - | 17.6 | 16.1 |
| Visocrete 6100 High Water Reducing Agent [oz] | 56 | 75 | 56 | - | - |
| Daracem-55 Water Reducing Agent [oz] | - | - | - | 17.6 | 16.1 |
| Rapid-1 Accelerator [oz] | 120 | 100 | 120 | - | - |
| Daraccel Accelerator [oz] | - | - | - | 47 | 42.9 |
| Unit Weight [lb/cft] | 141.7 | 144.5 | 143.6 | 149.87 | 149.52 |
| W/C Ratio | 0.38 | 0.38 | 0.38 | 0.52 | 0.57 |

### SUBASSEMBLY A: JVI CONNECTOR

#### SUBASSEMBLY DETAILS A

The specimen tested represents a JVI Vector connection used as a connector between DT panels. The connectors are welded to a 3.5-in. x 1-in. x 3/8-in. rectangular slug. Details of the specimen are shown in Figure A.

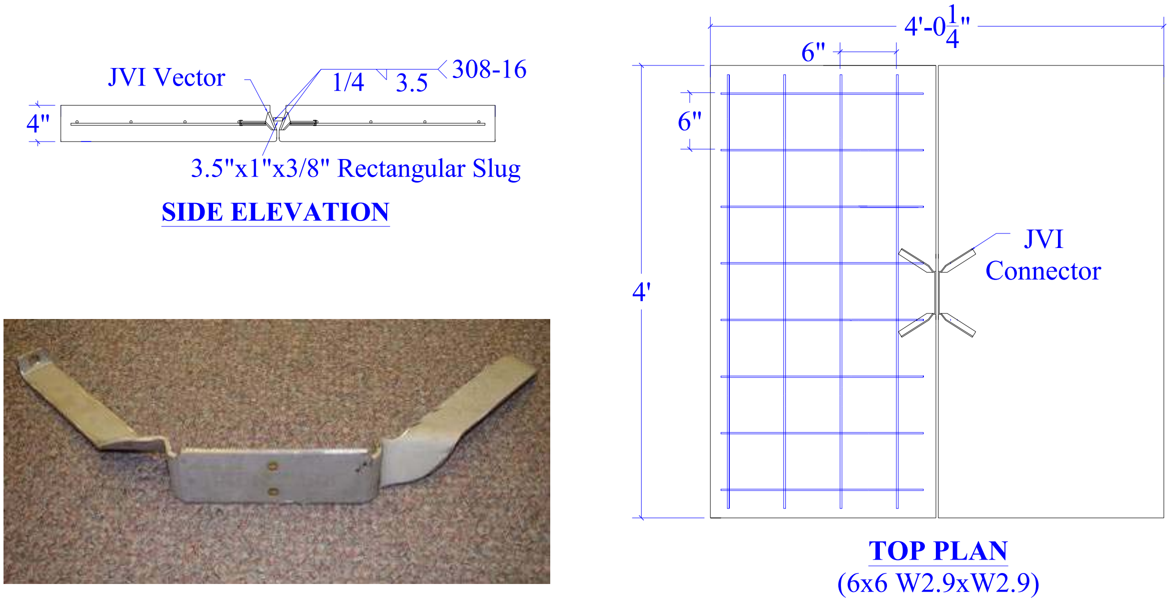


Figure A: Subassembly A

#### MATERIAL PROPERTIES A

The base 4-in. pre-cast panel was fabricated using high early strength self consolidating concrete with a design strength of 7000 psi. The WWR used in the base panel met the requirements of ASTM A185 grade 65 steel. The connector was fabricated from ASTM A240 Type 304 stainless steel. The measured concrete strengths and mill certified steel properties are presented in Table A.

Table A: Material Properties Capacity

| Test | Location in Subassembly (mix) | Compressive Strength, f'c [psi] |
|---|---|---|
| A-1 | Base Panels (P1) | 6983 ± 745 |
| A-2 | Base Panels (P1) | 6983 ± 745 |
| A-3 | Base Panels (P1) | 6996 ± 202 |
| A-4 | Base Panels (P2) | 7413 ± 269 |

| Size | Reinforcement Usage | Grade | Yield Stress [ksi] | Ultimate Strength [ksi] |
|---|---|---|---|---|
| JVI-Vector | Connector | Stainless 304 | 51.45 | 96.85 |
| PL 3.5-in. x 1-in. x 3/8-in | Slug | Stainless 304 | 51.45 | 96.85 |
| #4 | Reinforcing Bars | A706 | 65.79 | 91.39 |
| W2.9XW2.9 6X6 | Pre-cast Panel Mesh | A185 Gr.65 | 65.00* | 108.5 |
| * Mill certificate data unavailable, value assumed | | | | |

## TEST A-1: MONOTONIC TENSION WITH $\Delta V = 0$

The performance of the JVI Vector connector subjected to monotonic tension is presented in this section. The panel was subjected to tensile displacement with the shear displacement restrained, $\Delta V=0$. Panel failure consisted of cracking near the connector faceplates in both panels followed by slip of the connector legs and finally tearing resulting in complete fracture of the slug-to-connector weld. The observed events and corresponding displacement cycle is presented in Table A1-1. The photos of the damage are presented in Figure A-1.1. The global force deformation response and backbone curve are presented in Table A-1.2 and Figure A-1.2.

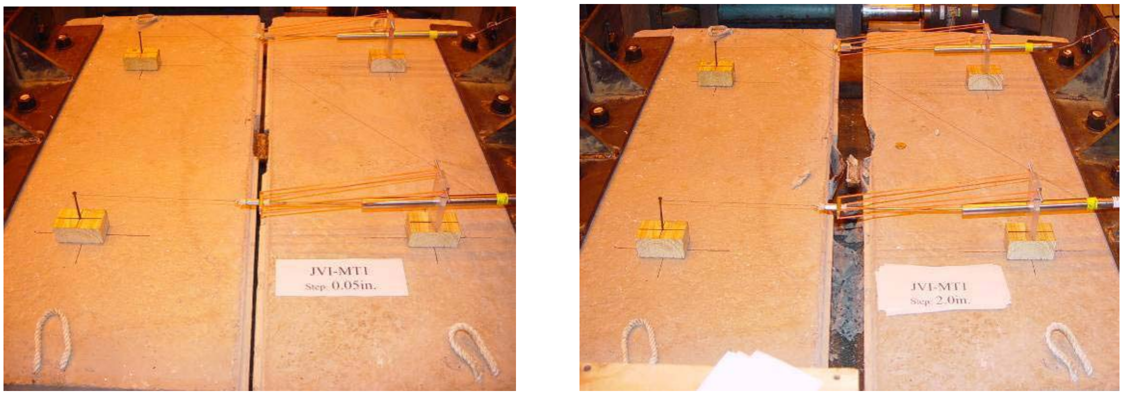


Figure A-1.1: Damage state at 0.05 and 2.0-in. tensile opening

| Table A-1.1: Key Test Observations | | |
|---|---|---|
| Event # | Tension Step $\Delta$ [in.] | Event Description |
| 1 | 0.08 | Unsymmetrical bending of faceplate in fixed panel. |
| 2 | 0.2 | Free panel cracked by faceplate. Bending of faceplate in free panel. |
| 3 | 0.3 | Free panel cracking progressed. Fixed panel cracked by faceplate. |
| 4 | 0.4 | Cracking on both panels progressed. Connector slug rotated slightly. |
| 5 | 0.6 | Pullout of connector leg in free panel. |
| 6 | 0.7 | Concrete spalling by connector leg in free panel. |
| 8 | 0.8 | Connector leg pullout in free panel progressed. Pullout in fixed panel initiated. |
| 10 | 1.0 | Pullout of diagonally opposite connector legs on both panels progressed. |
| 11 | 1.2 | Concrete spalling by connector leg in fixed panel. |
| 12 | 1.4 | Weld tearing initiated between fixed panel connector and slug. |
| 13 | 1.8 | Weld tearing progressed. |
| 15 | 1.2 | Connector failed due to weld fracture. |

| Table A-1.2: Experimental Results Backbone Curve | | |
|---|---|---|
| Step | Tensile Displacement | Tensile Force |
| - | 0 | 0 |
| ~75% Max Load | 0.065 | 5.73 |
| Max Load | 1.257 | 9.69 |
| Weld Tearing | 1.313 | 8.77 |
| Weld Tearing | 1.559 | 8.34 |
| Weld Tearing | 1.701 | 8.80 |
| Weld Tearing | 1.837 | 7.76 |
| Weld Fracture | 1.865 | 5.69 |
| | 1.997 | 4.86 |
| End of test | 2.01 | 0 |

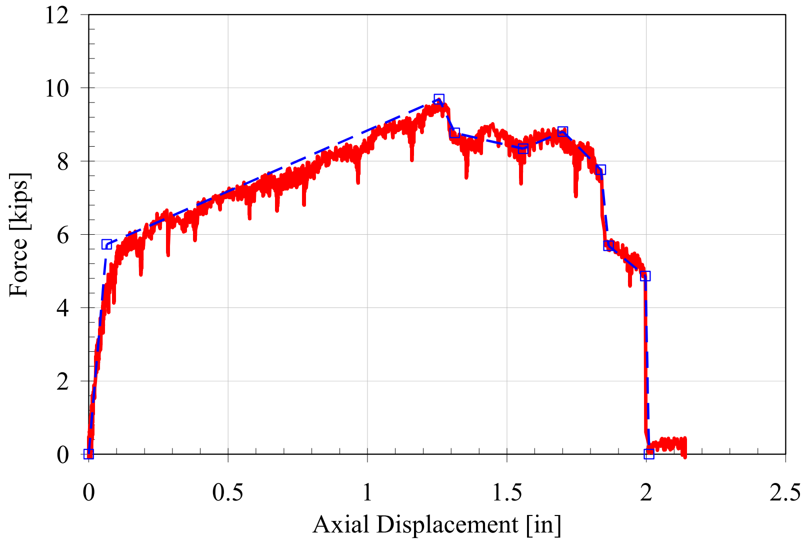

Figure A-1.2: Tensile force and displacement

## TEST A-2: MONOTONIC SHEAR WITH ΔT = 0

The performance of the JVI Vector connector subjected to monotonic shear is presented in this section. The panel was subjected to shear displacement with the tensile displacement restrained, ΔT=0. Panel failure consisted of diagonal cracking from the connector to the support in the fixed panel followed by pullout of the tension leg in the fixed panel characterized by a concrete pullout failure cone. The observed events and corresponding displacement cycle is presented in Table A-2.1. The photos of the damage are presented in Figure A-2.1. The global force deformation response and backbone curve is presented in Table A-2.2 and Figure A-2.2.

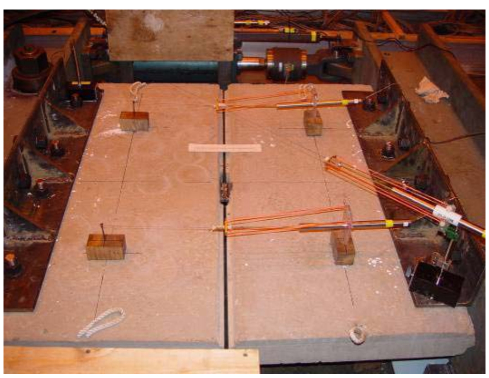
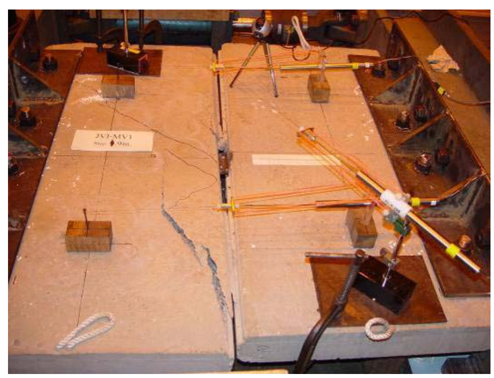
Figure A-2.1: Damage state at 0 and 1.9-in. shear opening

| Table A-2.1: Key Test Observations | | |
|---|---|---|
| Event # | Shear Step Δ [in.] | Event Description |
| 1 | 0.04 | Cracking noises audible. |
| 2 | 0.08 | Cracking noises audible. |
| 3 | 0.4 | Cracking at the end of the supports. |
| 4 | 0.7 | Shear cracking on fixed panel. |
| 5 | 0.8 | Additional shear cracking on fixed panel. Cracking at free panel connector face. |
| 6 | 0.9 | Progression of shear cracking. Cracking at fixed panel connector face. |
| 7 | 1 | Cracking noises audible. |
| 8 | 1.5 | Tension leg pullout in fixed panel. Concrete pullout cone failure occurs. |
| 9 | 1.6 | Progression of tension leg pullout. |
| 10 | 1.7 | End of test. |

| Table A-2.2: Experimental Results Backbone Curve [kip. in.] | | | | |
|---|---|---|---|---|
| Shear force-deformation | | | Axial force – Shear deformation | |
| Step | Shear Displacement | Shear Force | Shear Displacement | Axial Force |
| Softening of initial panel stiffness | 0.062 | 11.05 | 0 | 1.24 |
| Max Load – Shear cracking | 0.767 | 35.87 | 0.276 | -4.25 |
| - | 1.102 | 22.84 | 0.736 | -24.66 |
| - | 1.179 | 22.36 | 1.116 | -7.30 |
| - | 1.215 | 21.36 | 1.223 | -5.91 |
| Tension leg pullout | 1.401 | 21.47 | 1.324 | -6.41 |
| Tension leg pullout | 1.494 | 16.12 | 1.491 | -3.39 |
| - | 1.538 | 7.86 | 1.614 | -2.99 |
| End of test | 1.614 | 5.57 | | |

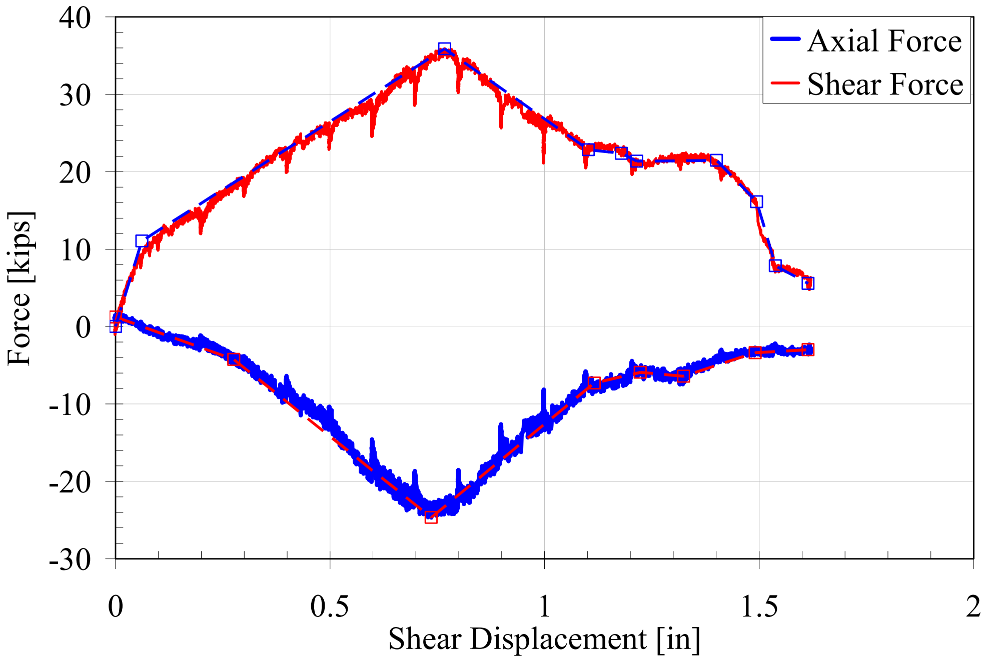


Figure A-2.2: Shear force and displacement

### TEST A-3: MONOTONIC TENSION & SHEAR WITH ΔT /ΔV = 0.5

The performance of the JVI Vector connector subjected to combined shear and tension deformation is presented in this section. Tension deformation to shear deformation was applied at a constant ratio of ΔT/ΔV = 0.5. Panel failure consisted of local cracking in both panels followed by pullout of the tension leg in the fixed panel accompanied by a concrete pullout failure cone. The observed events and corresponding displacement cycle is presented in Table A-3.1. The photos of the damage are presented in Figure A-3.1. The global force deformation response and backbone curve is presented in Table A-3.2, Figure A-3.2 and Figure A-3.3.

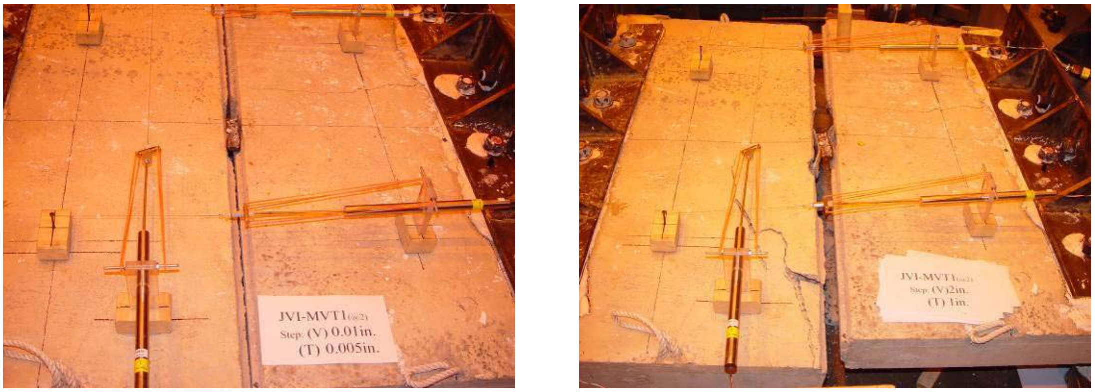

Figure A-3.1: Damage state at 0.01 and 2.0-in. shear opening

| Table A-3.1: Key Test Observations | | |
|---|---|---|
| Event # | Shear Step Δ [in.] | Event Description |
| 1 | 0.1 | Concrete cracking audible. |
| 2 | 0.24 | Small cracking seen close to the connector. Connector slug twisted slightly. |
| 3 | 0.32 | Cracking elongated. Connector tension leg pulled out slightly. |
| 4 | 0.4 | Concrete cracking at tension leg in fixed panel. |
| 5 | 0.48 | Spalling occurred. |
| 6 | 0.56 | Connector tension leg pullout more pronounced. |
| 7 | 0.6 | Connector slug rotation more pronounced. Concrete spalling near tension leg. |
| 8 | 0.64 | Concrete spalling audible. |
| 9 | 0.72 | Concrete spalling near tension leg. |
| 10 | 0.88 | Concrete cracking audible. |
| 11 | 0.96 | Concrete spalling at tension leg in free panel. |
| 12 | 1.2 | Compression leg in fixed panel buckled. |
| 13 | 1.48 | Concrete cracking audible. |
| 14 | 1.56 | Tension leg pullout in fixed panel. Concrete pullout cone failure occurs. |

| Table A-3.2: Experimental Results Backbone Curves [kip. in.] | | | | | | |
|---|---|---|---|---|---|---|
| Shear force-deformation | | | | Axial force-deformation | | |
| Step | Axial Δ | Shear Δ | Shear Force | Axial Δ | Shear Δ | Axial Force |
| 75% Max Load | 0.058 | 0.116 | 20.60 | 0 | 0 | 0.11 |
| Max Load | 0.1 | 0.209 | 27.40 | 0.1 | 0.210 | -6.26 |
| - | 0.1695 | 0.339 | 20.47 | 0.167 | 0.334 | -0.73 |
| Fixed panel tension leg pullout | 0.205 | 0.410 | 18.90 | 0.761 | 1.455 | 1.48 |
| Fixed panel tension leg pullout | 0.3545 | 0.709 | 22.66 | 0.817 | 1.519 | -1.62 |
| Free panel tension leg pullout | 0.4515 | 0.903 | 21.25 | 1.133 | 2.156 | -0.37 |
| Fixed panel tension leg pullout | 0.75 | 1.441 | 24.51 | | | |
| - | 0.787 | 1.508 | 5.79 | | | |
| End of test | 1.133 | 2.156 | 3.71 | | | |

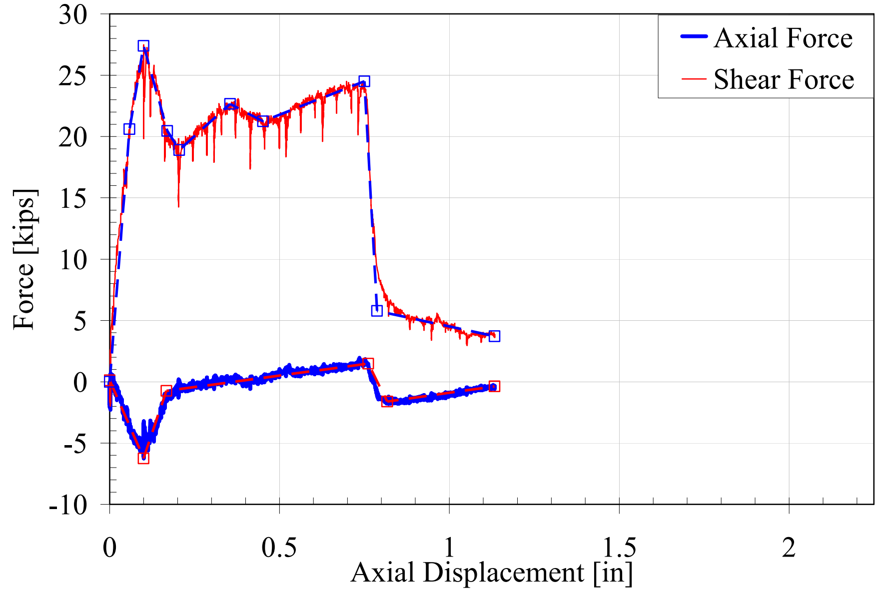

Figure A-3.2: Force and Axial displacement

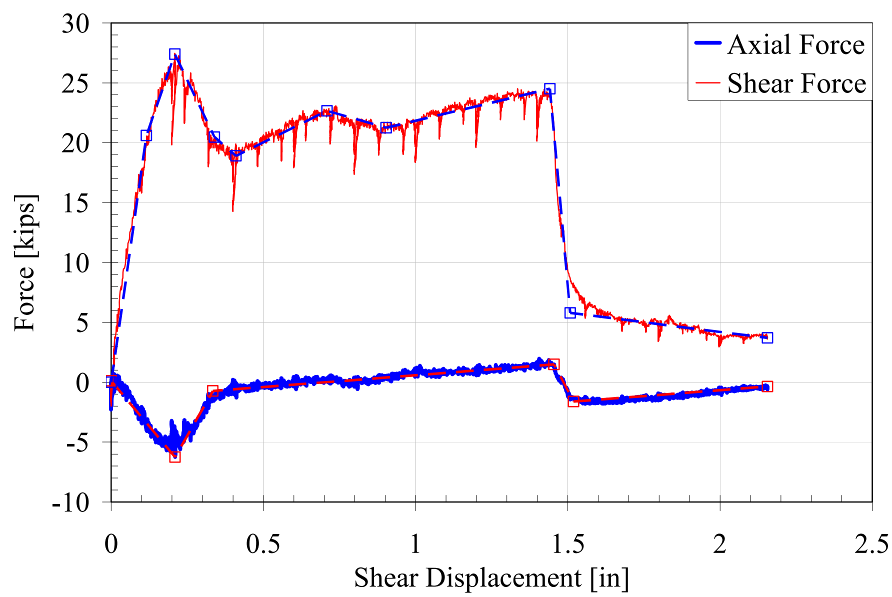

Figure A-3.3: Force and Shear displacement

## TEST A-4: CYCLIC TENSION & COMPRESSION WITH ΔV = 0

The performance of the JVI Vector connector subjected to cyclic tension and compression is presented in this section. The panel was subjected to axial displacement with the shear displacement restrained, ΔV=0. Panel failure consisted of weld tearing between the connector slug and the free panel connector followed by fracture of the slug-to-connector weld. The observed events and corresponding displacement cycle is presented in Table A-4.1. The photos of the damage are presented in Figure A-4.1. The global force deformation response and backbone curve is presented in Table A-4.2 and Figure A-4.2.

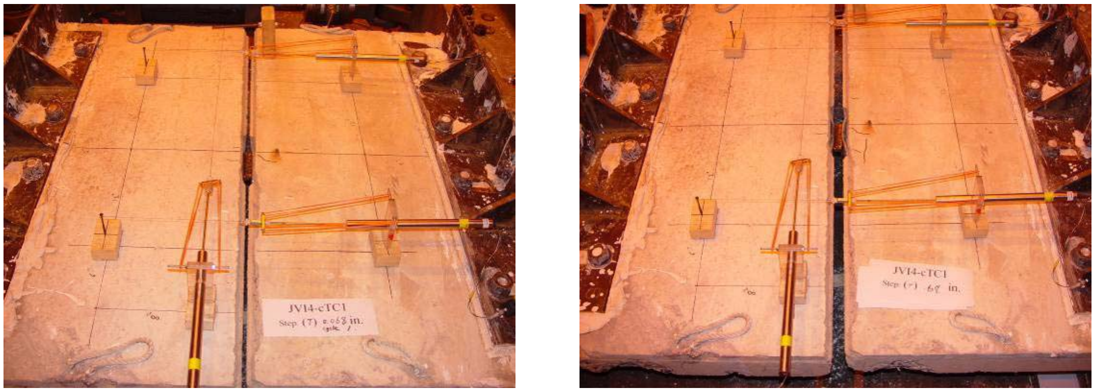

Figure A-4.1: Damage state at 0.068 and 0.68-in. tensile opening

| Table A-4.1: Key Test Observations | | |
|---|---|---|
| Event # | Axial Step Δ [in.] | Event Description |
| 1 | 0.51 | Weld tearing initiated between slug and free panel connector. |
| 2 | 0.68 | Weld tearing ~ 0.25-in. – 0.5-in. from both corners. |
| 3 | 1.02 | Connector failed through weld fracture between slug and free panel connector. |

| Table A-4.2: Experimental Results Backbone Curves [kip. in.] | | |
|---|---|---|
| Step | Tensile Displacement | Tensile Force |
| - | 0.008 | 1.14 |
| - | 0.065 | 3.14 |
| - | 0.168 | 4.43 |
| - | 0.337 | 5.40 |
| Max Load | 0.498 | 5.90 |
| - | 0.667 | 5.48 |
| - | 0.752 | 4.41 |
| End of test | 0.773 | 0 |

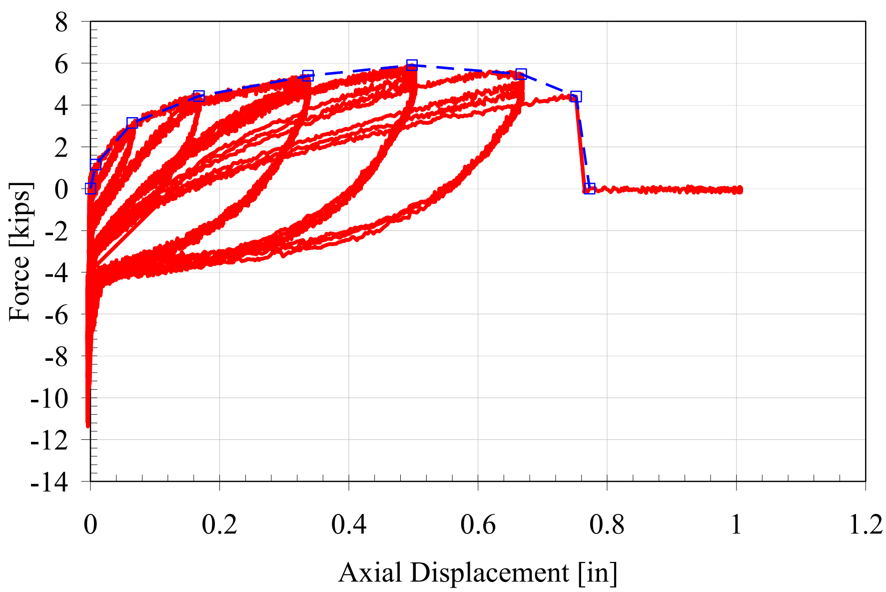


Figure A-4.2: Axial force and displacement

## SUBASSEMBLY B: CHORD CONNECTOR

### SUBASSEMBLY DETAILS B

The specimen tested represents a typical dry chord connector between two DT flanges used to resist axial forces in the diaphragm. The connectors are welded to 7-in. #6 round bar slug. Details of the specimen are shown in Figure B.

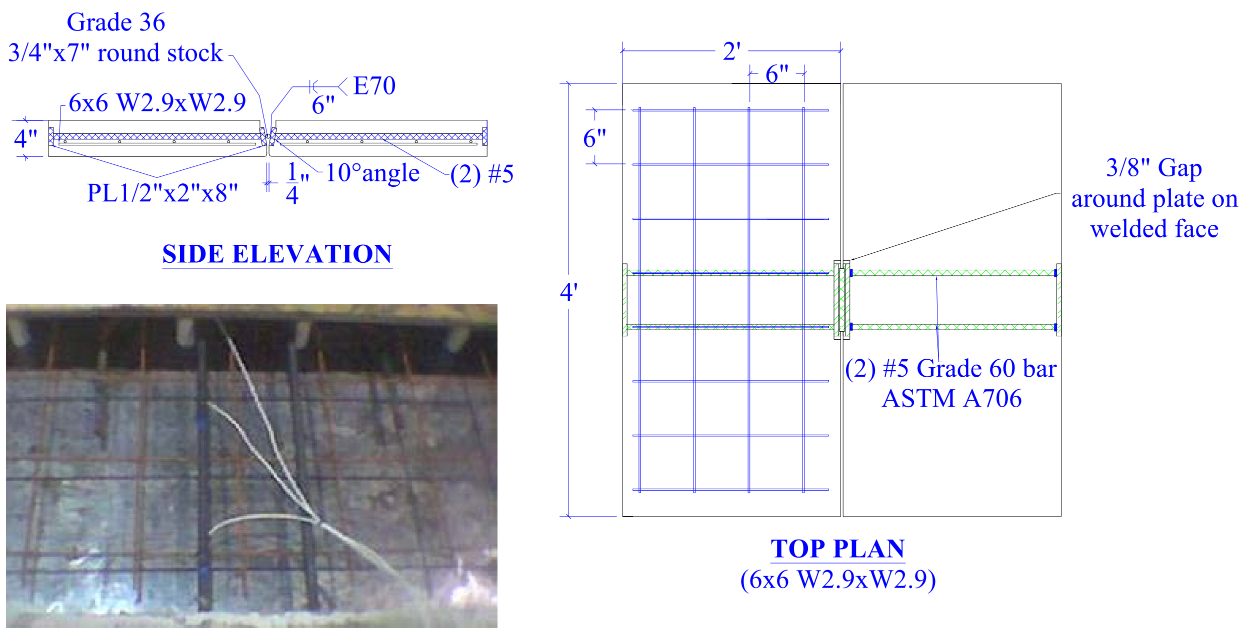


Figure B: Subassembly B

### MATERIAL PROPERTIES B

The base 4-in. pre-cast panel was fabricated using high early strength self consolidating concrete with a design strength of 7000 psi. The WWR used in the base panel met the requirements of ASTM A185 grade 65 steel. The connector was fabricated from ASTM A706 grade 60 reinforcing bars. All plate material conformed to ASTM A36. The measured concrete strengths and mill certified steel properties are presented in Table B.

Table B: Material Properties Capacity

| Test | Location in Subassembly (mix) | Compressive Strength, f'c [psi] |
|---|---|---|
| B-1 | Base Panels (P1) | 7520 ± 635 |
| B-2 | Base Panels (P1) | 6996 ± 202 |
| B-3 | Base Panels (P1) | 7911 ± 240 |
| B-4 | Base Panels (P1) | 7911 ± 240 |

| Size | Reinforcement Usage | Grade | Yield Stress [ksi] | Ultimate Strength [ksi] |
|---|---|---|---|---|
| #5 | Connector | A706 | 67.61 | 95.56 |
| #6 | Round Slug | A36 | 41.05 | 60.6 |
| #4 | Reinforcing Bars | A706 | 65.79 | 91.39 |
| W2.9XW2.9 6X6 | Pre-cast Panel Mesh | A185 Gr.65 | 65.00* | 108.5 |

* Data unavailable, value assumed

## TEST B-1: MONOTONIC TENSION WITH $\Delta V = 0$

The performance of an pre-topped welded chord connector subjected to monotonic tension is presented in this section. The panel was subjected to tensile displacement with the shear displacement restrained, $\Delta V=0$. Panel failure consisted of tensile cracking on the free panel parallel to the joint, followed by weld tearing at the connector slug, and eventually anchorage bar fractures at the weld toe in the free panel. The observed events and corresponding displacement cycle is presented in Table B-1.1. The photos of the damage are presented in Figure B-1.1. The global force deformation response and backbone curve is presented in Table B-1.2 and Figure B-1.2.

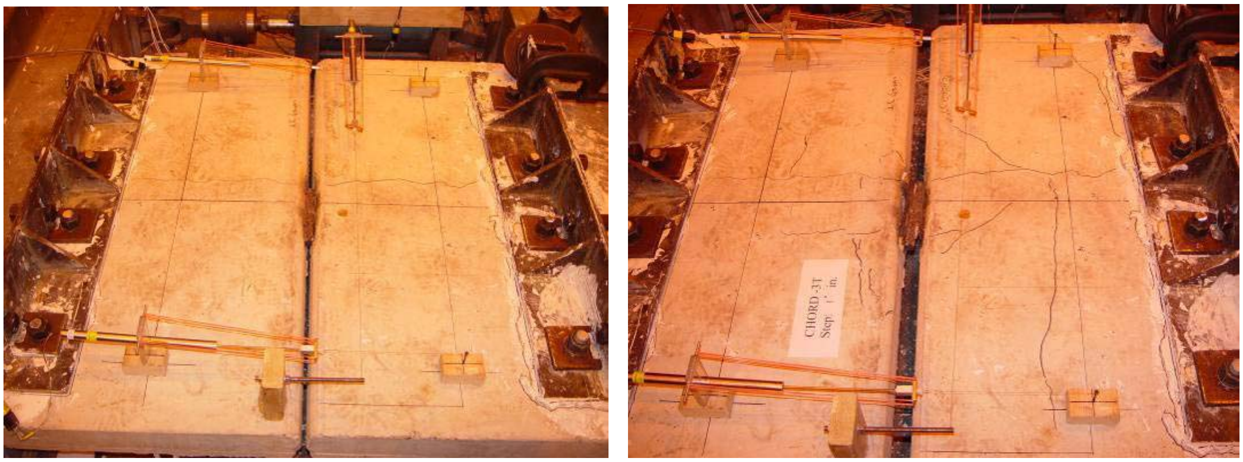

Figure B-1.1: Damage state at 0 and 1-in. tensile opening

| Table B-1.1: Key Test Observations | | |
|---|---|---|
| Event # | Tension Step $\Delta$ [in.] | Event Description |
| 1 | 0.2 | Tension cracking on both panels. |
| 2 | 0.4 | More cracking developed. |
| 3 | 0.6 | Loud noise heard. Weld tearing seen. |
| 4 | 0.7 | Concrete cracking audible. |
| 5 | 0.8 | Concrete cracking audible. |
| 6 | 1.0 | New tension cracks formed. Both bars fractured in free panel. |

| Table B-1.2: Experimental Results Backbone Curve [kip. in.] | | |
|---|---|---|
| Step | Tensile Displacement | Tensile Force |
| 0.75% Max Load | 0.042 | 28.00 |
| Max Load | 0.324 | 36.37 |
| Weld tearing | 0.396 | 31.64 |
| Weld tearing | 0.464 | 30.15 |
| Weld tearing | 0.529 | 30.00 |
| Weld tearing | 0.675 | 26.21 |
| Bar fracture | 0.922 | 20.67 |
| End of test | 0.963 | 0 |

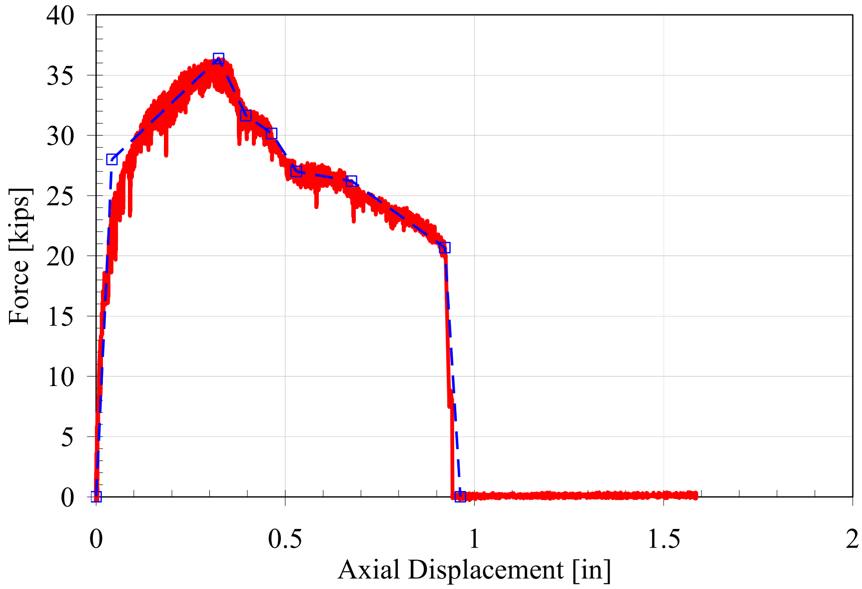


Figure B-1.2: Tension force and displacement

## TEST B-2: MONOTONIC SHEAR WITH ΔT = 0

The performance of a pre-topped welded chord connector subjected to monotonic shear is presented in this section. The panel was subjected to shear displacement with the tensile displacement restrained, ΔT=0. Panel failure consisted of diagonal cracking from the connector to the support in the both panels followed by local cracking at the connector face in the free panel. Stroke was limited due to control issues; consequently the connector did not fail during the test. The observed events and corresponding displacement cycle is presented in Table B-2.1. The photos of the damage are presented in Figure B-2.1. The global force deformation response and backbone curve is presented in Table B-2.2 and Figure B-2.2.

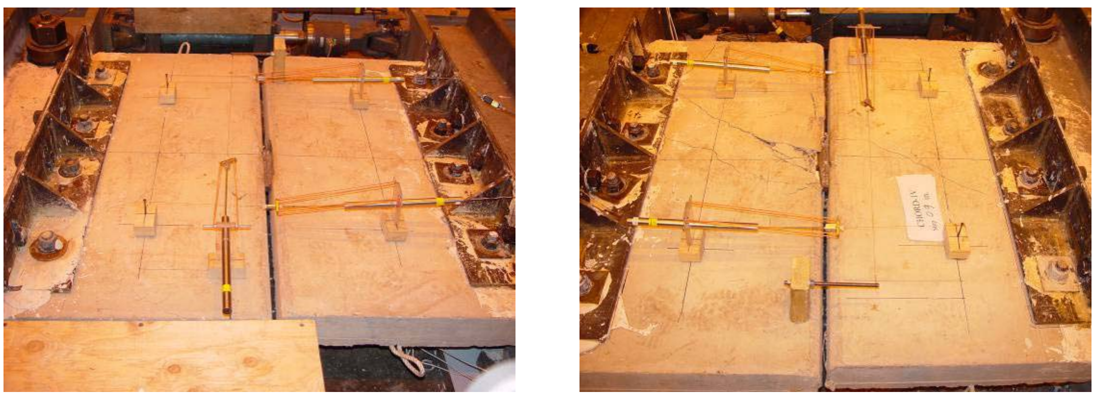

Figure B-2.1: Damage state at 0 and 0.9-in. shear opening

| Table B-2.1: Key Test Observations | | |
|---|---|---|
| Event # | Shear Step Δ [in.] | Event Description |
| 1 | 0.1 | Cracking noises audible. |
| 2 | 0.2 | Cracking noises audible. Shear cracking on both panels. |
| 3 | 0.3 | Progression of existing cracking seen. Additional shear cracking on free panel. |
| 4 | 0.4 | Progression of existing crack. Face cracking near connector face on free panel. |
| 5 | 0.5 | Cracking noise audible. |
| 6 | 0.6 | Cracking noise audible. |
| 7 | 0.8 | Surface spalling of concrete near connector weld face. |
| 8 | 0.9 | End of test. |

| Table B-2.2: Experimental Results Backbone Curve [kip. in.] | | | | |
|---|---|---|---|---|
| Shear force-deformation | | | Axial force – Shear deformation | |
| Step | Shear Displacement | Shear Force | Shear Displacement | Axial Force |
| 0.75% Max Load | 0.046 | 42.67 | 0.090 | -37.40 |
| Max Load – Shear cracking | 0.131 | 56.90 | 0.131 | -49.86 |
| Shear cracking | 0.206 | 30.29 | 0.200 | -20.42 |
| Cracking at connector face | 0.321 | 18.36 | 0.319 | -7.75 |
| - | 0.351 | 15.44 | - | - |
| - | 0.521 | 12.42 | - | - |
| End of test | 0.900 | 10.67 | 0.353 | -2.26 |

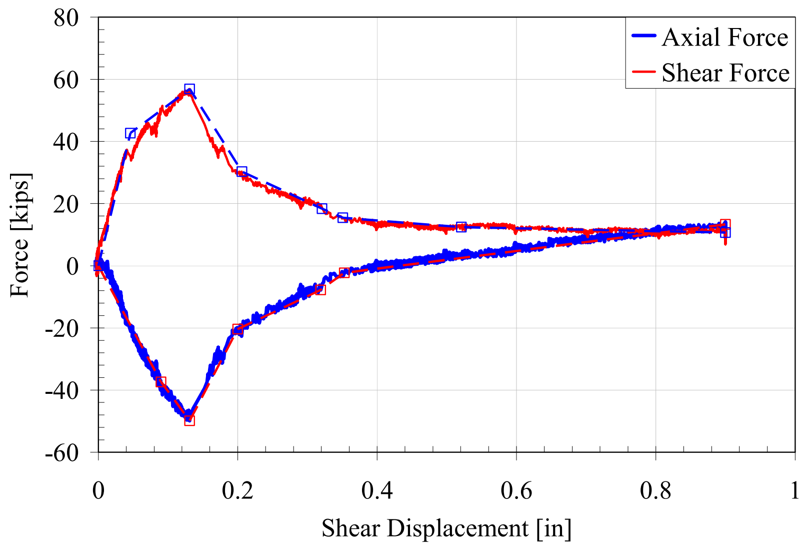

Figure B-2.2: Shear force and displacement

### TEST B-3: MONOTONIC TENSION & SHEAR WITH ΔT/ΔV = 0.5

The performance of an pre-topped welded chord connector subjected to combined tension and shear deformation is presented in this section. Tension deformation to shear deformation was applied at a constant ratio of ΔT/ΔV = 0.5. Panel failure consisted of diagonal cracking from the connector to the support in both panels, followed by fracture of the left connector bar in the free panel followed by tearing of the weld at the connector slug. Complete fracture of the connector did not occur. The observed events and corresponding displacement cycle is presented in Table B-3.1. The photos of the damage are presented in Figure B-3.1. The global force deformation response and backbone curve is presented in Table B-3.2, Figure B-3.2 and Figure B-3.3.


Figure B-3.1: Damage state at 0 and 3.0-in. shear opening

| Table B-3.1: Key Test Observations | | |
|---|---|---|
| Event # | Shear Step Δ [in.] | Event Description |
| 1 | 0.02 | Small crack formation over connector legs on both panels. |
| 2 | 0.10 | Concrete cracking audible. Shear cracking on free panel. |
| 3 | 0.20 | Concrete cracking audible. Shear cracking on fixed panel. |
| 4 | 0.32 | Concrete cracking audible. Progression of existing cracking. |
| 5 | 0.40 | Formation of new small cracks. Progression of existing cracking. |
| 6 | 0.48 | Two fracture noises heard. |
| 7 | 0.60 | Three fracture noises heard. |
| 8 | 0.64 | Loud fracture heard. |
| 9 | 0.72 | Concrete cracking audible. Concrete spalling. |
| 10 | 0.80 | Concrete cracking audible. |
| 11 | 0.96 | Fracture of left connector bar in free panel. |
| 12 | 1.40 | Weld tearing between slug and free panel connector. |

| Table B-3.2: Experimental Results Backbone Curve [kip. in.] | | | | | | |
|---|---|---|---|---|---|---|
| Shear force-deformation | | | | Axial force-deformation | | |
| Step | Axial Δ | Shear Δ | Shear Force | Axial Δ | Shear Δ | Axial Force |
| Local connector cracking | 0.0165 | 0.026 | 13.20 | 0.013 | 0.033 | 10.26 |
| Shear cracking | 0.048 | 0.141 | 21.33 | 0.071 | 0.096 | 14.41 |
| Max Load | 0.129 | 0.270 | 34.91 | 0.129 | 0.287 | 11.38 |
| | 0.206 | 0.432 | 16.76 | 0.200 | 0.447 | 26.94 |
| Bar fracture | 0.367 | 0.890 | 12.14 | 0.421 | 0.8 | 33.78 |
| - | 0.401 | 0.905 | 4.06 | 0.451 | 0.853 | 24.42 |
| | 0.427 | 1.109 | 9.78 | 0.555 | 0.89 | 23.57 |
| Weld tearing | 0.444 | 1.677 | 4.34 | 0.864 | 0.902 | 7.44 |
| End of test | 1.513 | 2.959 | 5.05 | 1.513 | 2.959 | 1.60 |

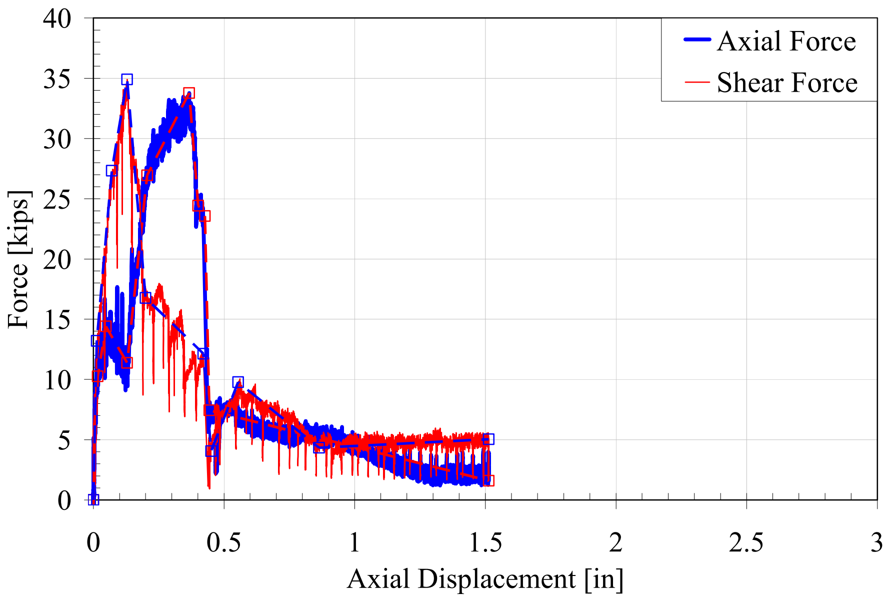


Figure B-3.2: Force and Axial displacement

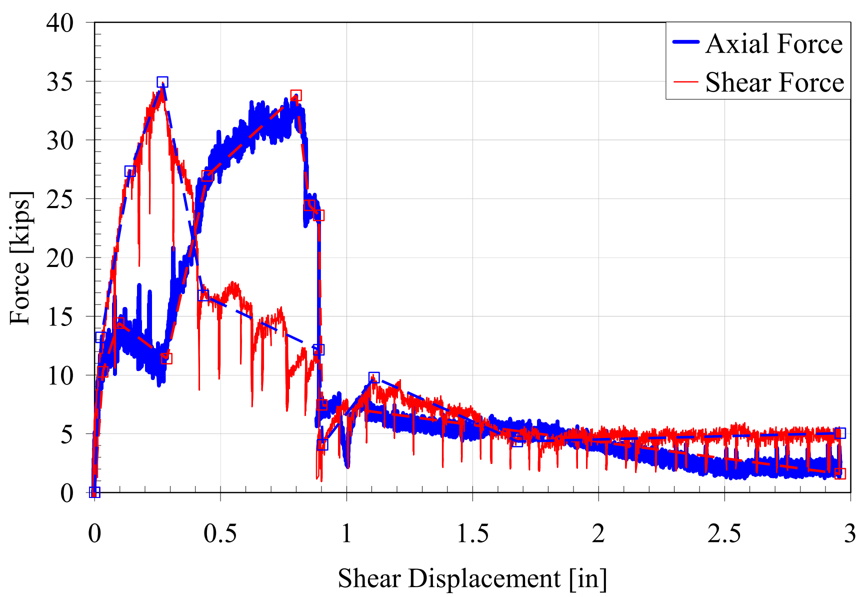


Figure B-3.3: Force and Shear displacement

## TEST B-4: CYCLIC SHEAR WITH ΔT = 0

The performance of an pre-topped welded chord connector subjected to cyclic shear is presented in this section. The panel was subjected to shear displacement with the tensile displacement restrained, ΔT=0. Panel failure consisted of diagonal cracking from the connector to the support in both panels followed by local cracking at the connector face in the free panel and finally fracture of one connector bar in the free panel. The observed events and corresponding displacement cycle is presented in Table B-4.1. The photos of the damage are presented in Figure B-4.1. The global force deformation response and backbone curve is presented in Table B-4.2 and Figure B-4.2.

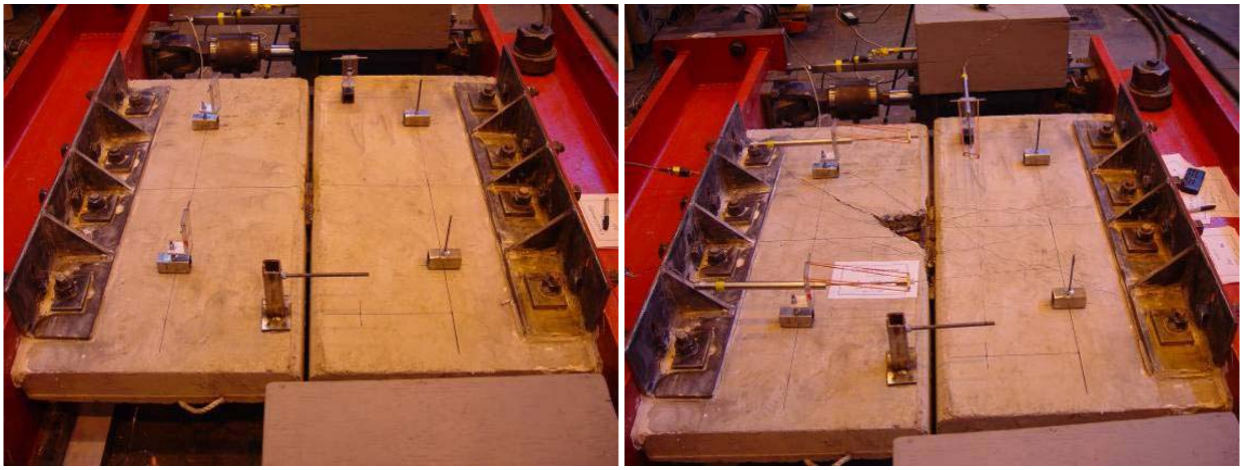

Figure B-4.1: Damage state at 0 and +0.96-in. shear deformation

| Table B-4.1: Key Test Observations | | |
|---|---|---|
| Event # | Shear Step Δ [in.] | Event Description |
| 1 | 0 | Initial surface crack on fixed panel noted. |
| 2 | 0.06 | Surface crack progresses into face and widens slightly. |
| 3 | 0.08 | Concrete cracking audible. |
| 4 | 0.16 | Diagonal shear crack on fixed panel. Cracking on free panel at connector leg. |
| 5 | -0.16 | More transverse cracking on fixed panel & on opposite leg on free panel. |
| 6 | 0.24 | Shear cracking on free panel. |
| 7 | 0.32 | Concrete cracking audible. Progression of concrete cracking spalling. |
| 8 | 0.48 | Popping noise heard. Concrete crushing on fixed panel seen. |
| 9 | 0.64 | Concrete cracking audible. Long crack developed. |
| 10 | 0.8 | Concrete cracking audible. |
| 11 | 0.96 | Large mass of concrete spalling off at connector leg in free panel. |
| 12 | -0.96 | Fracture of connector leg in free panel. |

| Table B-4.2: Experimental Results Backbone Curve [kip. in.] | | | |
|---|---|---|---|
| Step | Shear Displacement | Shear Force | Axial Force |
| Connector leg fracture in free panel | -0.959 | -0.64 | -0.88 |
| - | -0.318 | -11.97 | -2.50 |
| Max Load - Shear cracking free panel | -0.316 | -41.98 | -34.32 |
| Shear cracking fixed panel | -0.118 | -27.48 | -20.02 |
| - | 0 | 0 | 0 |
| Shear cracking fixed panel | 0.118 | 43.62 | -36.59 |
| Max Load - Shear cracking free panel | 0.235 | 63.80 | -60.52 |
| - | 0.295 | 62.74 | -4.68 |
| - | 0.325 | 14.60 | 6.33 |
| - | 0.960 | 2.48 | 1.02 |

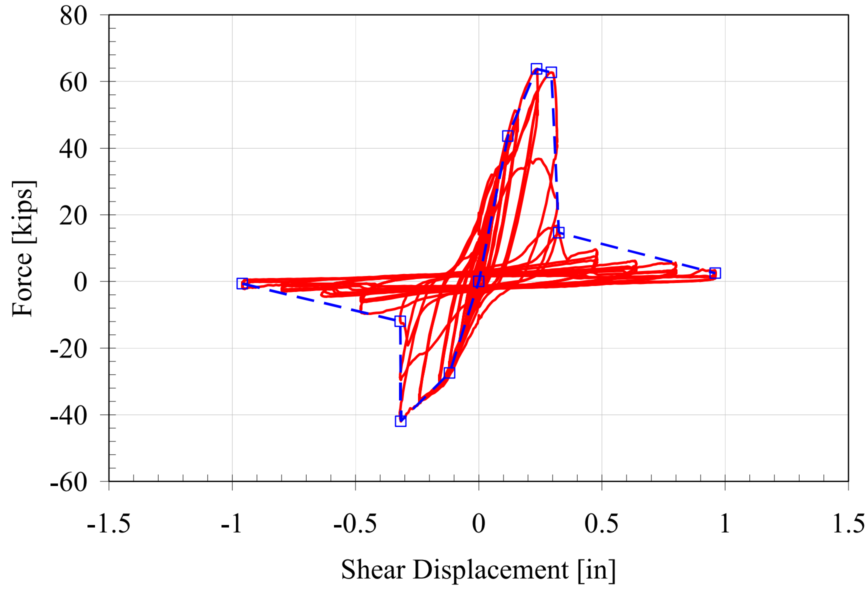

Figure B-4.2: Shear force and displacement

## Subassembly C: Un-topped Hairpin Connector

### Subassembly Details C

The specimen tested represents a topped hairpin connection used as a connector between DT panels. The 2-in. thickness replicates typical roof diaphragms. The embedded connectors are joined through a welded deformed #4 bar slug. Details of the specimen are shown in Figure C.

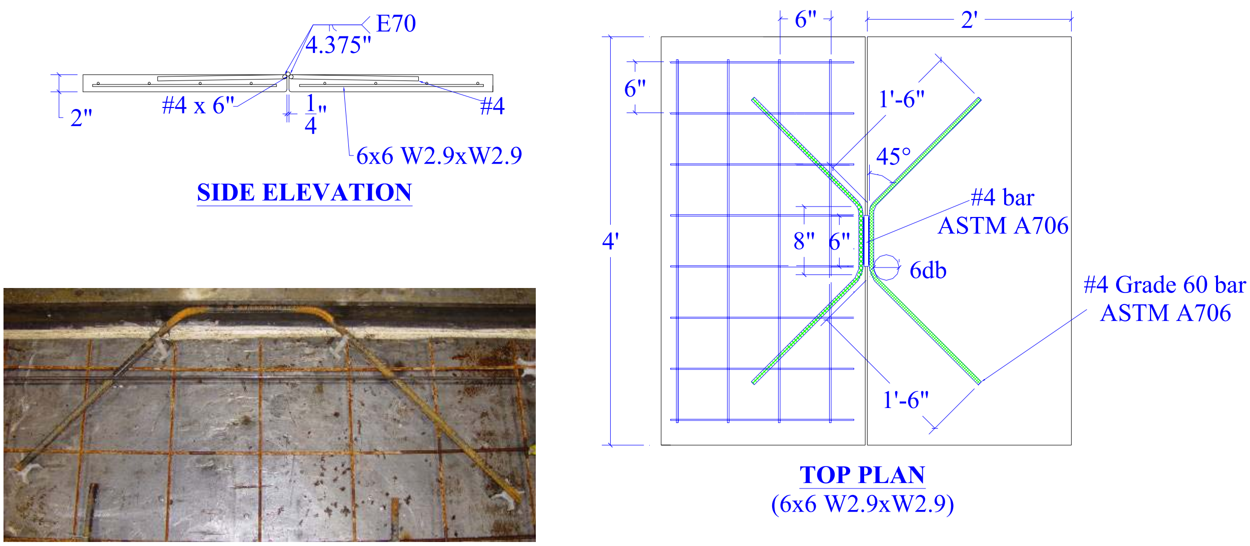


Figure C: Subassembly C

### Material Properties C

The 2-in. thick pre-cast panel was fabricated using high early strength self consolidating concrete with a design strength of 7000 psi. The WWR used in the base panel met the requirements of ASTM A185 grade 65 steel. The connector was fabricated from ASTM A706 grade 60 reinforcing bars. The measured concrete strengths and mill certified steel properties are presented in Table C.

| Table C: Material Properties Capacity | | | | |
|---|---|---|---|---|
| Test | Location in Subassembly (mix) | Compressive Strength, f'c [psi] | | |
| C-1 | Base Panels (P2) | 7274 ± 84 | | |
| C-2 | Base Panels (P2) | 6954 ± 148 | | |
| C-3 | Base Panels (P2) | 6954 ± 148 | | |
| Size | Reinforcement Usage | Grade | Yield Stress [ksi] | Ultimate Strength [ksi] |
| #4 | Reinforcing Bars | A706 | 65.79 | 91.39 |
| W2.9XW2.9 6X6 | Pre-cast Panel Mesh | A185 Gr.65 | 65.00* | 108.5 |
| * Data unavailable, value assumed | | | | |

## TEST C-1: MONOTONIC TENSION WITH ΔV = 0

The performance of an un-topped hairpin web connector subjected to monotonic tension is presented in this section. The panel was subjected to tensile displacement with the shear displacement restrained, ΔV=0. Panel damage consisted of bending of the straight welded length of the connector bars, which initiated weld tearing, followed by concrete cracking near the connector legs. The weld tearing propagated through the left leg of the free panel connector resulting in a complete fracture. The observed events and corresponding displacement cycle is presented in Table C-1.1. The photos of the damage are presented in Figure C-1.1. The global force deformation response and backbone curve is presented in Table C-1.2 and Figure C-1.2.

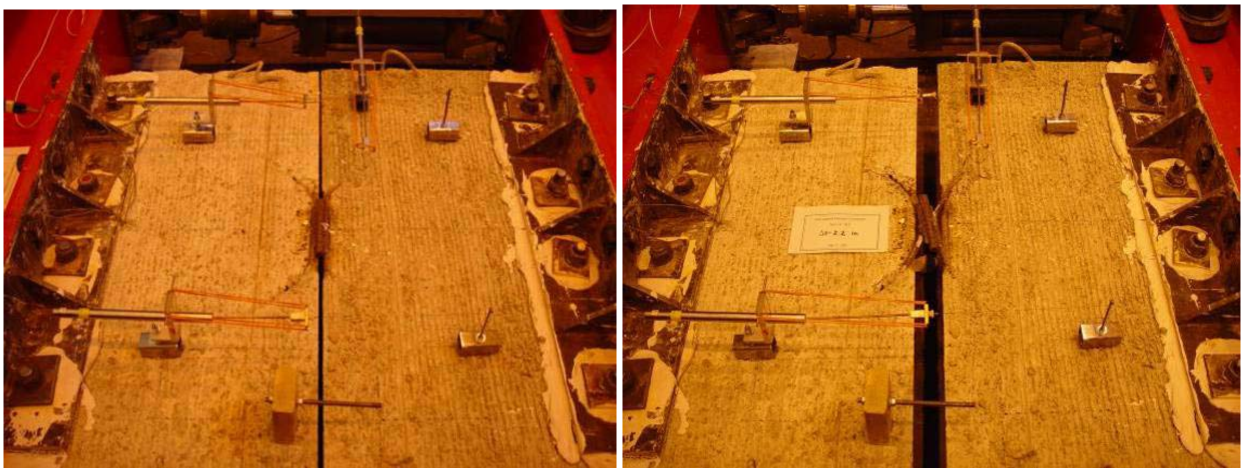

Figure C-1.1: Damage state at 0.03 and 2.2-in. shear opening

Table C-1.1: Key Test Observations

| Event # | Tension Step Δ [in.] | Event Description |
|---|---|---|
| 1 | 0.08 | Concrete cracking audible. |
| 2 | 0.25 | Concrete cracking audible. |
| 3 | 0.4 | Concrete cracking audible. |
| 4 | 0.5 | Concrete cracking audible. |
| 5 | 0.7 | Bending of straight welded length of connector bars seen. Weld tearing initiated. |
| 6 | 1.2 | Cracking near the connector legs seen. |
| 7 | 2 | Left leg bar fractured at free panel. |

Table C-1.2: Experimental Results Backbone Curve [kip. in.]

| Step | Tensile Displacement | Tensile Force |
|---|---|---|
| - | 0.091 | 2.60 |
| - | 0.252 | 3.83 |
| Weld tearing | 1.073 | 6.95 |
| Max Load | 1.444 | 7.71 |
| Fracture of Connector leg. | 1.833 | 5.28 |
| - | 1.871 | 0 |

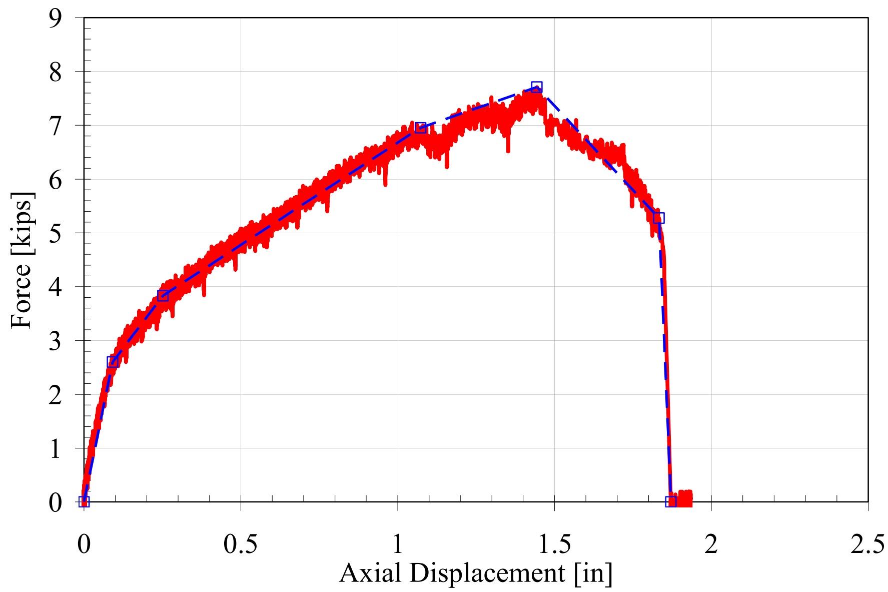

Figure C-1.2: Tensile force and displacement

### TEST C-2: MONOTONIC SHEAR (1) WITH ΔT = 0

The performance of an un-topped hairpin web connector subjected to monotonic shear is presented in this section. The panel was subjected to shear displacement with the tensile displacement restrained, ΔT=0. Panel damage consisted of concrete crushing at the compression leg in the free panel, followed by concrete spalling over the tension leg in the free panel. The connector failed due to pullout of the tension leg in the free panel. The observed events and corresponding displacement cycle is presented in Table C-2.1. The photos of the damage are presented in Figure C-2.1. The global force deformation response and backbone curve is presented in Table C-2.2 and Figure C-2.2.

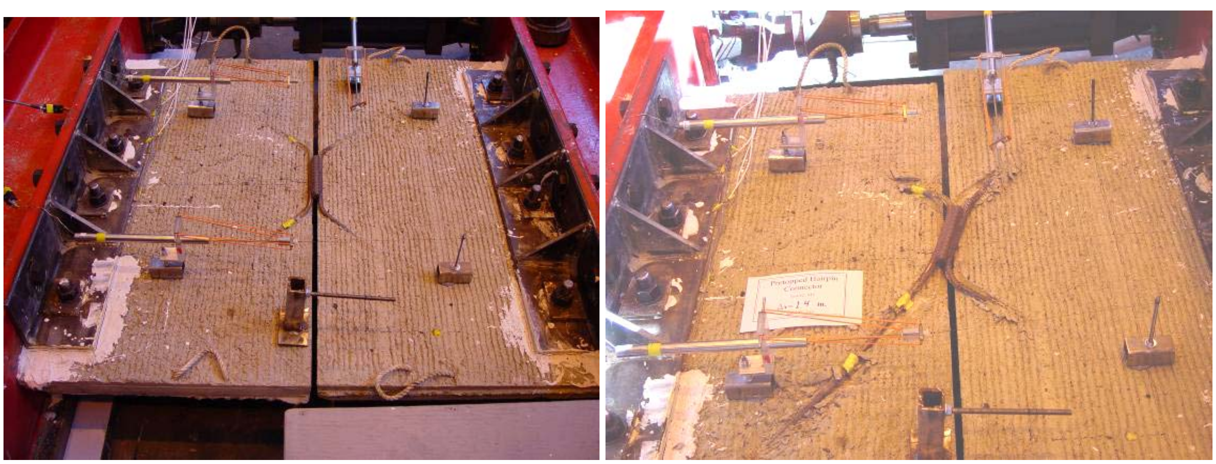
Figure C-2.1: Damage state at 0 and 1.4-in. shear opening

| Table C-2.1: Key Test Observations | | | |
|---|---|---|---|
| Event # | Shear Step Δ [in.] | Tension Step Δ [in.] | Event Description |
| 1 | 0.08 | 0 | Concrete cracking audible. |
| 2 | 0.2 | 0 | Cracks form at compression leg bend in free panel. |
| 3 | 0.3 | 0 | Cracks form at compression leg bend in free panel. |
| 4 | 0.4 | 0 | Tension leg pullout in free panel initiated. |
| 5 | 0.5 | 0 | Concrete spalling at tension leg in free panel. Twisting of connector apparent. |
| 6 | 0.6 | 0 | Concrete spalling at compression leg in free panel. |
| 7 | 1.3 | 0 | Tension leg pullout in free panel. |
| 8 | 1.4 | 0 | Tension leg pullout in free panel. Tension leg embedment length ~ 2-in. |
| 9 | 1.9 | 0 | Complete tension leg pullout in free panel. |
| 10 | 2 | 0 | Slip of tension leg connector reinforcement in the free panel over the topping. |

| Table C-2.2: Experimental Results Backbone Curve [kip. in.] | | | | |
|---|---|---|---|---|
| Shear force-deformation | | | Axial force – Shear deformation | |
| Step | Shear Displacement | Shear Force | Shear Displacement | Axial Force |
| Concrete crushing at comp. leg | 0.082 | 4.52 | 0.003 | 0.91 |
| Tension leg pullout | 0.492 | 4.26 | 0.764 | 2.02 |
| Comp. leg bearing on concrete | 0.720 | 5.27 | 1.256 | 4.56 |
| - | 0.842 | 5.26 | 1.328 | 0.49 |
| Max load | 1.265 | 8.74 | 1.734 | 0.07 |
| - | 1.321 | 2.06 | 1.776 | -0.13 |
| Tension leg pullout | 1.753 | 2.29 | | |
| - | 1.778 | 1.50 | | |
| End of test | 2.798 | 1.08 | | |

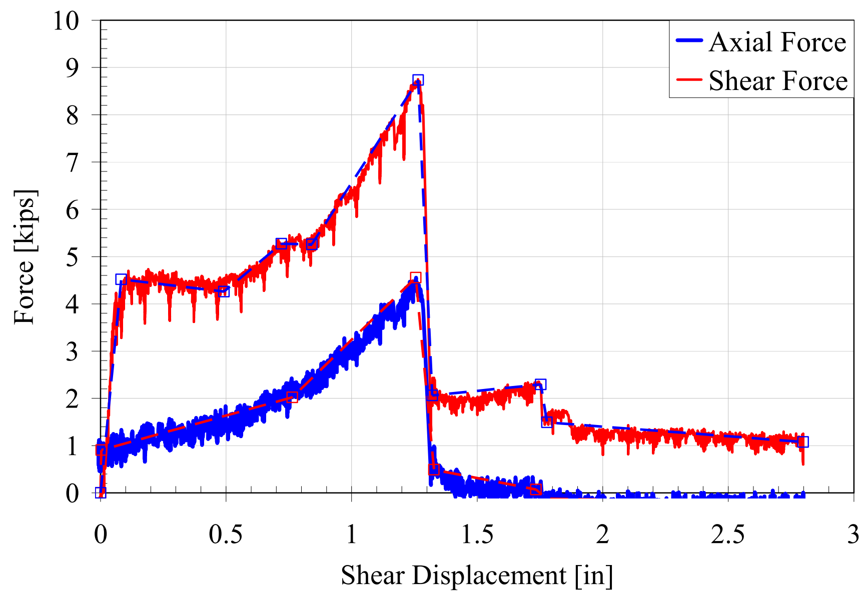


Figure C-2.2: Shear force and displacement

### TEST C-3: MONOTONIC SHEAR (2) WITH ΔT = 0

The performance of an un-topped hairpin web connector subjected to monotonic shear was repeated to provide further information on the ultimate deformation capacity. The panel was subjected to shear displacement with the tensile displacement restrained, ΔT=0. Panel damage consisted of concrete crushing at the compression leg in the free panel, followed by concrete spalling over the tension leg in the free panel. The connector failed due to pullout of the tension leg in the free panel. The observed events and corresponding displacement cycle is presented in Table C-3.1. The photos of the damage are presented in Figure C-3.1. The global force deformation response and backbone curve is presented in Table C-3.2 and Figure C-3.2.

Figure C-3.1: Damage state at 0 and 2.5-in. shear opening

| Table C-3.1: Key Test Observations | | | |
|---|---|---|---|
| Event # | Shear Step Δ [in.] | Tension Step Δ [in.] | Event Description |
| 1 | 0.06 | 0 | Cracking near right bend of free panel connector. |
| 2 | 0.08 | 0 | Surface concrete spalling on fixed panel at connector bends. |
| 3 | 0.1 | 0 | Cracking noticed at connector tension legs. |
| 4 | 0.2 | 0 | Cracking progressed at connector tension legs. |
| 5 | 0.3 | 0 | Cracking noticed over connector legs. |
| 6 | 0.4 | 0 | Concrete spalling exposing connector tension legs. |
| 7 | 0.5 | 0 | Concrete block sheared off at connector compression leg in free panel bearing between gap. |
| 8 | 0.6 | 0 | Connector rotation visible. |
| 9 | 0.9 | 0 | Cracking over connector tension legs exposes legs further. |
| 10 | 1.0 | 0 | Concrete spalling off at connector compression leg in free panel. |
| 11 | 1.3 | 0 | Concrete spalling over tension legs exposing: free panel ~8-in. fixed |
| 12 | 1.4 | 0 | Large spalling over connector tension leg (leg complete pulls out). |
| 13 | 1.9 | 0 | Loud noise audible: Tension leg in fixed panel dislodged from exposed plastic form chair. |
| 14 | 2.2 | 0 | Spalling over free tension leg exposing the full tension leg length. |

| Table C-3.2: Experimental Results Backbone Curve [kip. in.] | | | | |
|---|---|---|---|---|
| Shear force-deformation | | | Axial force – Shear deformation | |
| Step | Shear Displacement | Shear Force | Shear Displacement | Axial Force |
| Concrete cracking at comp. leg | 0.034 | 4.147 | 0.111 | 0.48 |
| Cracking at tension legs | 0.116 | 5.292 | 0.396 | 0.42 |
| - | 0.186 | 4.693 | 1.182 | 3.10 |
| Connector rotation | 0.582 | 4.706 | 1.301 | 4.52 |
| Cracking at tension leg | 1.134 | 6.483 | 1.354 | 1.261 |
| Max load-tension leg pullout | 1.298 | 8.58 | 1.581 | 0.21 |
| Tension leg pullout | 1.359 | 2.929 | 1.836 | -0.34 |
| Tension leg pullout | 1.84 | 1.79 | 2.417 | -0.21 |
| End of test | 2.418 | 1.53 | | |

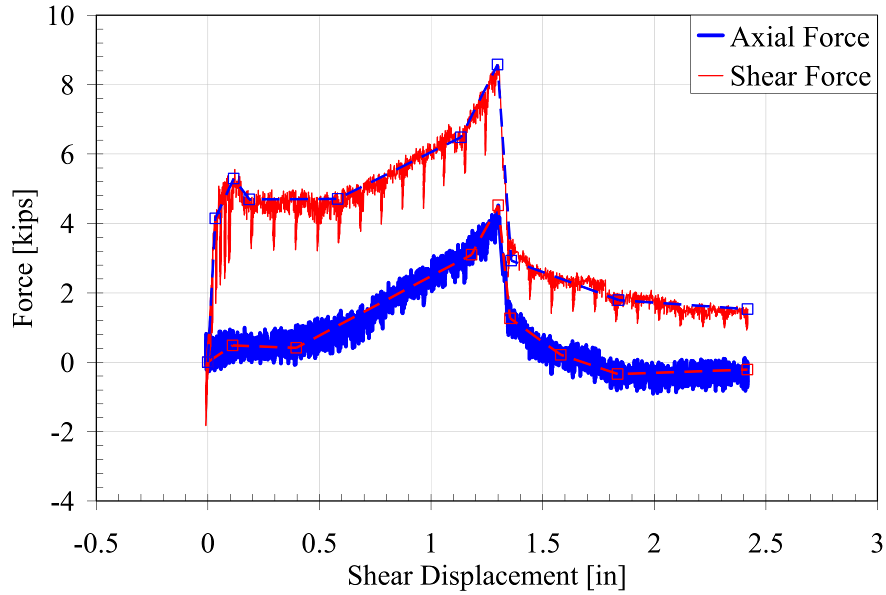

Figure C-3.2: Shear force and displacement

## Subassembly D: Topped Hairpin Connector

### Subassembly Details D

The specimen tested represents a topped hairpin connection used as a connector between DT panels. The bars are connected by a deformed #4 bar slug. Details of the specimen are shown in Figure D.

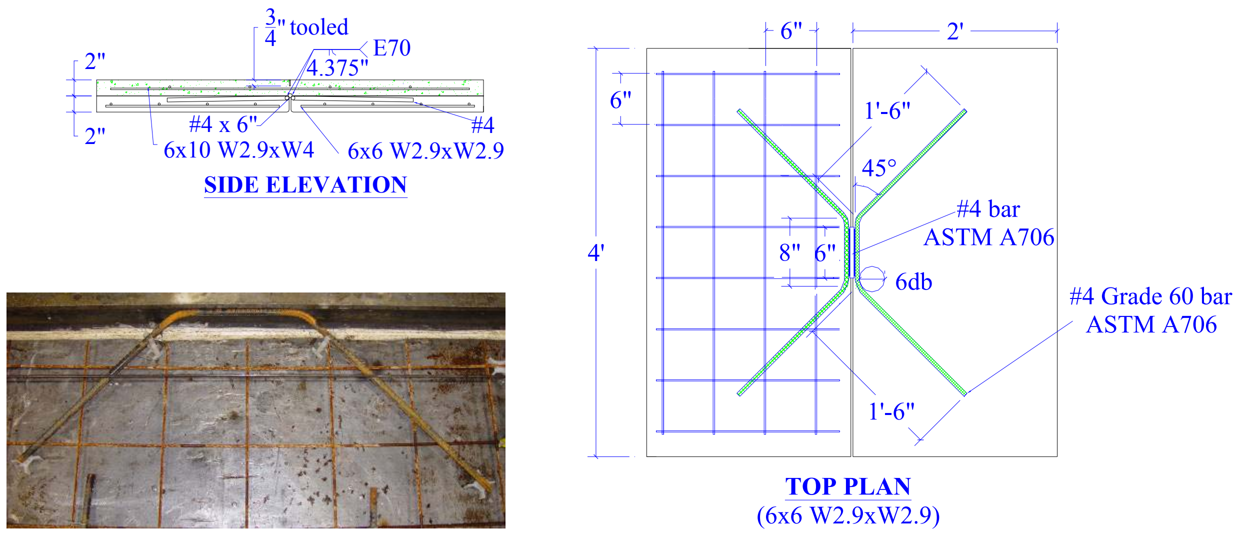


Figure D: Subassembly D

### Material Properties D

The base 2-in. pre-cast panel was fabricated using high early strength self consolidating concrete with a design strength of 7000 psi. A ready mix topping was used to simulate field topped conditions. The design strength of the topping was 4000 psi. The WWR used in the topping and base panel met the requirements of ASTM A185 grade 65 steel. The connector was fabricated from ASTM A706 grade 60 reinforcing bars. The measured concrete strengths and mill certified steel properties are presented in Table D.

Table D: Material Properties Capacity

| Test | Location in Subassembly (mix) | Compressive Strength, f'c [psi] |
|---|---|---|
| D-1 | Topping (T1) | 4337 ± 147 |
| | Base Panels (P2) | 8416 ± 175 |
| D-2 | Topping (T1) | 4337 ± 147 |
| | Fixed Panel (P2) | 7633 ± 797 |
| | Free Panel (P2) | 6954 ± 148 |
| D-3 | Topping (T1) | 4337 ± 147 |
| | Base Panels (P2) | 7020 ± 684 |
| D-4 | Topping (T2) | 4032 ± 600 |
| | Base Panels (P2) | 8416 ± 175 |
| D-5 | Topping (T1) | 4337 ± 147 |
| | Fixed Panel (P2) | 7274 ± 84 |
| | Free Panel (P2) | 7020 ± 684 |

| Size | Reinforcement Usage | Grade | Yield Stress [ksi] | Ultimate Strength [ksi] |
|---|---|---|---|---|
| #4 | Reinforcing Bars | A706 | 65.79 | 91.39 |
| W2.9XW4 6X10 | Topping Mesh | A185 Gr.65 | 65.00* | 103.3 |
| W2.9XW2.9 6X6 | Pre-cast Panel Mesh | A185 Gr.65 | 65.00* | 108.5 |

* Data unavailable, value assumed

### Test D-1: Monotonic Tension with Fv = 0

The performance of a topped hairpin web connector subjected to monotonic tension is presented in this section. The panel was subjected to tensile displacement with the shear displacement unrestrained, Fv=0. The panel failed due to fracture of the WWR followed by tearing of the slug to connector weld followed by fracture through the hairpin connector. The observed events and corresponding displacement cycle is presented in Table D-1.1. The photos of the damage are presented in Figure D-1.1. The global force deformation response and backbone curve is presented in Table D-1.2 and Figure D-1.2.

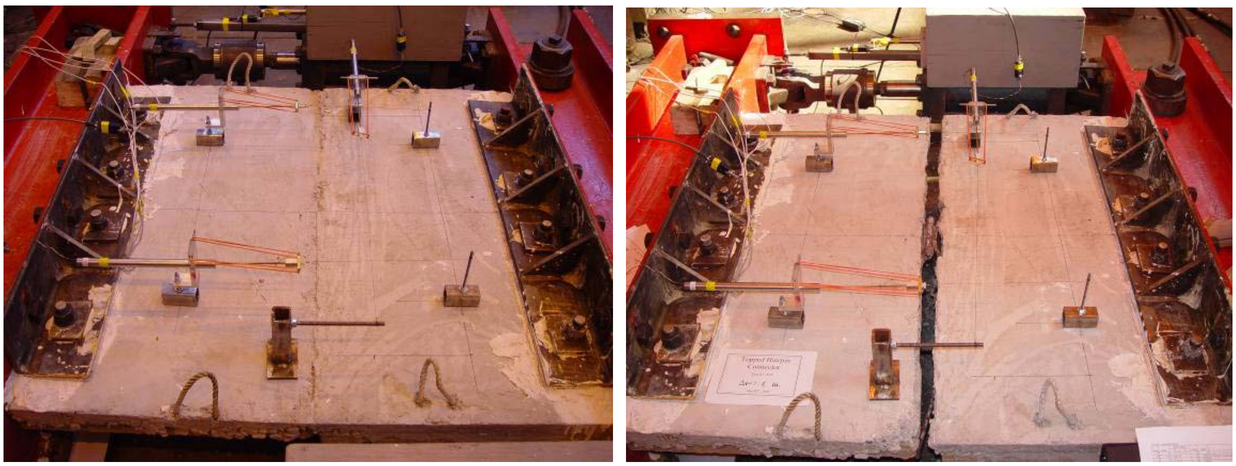

Figure D-1.1: Damage state at 0 and 1.6-in. shear opening

| Table D-1.1: Key Test Observations | | |
|---|---|---|
| Event # | Tension Δ [in.] | Event Description |
| 1 | 0.01 | Centerline crack formed. |
| 2 | 0.06 | Concrete cracking audible. |
| 3 | 0.2 | Six WWR wires fractured. |
| 4 | 1 | Weld tearing initiated. |
| 5 | 1.4 | Progression of weld tearing. |
| 6 | 1.7 | Weld tear failure. |

| Table D-1.2: Experimental Results Backbone Curve [kip. in.] | | |
|---|---|---|
| Step | Tensile Displacement | Tensile Force |
| 75% Max Load | 0.014 | 15.80 |
| Max Load | 0.048 | 25.00 |
| Fracture of WWR | 0.124 | 19.45 |
| Fracture of WWR | 0.158 | 3.35 |
| Weld tearing | 1.323 | 8.78 |
| Weld tear failure | 1.696 | 6.06 |
| End of test | 1.696 | 0 |

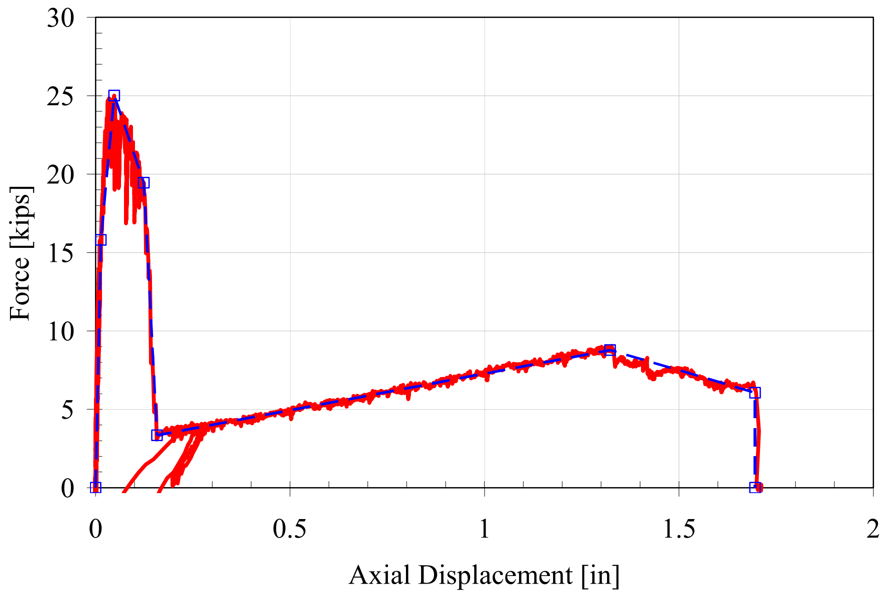


Figure D-1.2: Tensile force and displacement

### **TEST D-2: MONOTONIC SHEAR (1) WITH $\Delta T = 0.1$-IN.**

The performance of a topped hairpin web connector subjected to monotonic shear is presented in this section. The panel was pre-cracked by applying a tensile opening of 0.1-in. A shear displacement was the applied with the tensile displacement restrained at the 0.1-in. opening. Panel damage consisted of diagonal cracking from the connector to the support in the fixed panel, followed by diagonal cracking from the connector to the support in the free panel and finally fractures of the WWR in the topping coupled with slippage of the main reinforcement. A max shear deformation of 1.8in was applied due to a limitation of the control system. The observed events and corresponding displacement cycle is presented in Table D-2.1. The photos of the damage are presented in Figure D-2.1. The global force deformation response and backbone curve is presented in Table D-2.2 and Figure D-2.2.

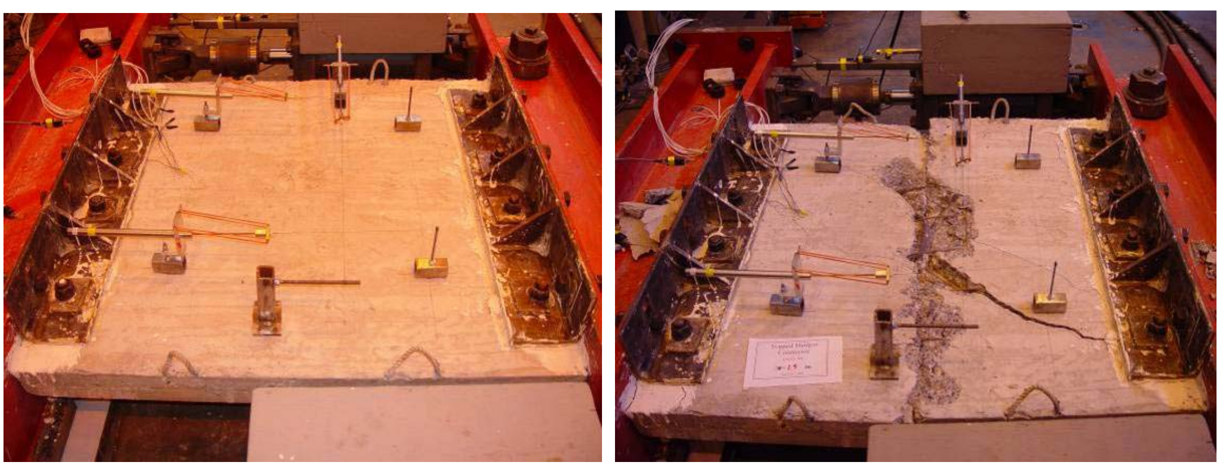

Figure D-2.1: Damage state at 0 and 1.8-in. shear opening

| Table D-2.1: Key Test Observations | | | |
|---|---|---|---|
| Event # | Shear Δ [in.] | Tension Δ [in.] | Event Description |
| 1 | 0 | 0.01 | Centerline crack formed. |
| 2 | 0.04 | 0.1 | Concrete cracking audible. |
| 3 | 0.2 | 0.1 | Concrete cracking audible. |
| 4 | 0.3 | 0.1 | Shear crack formation on fixed panel. |
| 5 | 0.4 | 0.1 | Concrete cracking audible. Shear crack widened. |
| 6 | 0.5 | 0.1 | Concrete cracking audible. Shear cracking in free panel. |
| 7 | 0.6 | 0.1 | Concrete cracking audible. |
| 8 | 0.7 | 0.1 | Three WWR wires fractured. |
| 9 | 0.8 | 0.1 | Two WWR wires fractured. |
| 10 | 1.0 | 0.1 | Two WWR wires fractured. |
| 11 | 1.1 | 0.1 | One WWR wires fractured. |
| 12 | 1.2 | 0.1 | One WWR wires fractured. |
| 13 | 1.5 | 0.1 | Two WWR wires fractured. |
| 14 | 1.6 | 0.1 | Two WWR wires fractured. |
| 15 | 1.8 | 0.1 | One WWR wires fractured. |

| Table D-2.2: Experimental Results Backbone Curve [kip. in.] | | | | |
|---|---|---|---|---|
| Shear force-deformation | | | Axial force – Shear deformation | |
| Step | Shear Displacement | Shear Force | Shear Displacement | Axial Force |
| - | 0.023 | 8.33 | 0.002 | 28.46 |
| ~ 75% Max Load | 0.114 | 41.97 | 0.128 | -9.97 |
| Max Load-Shear crack in fixed panel | 0.206 | 47.62 | 0.238 | -17.84 |
| Shear crack in free panel | 0.482 | 41.15 | 0.564 | -3.81 |
| - | 0.559 | 31.42 | 0.916 | -11.26 |
| Fracture of WWR | 1.246 | 26.08 | 1.375 | 3.87 |
| Fracture of WWR | 1.552 | 20.35 | 1.571 | 4.97 |
| Fracture of WWR | 1.681 | 13.56 | 1.616 | -1.36 |
| Fracture of WWR | 1.781 | 12.98 | 1.79 | -3.14 |

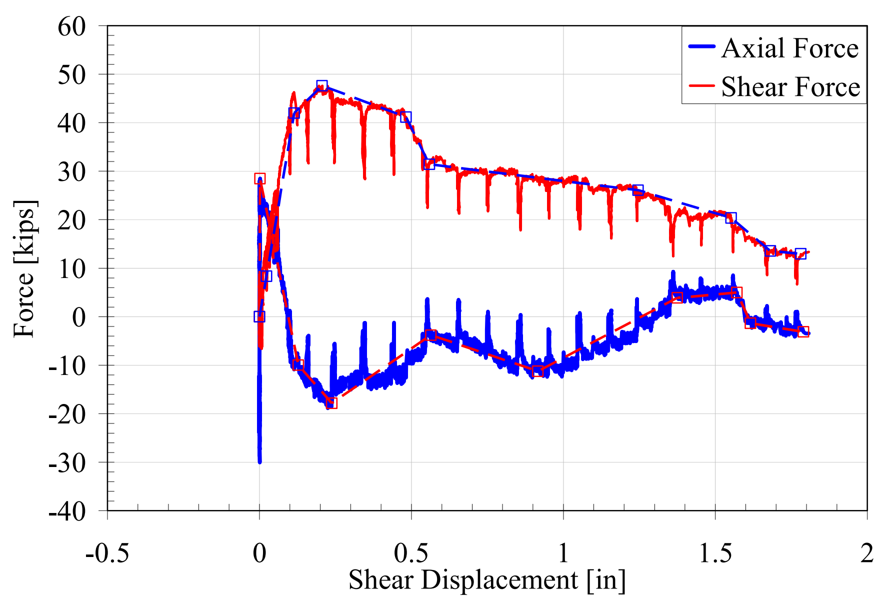


Figure D-2.2: Shear force and displacement

### TEST D-3: MONOTONIC SHEAR (2) WITH $\Delta T = 0.1$-IN.

The performance of a topped hairpin web connector subjected to monotonic shear was repeated to provide further information on the ultimate deformation capacity. The panel was pre-cracked by applying a tensile opening of 0.1-in. A shear displacement was the applied with the tensile displacement restrained at the 0.1-in. opening. Panel damage consisted of diagonal cracking from the connector to the support in both panels followed by fractures of the WWR in the topping and finally, fracture of the tension leg in the free panel close to the weld toe. The observed events and corresponding displacement cycle is presented in Table D-3.1. The photos of the damage are presented in Figure D-3.1. The global force deformation response and backbone curve is presented in Table D-3.2 and Figure D-3.2.

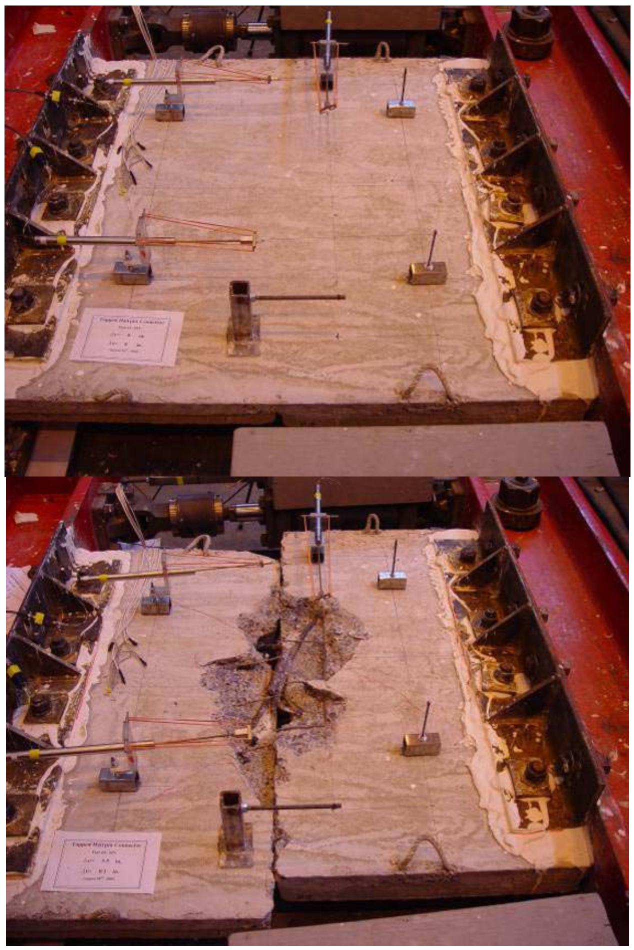

Figure D-3.1: Damage state at 0 and 3.5-in. shear opening

| Table D-3.1: Key Test Observations | | | |
|---|---|---|---|
| Event # | Shear Δ [in.] | Tension Δ [in.] | Event Description |
| 1 | 0 | 0.01 | Centerline crack formed. |
| 2 | 0.2 | 0.1 | Concrete cracking audible. |
| 3 | 0.3 | 0.1 | Concrete cracking audible. Surface spalling. |
| 4 | 0.4 | 0.1 | Concrete cracking audible. Surface spalling. Shear cracking on both panels. |
| 5 | 0.5 | 0.1 | Concrete cracking audible. Surface spalling & large block spalling off end. |
| 6 | 0.6 | 0.1 | Concrete cracking audible. Two WWR wires fractured. |
| 7 | 0.7 | 0.1 | Concrete cracking audible. Surface spalling exposed two WWR wires. |
| 8 | 0.8 | 0.1 | Concrete cracking audible. One WWR wire fractured. |
| 9 | 0.9 | 0.1 | Concrete cracking audible. Surface spalling. |
| 10 | 1.0 | 0.1 | Concrete cracking audible. Surface spalling. Two WWR wires fractured. |
| 11 | 1.1 | 0.1 | Concrete cracking audible. |
| 12 | 1.2 | 0.1 | Concrete cracking audible. Two WWR wires fractured. |
| 13 | 1.4 | 0.1 | Concrete cracking and spalling on the underside of the panel audible. |
| 14 | 1.5 | 0.1 | Concrete cracking audible. |
| 15 | 1.6 | 0.1 | Concrete cracking audible. Surface spalling. One WWR wire fractured. |
| 16 | 1.8 | 0.1 | Small popping noises heard. |
| 17 | 1.9 | 0.1 | Two WWR wires fractured. |
| 18 | 2.0 | 0.1 | One WWR wire fractured after cycle. Tension leg in both panels exposed: fixed panel ~ 7-in; free panel ~ 5-in |
| 19 | 2.2 | 0.1 | Spalling off of fixed panel tension leg. One WWR wire fractured. |
| 20 | 2.3 | 0.1 | One WWR wire fractured. |
| 21 | 2.5 | 0.1 | One WWR wire fractured. |
| 22 | 2.9 | 0.1 | Fracture of tension leg in free panel close to weld toe. |
| 23 | 3 | 0.1 | Tension leg in both panels exposed: fixed panel ~ 7-in; free panel ~ 5-in |

| Table D-3.2: Experimental Results Backbone Curve [kip. in.] | | | | |
|---|---|---|---|---|
| Shear force-deformation | | | Axial force – Shear deformation | |
| Step | Shear Displacement | Shear Force | Shear Displacement | Axial Force |
| 75% Max Load | 0.184 | 39.56 | 0 | 27.41 |
| Max Load-Shear cracking. | 0.342 | 54.94 | 0.250 | -11.84 |
| Fracture of WWR | 0.556 | 47.93 | 0.446 | -24.87 |
| Fracture of WWR | 0.704 | 28.90 | 0.711 | 0.22 |
| - | 1.333 | 20.94 | 2.007 | 5.32 |
| Fracture of WWR | 1.961 | 23.03 | 2.378 | 1.80 |
| Fracture of connector bar | 2.828 | 18.79 | 2.825 | 2.44 |
| - | 2.843 | 1.72 | 2.825 | -0.81 |
| End of test | 3.439 | 2.97 | 3.441 | -2.76 |
| | | | 3.494 | -1.25 |

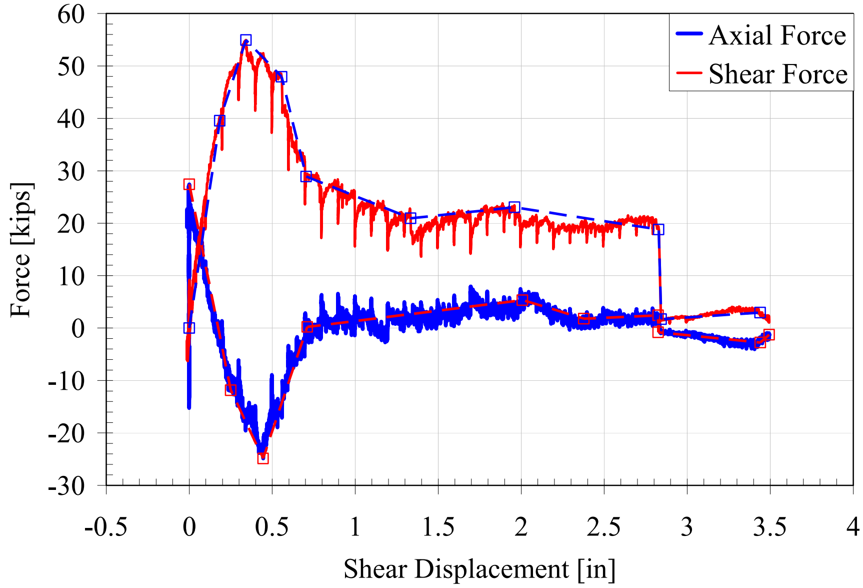


Figure D-3.2: Shear force and displacement

## TEST D-4: MONOTONIC TENSION & SHEAR WITH $\Delta T/\Delta V = 0.5$

The performance of a topped hairpin web connector subjected to monotonic tension & shear is presented in this section. Tension deformation to shear deformation was applied at a constant ratio of $\Delta T/\Delta V = 0.5$. Panel damage consisted of local cracking at the connector compression legs followed by fracture of the WWR in the topping and finally, fracture of the tension leg in the free panel close to the weld toe. The observed events and corresponding displacement cycle is presented in Table D-4.1. The photos of the damage are presented in Figure D-4.1. The global force deformation response and backbone curve is presented in Table D-4.2, Figure D-4.2 and Figure D-4.3.

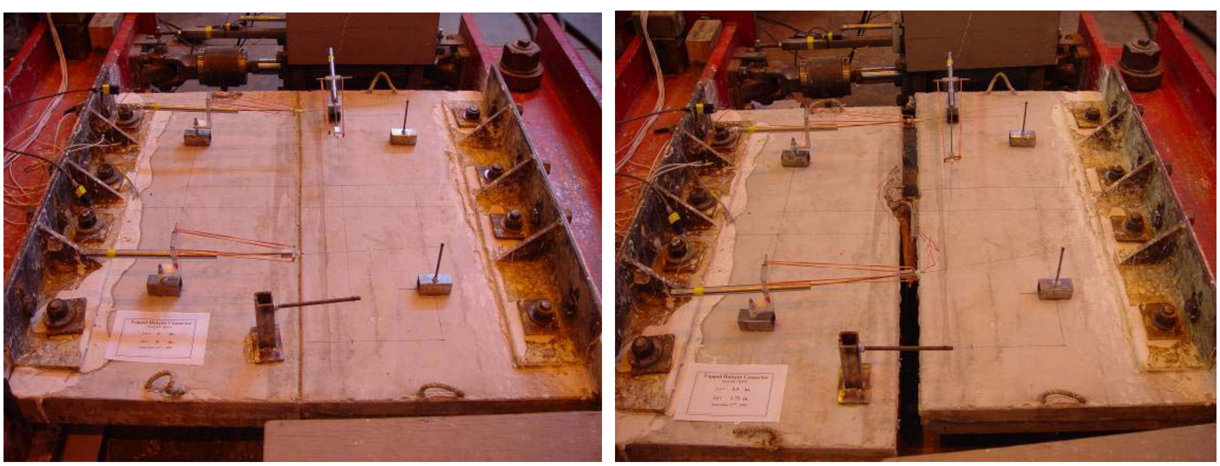

Figure D-4.1: Damage state at 0 and 3.5-in. shear opening

| Table D-4.1: Key Test Observations | | | |
|---|---|---|---|
| Event # | Shear Δ [in.] | Tension Δ [in.] | Event Description |
| 1 | 0.01 | 0.005 | Centerline crack formed. |
| 2 | 0.08 | 0.04 | Cracking at compression legs on both panels. |
| 3 | 0.2 | 0.1 | Concrete cracking audible. Crack widening. |
| 4 | 0.3 | 0.15 | Concrete cracking audible. Multiple wires fractured. |
| 5 | 0.4 | 0.2 | Concrete cracking audible. |
| 6 | 0.5 | 0.25 | Concrete cracking audible. |
| 7 | 0.6 | 0.3 | Tension leg in free panel fractured. Surface spalling exposed free panel connector. |
| 8 | 0.7 | 0.35 | Tension leg in free panel exposed. |

| Table D-4.2: Experimental Results Backbone Curve [kip. in.] | | | | | | |
|---|---|---|---|---|---|---|
| Shear force-deformation | | | | Axial force-deformation | | |
| Step | Axial Δ | Shear Δ | Shear Force | Axial Δ | Shear Δ | Axial Force |
| Centerline cracking | 0.007 | 0.014 | 12.78 | 0.005 | 0.01 | 3.461 |
| Cracking at comp. legs | 0.043 | 0.085 | 25.02 | 0.053 | 0.105 | 22.65 |
| Max Load-Fracture of WWR | 0.101 | 0.201 | 29.80 | 0.117 | 0.234 | 20.51 |
| Fracture of WWR | 0.143 | 0.285 | 28.99 | 0.139 | 0.278 | 14.67 |
| - | 0.159 | 0.318 | 22.68 | 0.152 | 0.304 | 0.30 |
| - | 0.207 | 0.414 | 23.36 | 0.274 | 0.548 | 0.64 |
| Tension leg fracture | 0.273 | 0.545 | 20.94 | 0.288 | 0.576 | -1.34 |
| - | 0.283 | 0.566 | 4.53 | 0.621 | 1.241 | -1.85 |
| End of test | 1.75 | 3.5 | 1.45 | 1.749 | 3.498 | 0.18 |

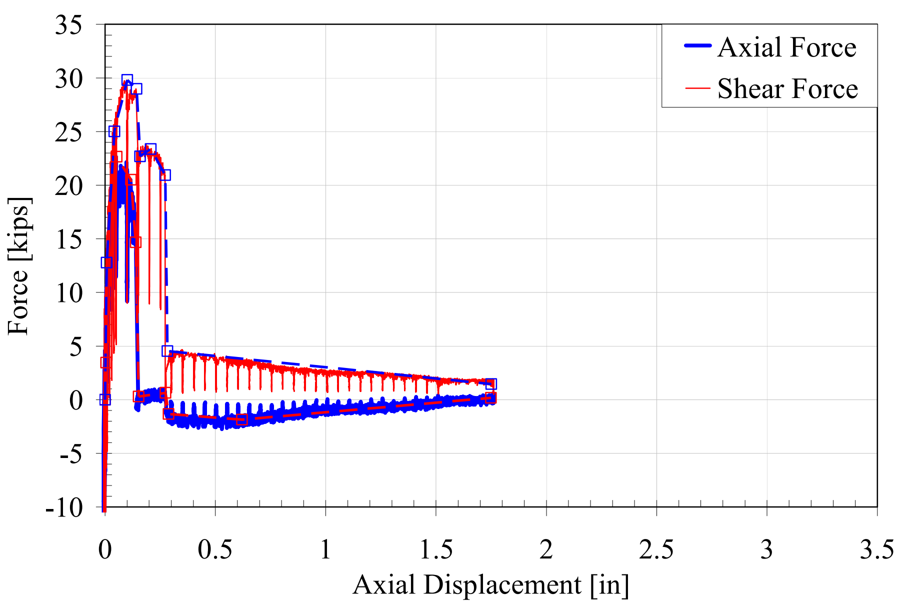

Figure D-4.2: Force and Axial displacement

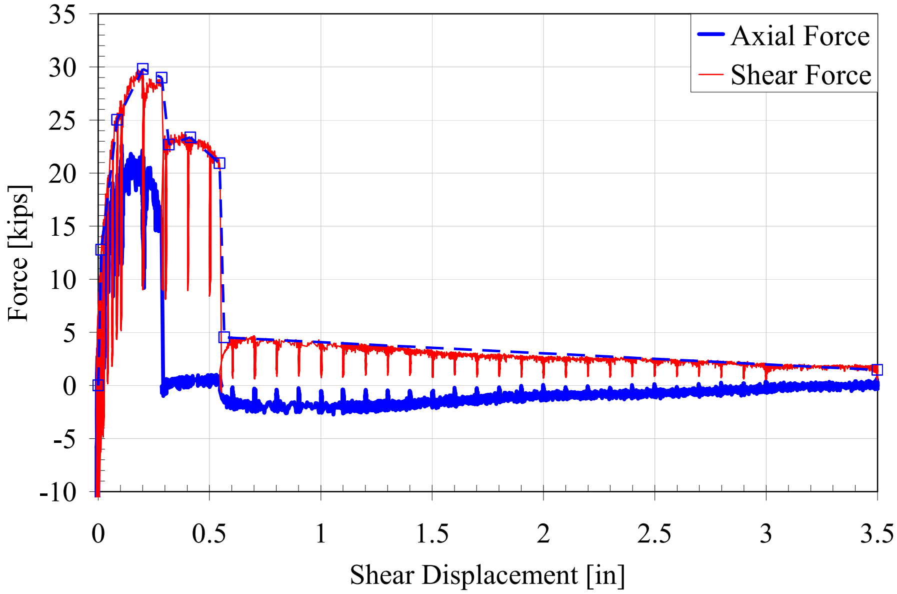


Figure D-4.3: Force and Shear displacement

### TEST D-5: CYCLIC SHEAR WITH ΔT = 0.1-IN.

The performance of a topped hairpin web connector subjected to cyclic shear was repeated to provide further information on the ultimate deformation capacity. The panel was pre-cracked by applying a tensile opening of 0.1-in. A cyclic shear displacement was the applied with tensile displacement restrained at the 0.1-in. opening. Panel damage consisted of diagonal cracking from the connector to the support in both panels followed by fractures of the WWR in the topping and finally, fracture of the tension legs in the free panel close to the weld toe. To fail the system, the panel was then subjected to a 3in tensile deformation which caused fracture of the main reinforcement bars. The observed events and corresponding displacement cycle is presented in Table D-5.1. The photos of the damage are presented in Figure D-5.1. The global force deformation response and backbone curve is presented in Table D-5.2, Figure D-5.2 and Figure D-5.3.

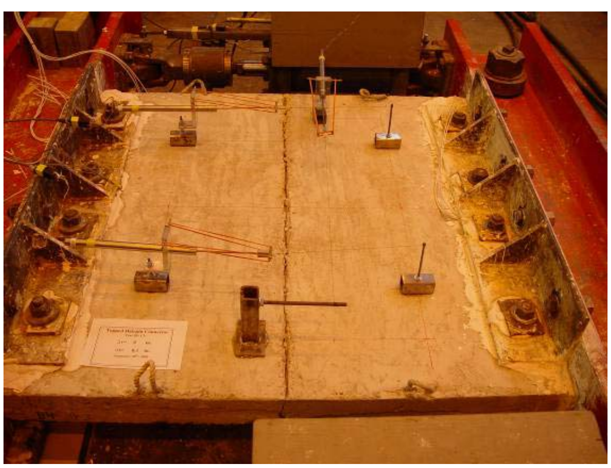

Figure D-5.1: Damage state at 0 and 2.734-in. shear opening

| Table D-5.1: Key Test Observations | | | |
|---|---|---|---|
| Event # | Shear Δ [in.] | Tension Δ [in.] | Event Description |
| 1 | 0 | 0 | Centerline crack pre-cracked. |
| 2 | 0.171 | 0.1 | Concrete cracking audible. |
| 3 | -0.171 | 0.1 | Shear cracking at connector legs. |
| 4 | 0.256 | 0.1 | Shear cracking through free panel. |
| 5 | 0.342 | 0.1 | Shear cracking. |
| 6 | 0.513 | 0.1 | Surface spalling followed by multiple WWR wire fractures. |
| 7 | -0.513 | 0.1 | Cracking extended. |
| 8 | -0.513 (2nd cycle) | 0.1 | Surface spalling exposed connector. |
| 9 | 0.683 | 0.1 | Popping noise heard. Cracking around connector in free panel. |
| 10 | -0.683 | 0.1 | Surface spalling. |
| 11 | 0.683 (3rd cycle) | 0.1 | Free panel left connector bar fracture. |
| 12 | -0.683 (3rd cycle) | 0.1 | Free panel right connector bar fracture. |
| 13 | 1.025 | 0.1 | WWR wires fractured. |
| 14 | 2.05 | 0.1 | 2 WWR wires over connector fractured. |

| Table D-5.2: Experimental Results Backbone Curve [kip. in.] | | | | |
|---|---|---|---|---|
| Shear force-deformation | | | Axial force – Shear deformation | |
| Step | Shear Displacement | Shear Force | Shear Displacement | Axial Force |
| - | -2.701 | -2.43 | -2.37 | -2.42 |
| Connector tensile bar fracture | -0.68 | -14.75 | -0.68 | -0.77 |
| Max Reverse Shear Load | -0.344 | -41.77 | -0.344 | -17.56 |
| Shear cracking | -0.172 | -36.10 | -0.172 | -7.07 |
| - | 0 | 0 | 0 | 0 |
| Shear cracking | 0.167 | 38.17 | 0.167 | -4.14 |
| Max Load-WWR wire fractures | 0.476 | 53.81 | 0.476 | -18.75 |
| Connector tensile bar fracture | 0.595 | 18.98 | 0.595 | -2.74 |
| WWR wire fractures | 1.019 | 4.34 | 1.019 | -2.04 |
| End of test | 2.723 | 2.27 | 2.723 | -1.40 |

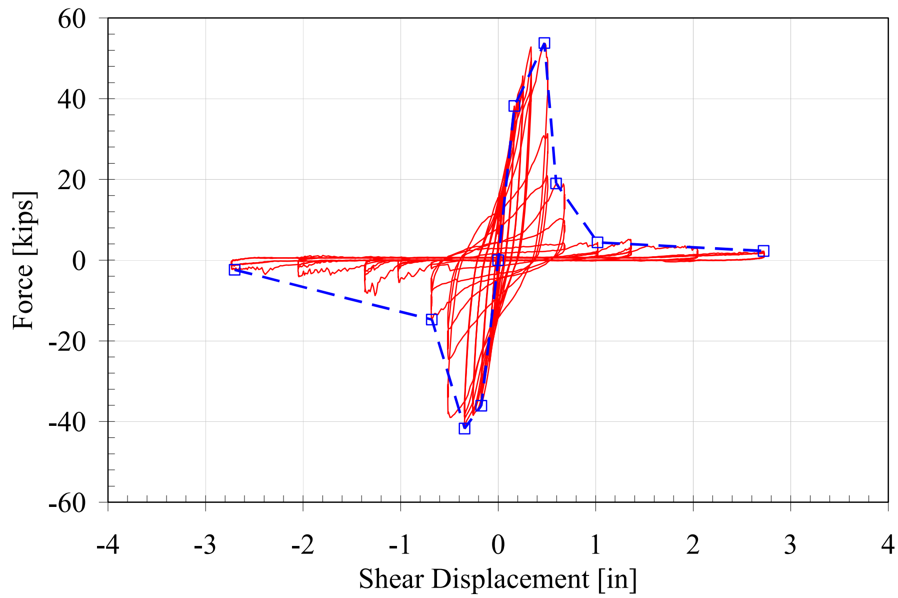


Figure D-5.2:  Shear force and displacement

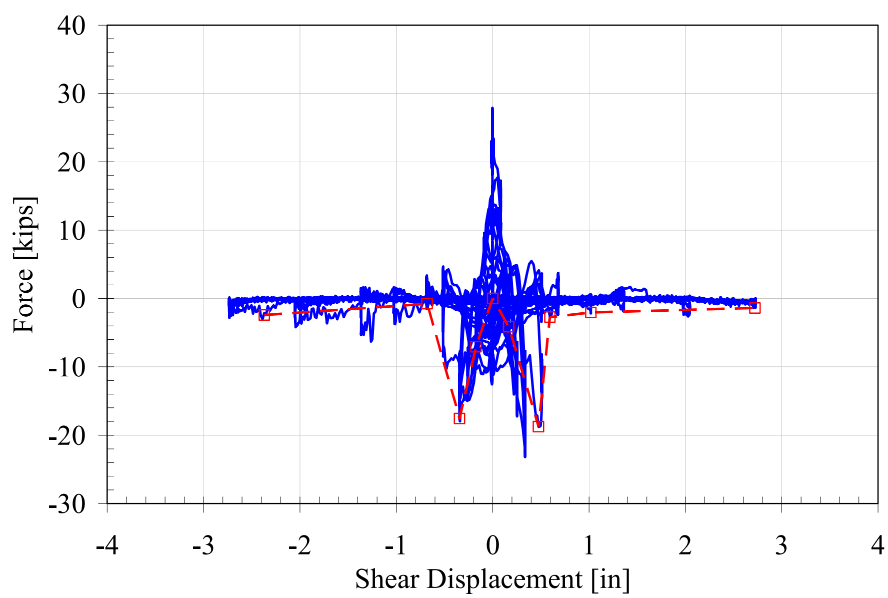


Figure D-5.2:  Axial and Shear displacement

## Subassembly E: Cover Plate Connector

### Subassembly Details E

The specimen tested represents a flat plate connection used for panel to wall connections or panel to panel web connections. It consists of a pair of #4 bars fillet welded to a rectangular flat plate. For panel to wall connections the plate is welded directly to a plate on the wall. For panel to panel connections the connector plates are welded to a square plate slug. Details of the specimen are shown in Figure E.

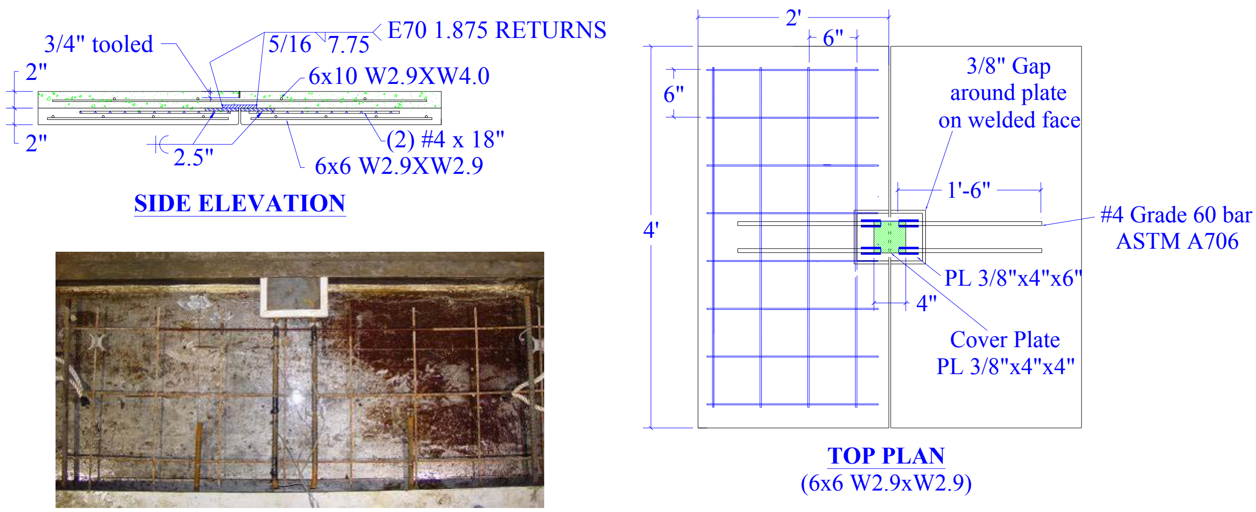


Figure E: Subassembly E

### Material Properties E

The base 2-in. pre-cast panel was fabricated using high early strength self consolidating concrete with a design strength of 7000 psi. A ready mix topping was used to simulate field topped conditions. The design strength of the topping was 4000 psi. The WWR used in the topping and base panel met the requirements of ASTM A185 grade 65 steel. The connector was fabricated from ASTM A706 grade 60 reinforcing bars. All plate material met the requirements of ASTM A36 grade 36 steel. The measured concrete strengths and mill certified steel properties are presented in Table E.

Table E: Material Properties Capacity

| Test | Location in Subassembly (mix) | Compressive Strength, f'c [psi] |
|---|---|---|
| E-1 | Topping (T1) | 4337 ± 147 |
| | Base Panels (P2) | 7633 ± 797 |
| E-2 | Topping (T1) | 4337 ± 147 |
| | Base Panels (P2) | 7633 ± 797 |
| E-3 | Topping (T1) | 4337 ± 147 |
| | Base Panels (P2) | 7633 ± 797 |
| E-4 | Topping (T1) | 4337 ± 147 |
| | Base Panels (P2) | 8416 ± 175 |

| Size | Reinforcement Usage | Grade | Yield Stress [ksi] | Ultimate Strength [ksi] |
|---|---|---|---|---|
| #4 | Connection | A706 | 65.79 | 91.39 |
| PL 3/8-in. x 4-in. x 6-in | Connection | A36 | 49.6 | - |
| PL 3/8-in. x 4-in. x 4-in | Connection | A36 | 48.2 | - |
| #4 | Reinforcing Bars | A706 | 65.79 | 91.39 |
| W2.9XW4 6X10 | Topping Mesh | A185 Gr.65 | 65.00* | 103.3 |
| W2.9XW2.9 6X6 | Pre-cast Panel Mesh | A185 Gr.65 | 65.00* | 108.5 |

* Data unavailable, value assumed

## TEST E-1: MONOTONIC TENSION WITH FV = 0

The performance of a topped cover-plate web connector subjected to monotonic tension is presented in this section. The panel was subjected to tensile displacement with the shear displacement unrestrained, Fv=0. Panel damage consisted of transverse tensile cracking in the topping at approximately the center of both panels. This cracking did not extend into the panels which suggest that delaminating of the topping occurred. This was followed by local cracking around the connector both in the topping and through the panel. The panel failed due to fracture of the WWR followed by tensile fracture of the two embedded #4 connector bar legs. The bar fractures were both tensile in nature and occurred just outside the bar weld region. The observed events and corresponding displacement cycle is presented in Table E-1.1. The photos of the damage are presented in Figure E-1.1. The global force deformation response and backbone curve is presented in Table E-1.2 and Figure E-1.2.

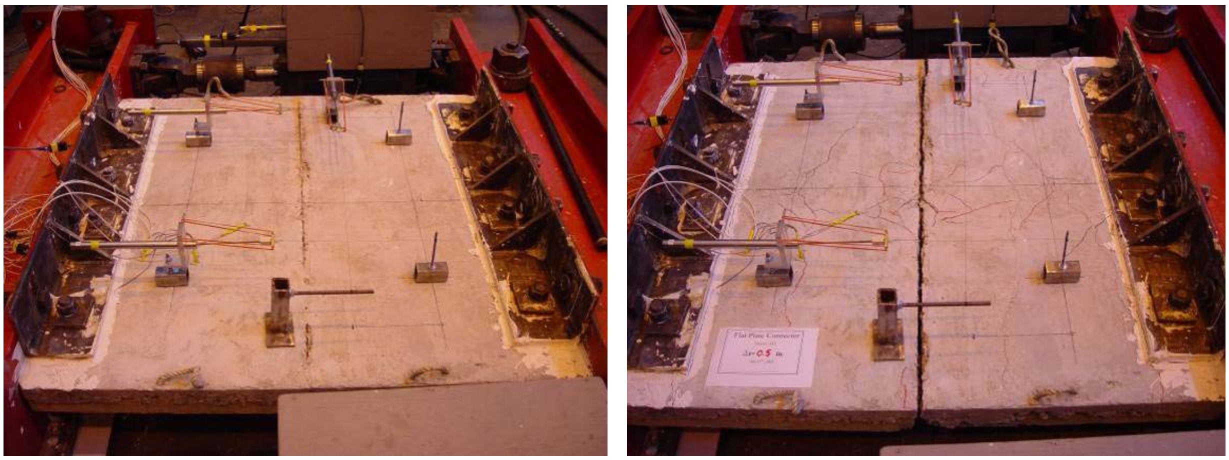

Figure E-1.1: Damage state at 0 and 0.5-in. tensile opening

Table E-1.1: Key Test Observations

| Event # | Tension Step Δ [in.] | Event Description |
|---|---|---|
| 1 | 0.01 | Center crack formation began. |
| 2 | 0.02 | Center crack completed. |
| 3 | 0.04 | Concrete cracking audible. |
| 4 | 0.08 | Tension cracks formed on both panels. |
| 5 | 0.1 | Tension cracks extended. |
| 6 | 0.2 | 3 WWR wires fractured. |
| 7 | 0.3 | 4 WWR wires fractured. |
| 8 | 0.4 | 1 WWR wire fractured. |
| 9 | 0.6 | Fracture of connector bars in free panel. End of test. |

| Table E-1.2: Experimental Results Backbone Curve [kip. in.] | | |
|---|---|---|
| Step | Tensile Displacement | Tensile Force |
| 75% Max Load | 0.020 | 36.56 |
| Max Load | 0.148 | 43.42 |
| Fracture of WWR | 0.182 | 41.86 |
| Fracture of WWR | 0.228 | 28.70 |
| Fracture of WWR | 0.287 | 28.85 |
| Fracture of WWR | 0.303 | 25.52 |
| Fracture of connector bar | 0.552 | 29.65 |
| Fracture of connector bar | 0.566 | 26.57 |
| End of test | 0.573 | 0 |

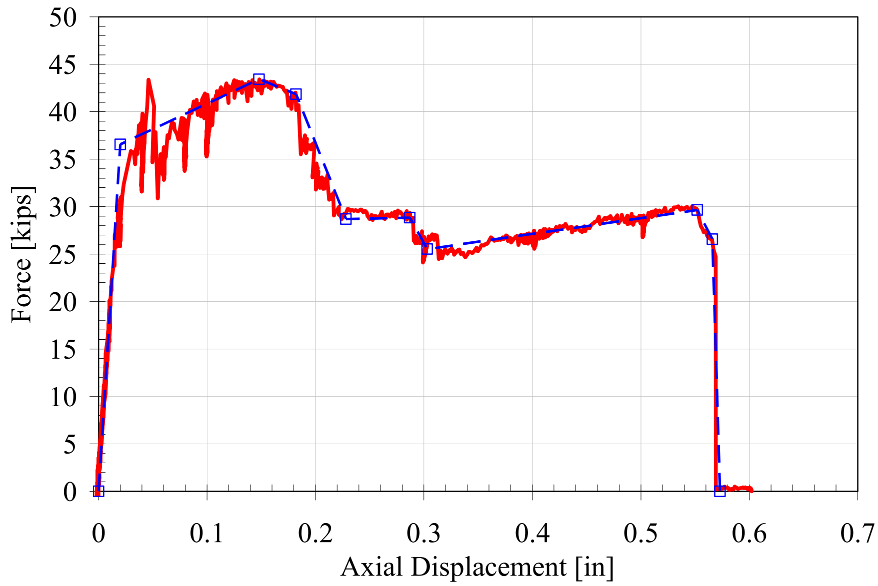


Figure E-1.2: Tensile force and displacement

### TEST E-2: MONOTONIC SHEAR WITH ΔT = 0.1-IN.

The performance of a topped cover-plate web connector subjected to monotonic shear is presented in this section. The panel was pre-cracked at the center by applying a tensile opening of 0.1-in. This was followed by a monotonically increasing shear displacement with the tensile displacement restrained at a 0.1-in. opening. Panel damage consisted of transverse tensile cracking in the topping at the middle of the fixed panel and close to the free panel supports during the 0.1-in. tensile step. This cracking did not extend into the panels, which suggest minor delamination, but no slip between the topping and the panel occurred. This was followed by diagonal cracking from the connector to the support on both panels, and then fracture of the WWR in the topping. The panel failed due to shear fracture of the two #4 connector bars close to the weld region near the plate. The observed events and corresponding displacement cycle is presented in Table E-2.1. The photos of the damage are presented in Figure E-2.1. The global force deformation response and backbone curve is presented in Table E-2.2 and Figure E-2.2.

Figure E-2.1: Damage state at 0 and 3.5-in. shear opening

| Table E-2.1: Key Test Observations | | | |
|---|---|---|---|
| Event # | Shear Δ [in.] | Tension Δ [in.] | Event Description |
| 1 | 0 | 0.01 | Centerline crack formed. |
| 2 | 0 | 0.1 | End of tension cycle. |
| 3 | 0.08 | 0.1 | Concrete cracking audible. Surface cracking over connector seen. |
| 4 | 0.1 | 0.1 | Concrete cracking audible. Cracking progressed. |
| 5 | 0.3 | 0.1 | Concrete cracking audible. Shear cracks developed. |
| 6 | 0.4 | 0.1 | Shear crack formed. Shear at center crack visible. |
| 7 | 0.5 | 0.1 | Spalling on surface. Cracking progressed at connector. |
| 8 | 0.6 | 0.1 | Concrete cracking audible. WWR wire fractured. |
| 9 | 0.9 | 0.1 | Concrete cracking audible. Tensile connector bar fractured in free panel. |
| 10 | 1.2 | 0.1 | Concrete cracking audible. WWR wire fractured. |
| 11 | 1.3 | 0.1 | Slight concrete cracking audible. Spalling at connector. Shear cracking. |
| 12 | 1.6 | 0.1 | Concrete cracking audible. Pop heard. |
| 13 | 1.9 | 0.1 | Pop heard. |
| 14 | 2.2 | 0.1 | One WWR wire fractured across center crack. |
| 15 | 2.3 | 0.1 | Four WWR wires fractured across center crack. |
| 16 | 2.6 | 0.1 | One WWR wire fractured across center crack. |
| 17 | 2.9 | 0.1 | Connector bar fractured in free panel. |

| Table E-2.2: Experimental Results Backbone Curve [kip. in.] | | | | |
|---|---|---|---|---|
| Shear force-deformation | | | Axial force – Shear deformation | |
| Step | Shear Displacement | Shear Force | Shear Displacement | Axial Force |
| 75% Max Load | 0.155 | 33.50 | 0 | 33.50 |
| Max Load – Shear Cracking | 0.338 | 53.89 | 0.167 | 3.16 |
| Fracture of WWR | 0.522 | 29.03 | 0.392 | -31.96 |
| Fracture of tensile connector bar | 0.897 | 15.97 | 0.51 | -6.04 |
| Fracture of WWR | 2.158 | 18.43 | 0.797 | 7.28 |
| Fracture of WWR | 2.33 | 8.93 | 1.615 | 15.06 |
| Fracture of comp. connector bar | 2.841 | 7.80 | 2.545 | 13.60 |
| - | 2.865 | 5.16 | 2.841 | 9.14 |
| End of test | 3.495 | 4.85 | 2.859 | 5.05 |
| | | | 3.494 | 5.39 |

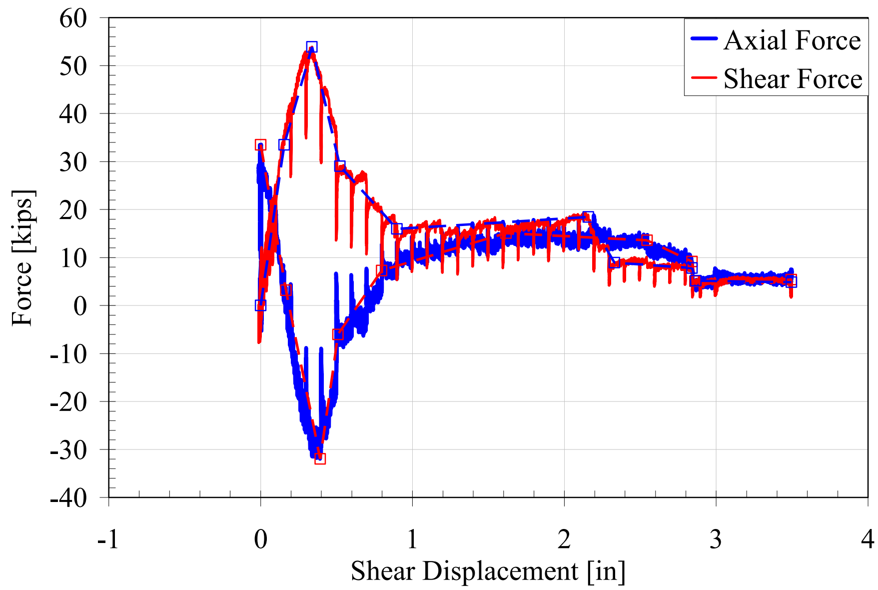


Figure E-2.2: Shear force and displacement

## TEST E-3: MONOTONIC TENSION & SHEAR WITH ΔT/ΔV = 0.5

The performance of a topped cover-plate web connector subjected to monotonic tension & shear is presented in this section. Tension deformation to shear deformation was applied at a constant ratio of ΔT/ΔV = 0.5. Panel damage consisted of diagonal cracking on both panels from the connector to the supports followed by fracture of the WWR in the topping. The connection capacity was lost due to tensile fracture of the two diagonally opposite #4 connector bars at the end of the flare bevel grove weld. After fracture of the bar the cover plate rotation increased resulting in flexure on the remaining connector bar in the free panel and fracture. The observed events and corresponding displacement cycle is presented in Table E-3.1. The photos of the damage are presented in Figure E-3.1. The global force deformation response and backbone curve is presented in Table E-3.2 and Figures E-3.2 and E-3.3.

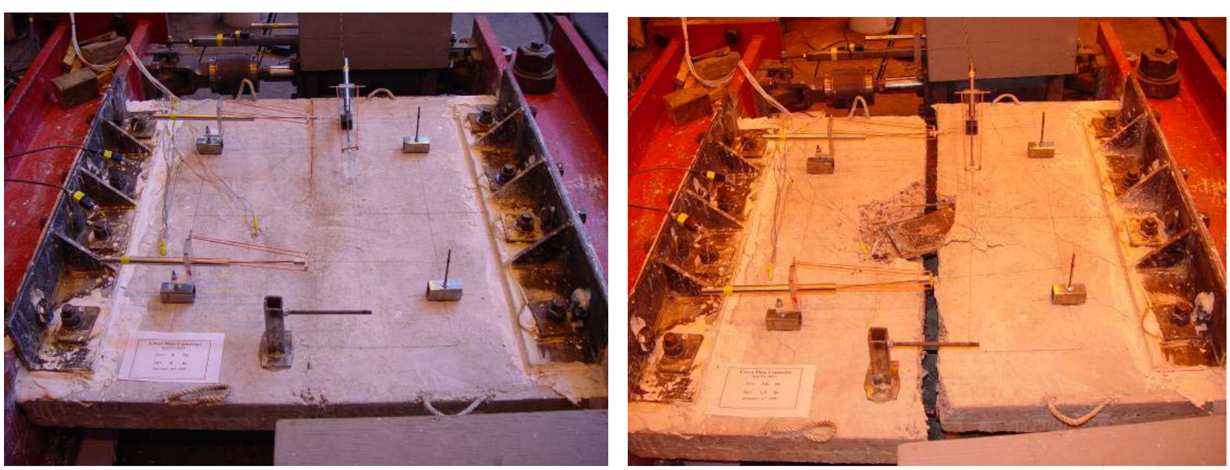

Figure E-3.1: Damage state at 0 and 3.0-in. shear opening

| Table E-3.1: Key Test Observations | | | |
|---|---|---|---|
| Event # | Shear Δ [in.] | Tension Δ [in.] | Event Description |
| 1 | 0.02 | 0.01 | Formation of center crack. |
| 2 | 0.06 | 0.03 | Shear cracking on fixed panel. |
| 3 | 0.08 | 0.04 | Concrete cracking audible. Shear cracking on free panel. |
| 4 | 0.1 | 0.05 | Concrete cracking audible. |
| 5 | 0.2 | 0.1 | Concrete cracking audible. Shear cracking on both panels. |
| 6 | 0.3 | 0.15 | 2 WWR wires fractured. Shear cracking on fixed panel. 1 WWR wire fracture after cycle. |
| 7 | 0.4 | 0.2 | Concrete cracking audible. 2 WWR wires fractured. Shear cracking on free panel. |
| 8 | 0.5 | 0.25 | Concrete cracking audible. 1 WWR wire fracture. Concrete over connector in free panel rose. |
| 9 | 0.6 | 0.3 | Concrete cracking audible. 1 WWR wire fracture. |
| 10 | 0.7 | 0.35 | Concrete cracking audible. |
| 11 | 0.8 | 0.4 | Connector exposed due to surface spalling. WWR around connector already fractured. |
| 12 | 0.9 | 0.45 | Concrete cracking audible. Connector appears to have rotated. |
| 13 | 1 | 0.5 | Connector bar fracture. |
| 14 | 1.2 | 0.6 | Connector bar fracture. |
| 15 | 3 | 1.5 | Connector bar fracture. |

| Table E-3.2: Experimental Results Backbone Curve [kip. in.] | | | | | | |
|---|---|---|---|---|---|---|
| Shear force-deformation | | | | Axial force-deformation | | |
| Step | Axial Δ | Shear Δ | Shear Force | Axial Δ | Shear Δ | Axial Force |
| Formation of center crack | 0.01 | 0.02 | 13.59 | 0.020 | 0.039 | 24.43 |
| Max Load – Shear cracking | 0.090 | 0.179 | 34.12 | 0.059 | 0.118 | 28.17 |
| Fracture of WWR | 0.205 | 0.41 | 8.25 | 0.092 | 0.184 | 9.47 |
| | 0.448 | 0.896 | 6.52 | 0.109 | 0.218 | 24.22 |
| Fracture of connector bar | 0.463 | 0.925 | 2.31 | 0.449 | 0.897 | 23.24 |
| - | 0.577 | 1.153 | 2.68 | 0.465 | 0.930 | 12.55 |
| Fracture of connector bar | 0.593 | 1.185 | -0.01 | 0.573 | 1.146 | 13.36 |
| - | 1.473 | 2.946 | -0.79 | 0.595 | 1.189 | 3.48 |
| - | 1.484 | 2.968 | 0.20 | 1.319 | 2.638 | 11.50 |
| Fracture of connector bar | 1.747 | 3.493 | 0.31 | 1.480 | 2.960 | 8.94 |
| End of test | | | | 1.480 | 2.960 | 0 |

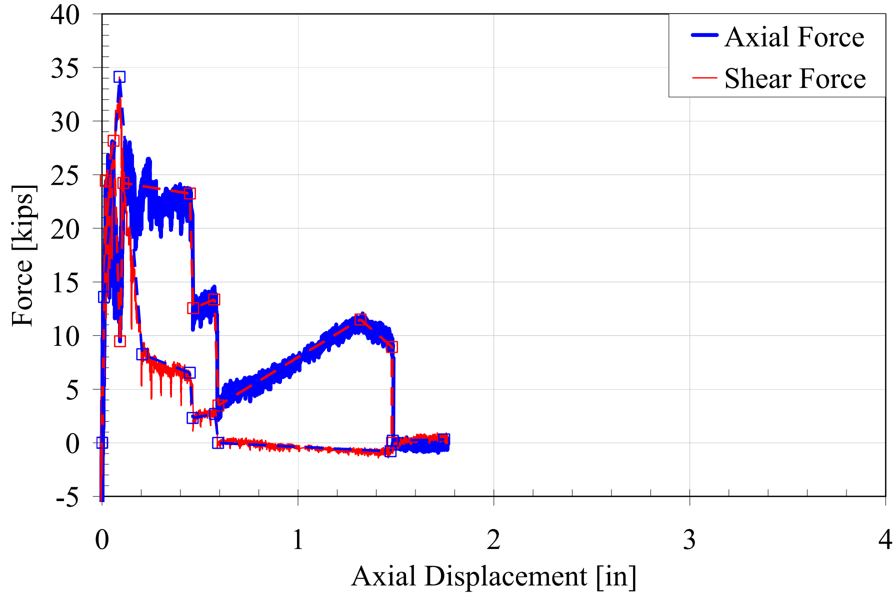

Figure E-3.2: Force and Axial displacement

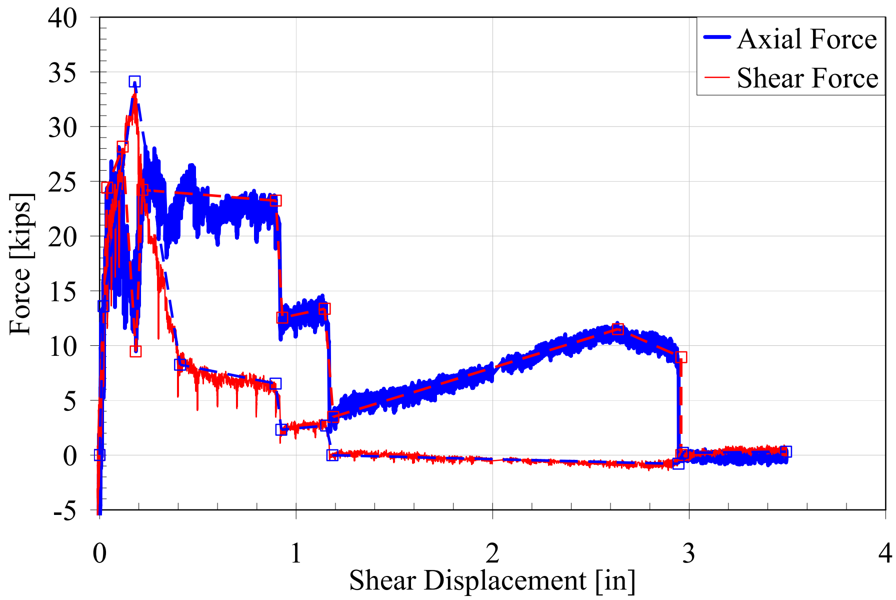

Figure E-3.3: Force and Shear displacement

### TEST E-4: CYCLIC SHEAR WITH ΔT = 0.1-IN.

The performance of a topped cover-plate web connector subjected to cyclic shear is presented in this section. The panel was pre-cracked at the center by applying a tensile opening of 0.1-in. This was followed by a cyclic shear displacement with the tensile displacement restrained at the 0.1-in. opening. Panel damage consisted transverse tensile cracking through the topping during the tension step, at approximately the middle of the free panel and close to the fixed panel supports. This cracking did not extend into the panels, which suggest minor delaminating, but no slip between the topping and the panel occurred during the tensile displacement. This was followed by local cracking around the connector legs and plate. The panel failed due to tension fracture of the two #4 connector bars close to the bar weld region in the fixed panel. To ensure failure of the system, the panel was then subjected to a 3in tensile deformation which ensured fracture of the main reinforcement bars. The observed events and corresponding displacement cycle is presented in Table E-4.1. The photos of the damage are presented in Figure E-4.1. The global force deformation response and backbone curve is presented in Table E-4.2, Figure E-4.2 and Figure E-4.3.

 

Figure E-4.1: Damage state at 0 and 2.704-in. shear opening

| Table E-4.1: Key Test Observations | | | |
|---|---|---|---|
| Event # | Shear Δ [in.] | ΔT [in.] | Event Description |
| 1 | 0 | 0.01 | Centerline cracked. |
| 2 | 0 | 0.04 | Cracking around the connector. |
| 3 | 0 | 0.06 | Tension cracking through both panels. |
| 4 | 0 | 0.1 | Concrete cracking audible. |
| 5 | 0.01 | 0.1 | Cracking over the connector on fixed panel. |
| 6 | 0.0845 | 0.1 | Concrete cracking audible. Longitudinal cracking on the free panel. |
| 7 | -0.0845 | 0.1 | Concrete cracking audible. |
| 8 | 0.169 | 0.1 | Concrete cracking audible. Cracking around the connector plate on free panel. |
| 9 | -0.169 | 0.1 | Concrete cracking audible. Cracking around the connector plate on free panel. |
| 10 | 0.2535 | 0.1 | Concrete cracking audible. Concrete crushing on free panel at the side of the connector plate. |
| 11 | -0.2535 | 0.1 | Concrete cracking audible. Concrete crushing on free panel at the side of the connector plate. |
| 12 | 0.338 | 0.1 | Concrete cracking audible. Crack development. |
| 13 | -0.338 | 0.1 | Concrete cracking audible. Crack development. |
| 14 | 0.338 (2nd cycle) | 0.1 | Concrete cracking audible. Spalling on fixed panel. |
| 15 | 0.507 | 0.1 | Concrete cracking audible. Surface spalling exposing connector. Crushing on fixed panel. |
| 16 | 0 | 0.1 | Concrete cracking audible. Surface spalling exposing connector. |
| 17 | -0.507 | 0.1 | Concrete cracking audible. Surface spalling exposing connector. Pops heard. |
| 18 | 0 | 0.1 | Concrete cracking audible. Surface spalling exposing connector. |
| 19 | 0.507 (2nd cycle) | 0.1 | Concrete cracking audible. Pop heard. |
| 20 | 0.676 | 0.1 | Concrete cracking audible. Concrete spalling. Concrete cracking causing concrete to rise on fixed panel. |
| 21 | -0.676 | 0.1 | Concrete spalling. Connector plate visible on fixed panel. Center 4 WWR wires visible still intact. |
| 22 | 0.676 (2nd cycle) | 0.1 | WWR wires fracture- wire just to the left of the connector (from fixed panel perspective). |
| 23 | 0.676 (3rd cycle) | 0.1 | WWR wires fracture- wire 2nd from the left of the connector (from fixed panel perspective). |
| 24 | -0.676 (3rd cycle) | 0.1 | Popping noise heard. |
| 25 | 1.014 | 0.1 | 2 WWR wires fracture- wires to the right of the connector (from fixed panel perspective). |

| Table E-4.2: Experimental Results Backbone Curve [kip. in.] | | | | |
|---|---|---|---|---|
| Shear force-deformation | | | Axial force – Shear deformation | |
| Step | Shear Displacement | Shear Force | Shear Displacement | Axial Force |
| - | -2.700 | -1.13 | -2.700 | -0.54 |
| WWR wires fracture | -0.859 | -4.19 | -0.859 | -1.18 |
| - | -0.614 | -7.714 | -0.614 | 0.429 |
| Max Reverse Shear Load | -0.160 | -22.36 | -0.160 | 9.41 |
| Cracks around connector | -0.083 | -18.98 | -0.083 | 22.09 |
| - | 0 | 0 | 0 | 0 |
| Cracking around connector | 0.088 | 19.79 | 0.088 | 25.61 |
| Max Load-Cracking at connector | 0.162 | 26.47 | 0.162 | 8.19 |
| Connector bar fracture | 0.651 | 9.01 | 0.651 | 8.22 |
| WWR wires fracture | 0.994 | 3.08 | 0.994 | -1.50 |
| End of test | 2.637 | 1.71 | 2.637 | -0.91 |

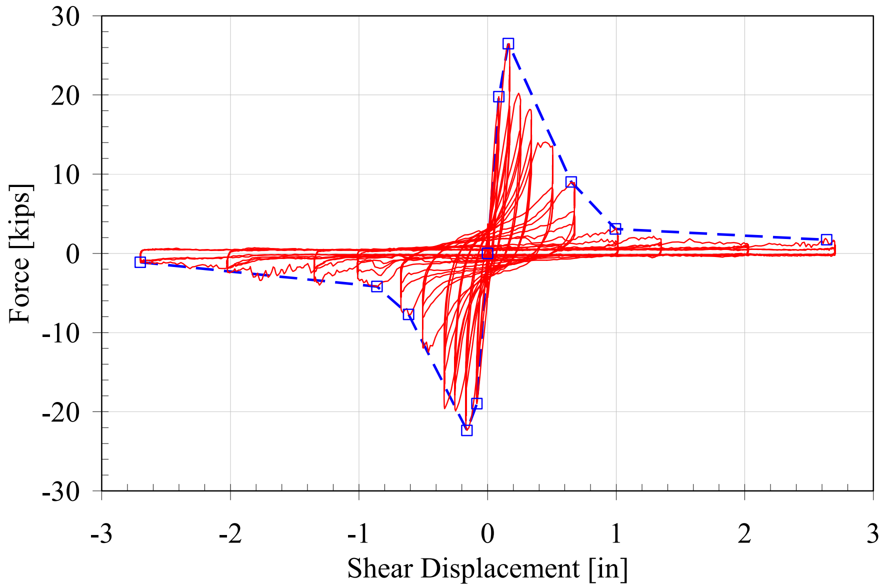


Figure E-4.2: Shear force and displacement

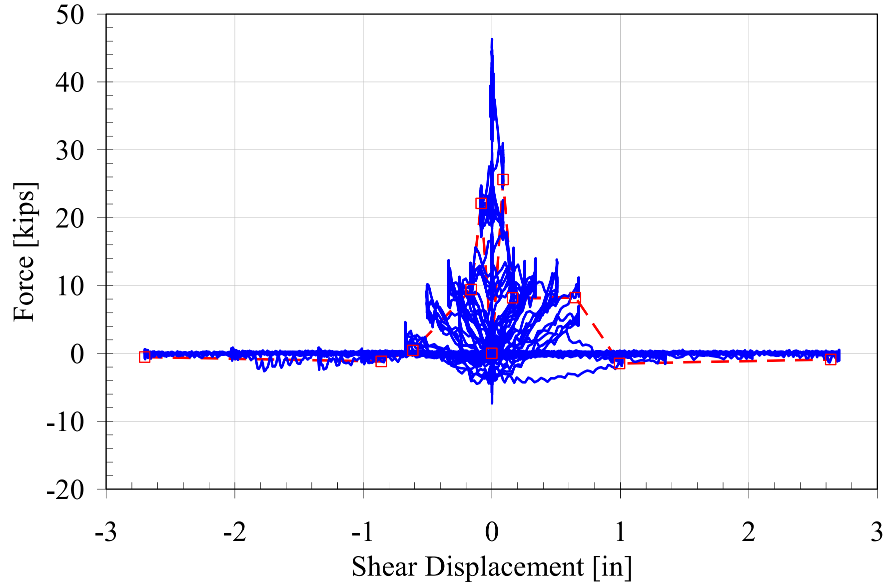


Figure E-4.3: Axial force and Shear displacement

## Subassembly F: Pour Strip Connector

### Subassembly Details F

The specimen tested represents a pour strip connection used as a chord in a topped floor diaphragm. In a conventional diaphragm pour strip reinforcement runs continuously over multiple panels. To ensure that the reinforcement in the test specimen matches the in-site behavior the bars are anchored at the ends to prevent premature slip of the bars from the panel. Details of the specimen are shown in Figure F.

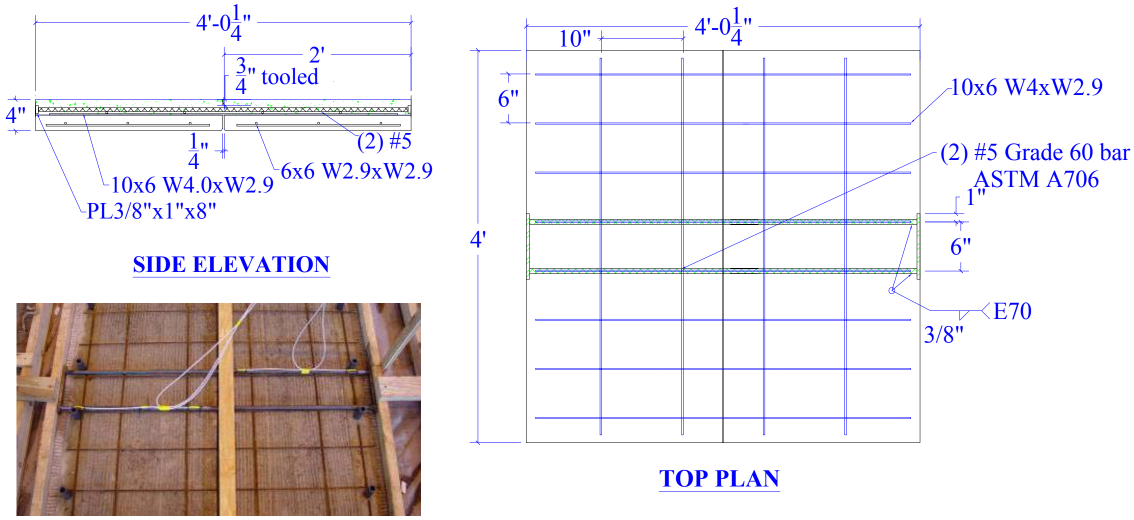


Figure F: Subassembly F

### Material Properties F

The base 2-in. pre-cast panel was fabricated using high early strength self consolidating concrete with a design strength of 7000 psi. A ready mix topping was used to simulate field topped conditions. The design strength of the topping was 4000 psi. The WWR used in the topping and base panel met the requirements of ASTM A185 grade 65 steel. The connector was fabricated from ASTM A706 grade 60 reinforcing bars. All plate material conformed to ASTM A36. The measured concrete strengths and mill certified steel properties are presented in Table F.

Table F: Material Properties Capacity

| Test | Location in Subassembly (mix) | Compressive Strength, f'c [psi] |
|---|---|---|
| F-1 | Topping (T1) | 4337 ± 147 |
| | Base Panels (P2) | 7274 ± 84 |
| F-2 | Topping (T1) | 4337 ± 147 |
| | Base Panels (P2) | 7274 ± 84 |
| F-3 | Topping (T2) | 4032 ± 147 |
| | Fixed Panel (P3) | 7406 ± 156 |
| | Free Panel (P3) | 7274 ± 84 |
| F-4 | Topping (T2) | 4032 ± 147 |
| | Base Panels (P3) | 7406 ± 156 |
| F-5 | Topping (T2) | 4032 ± 147 |
| | Base Panel (P3) | 7406 ± 156 |

| Size | Reinforcement Usage | Grade | Yield Stress [ksi] | Ultimate Strength [ksi] |
|---|---|---|---|---|
| #5 | Connection | A706 | 67.61 | 95.56 |
| #4 | Reinforcing Bars | A706 | 65.79 | 91.39 |
| W2.9XW4 6X10 | Topping Mesh | A185 Gr.65 | 65.00* | 103.3 |
| W2.9XW2.9 6X6 | Pre-cast Panel Mesh | A185 Gr.65 | 65.00* | 108.5 |

* Data unavailable, value assumed

## TEST F-1: MONOTONIC TENSION WITH FV = 0

The performance of a pour-strip chord connector subjected to monotonic tension is presented in this section. The panel was subjected to tensile displacement with the shear displacement unrestrained, Fv=0. Panel damage consisted transverse tensile cracking through the topping during the tension step, at approximately the middle of the fixed panel and close to the free panel supports. This cracking did not extend into the panels, which indicate delaminating of the topping during the tensile displacement. This was followed by cracking around the connector at the panel interface and fracture of the WWR in the topping. The panel failed due to fracture of the WWR followed by the fracture of the main connector reinforcement. The left connector bar fractured near the joint on its free length. The right bar fracture was not visible and most likely occurred within the topping. The observed events and corresponding displacement cycle is presented in Table F-1.1. The photos of the damage are presented in Figure F-1.1. The global force deformation response and backbone curve is presented in Table F-1.2 and Figure F-1.2.

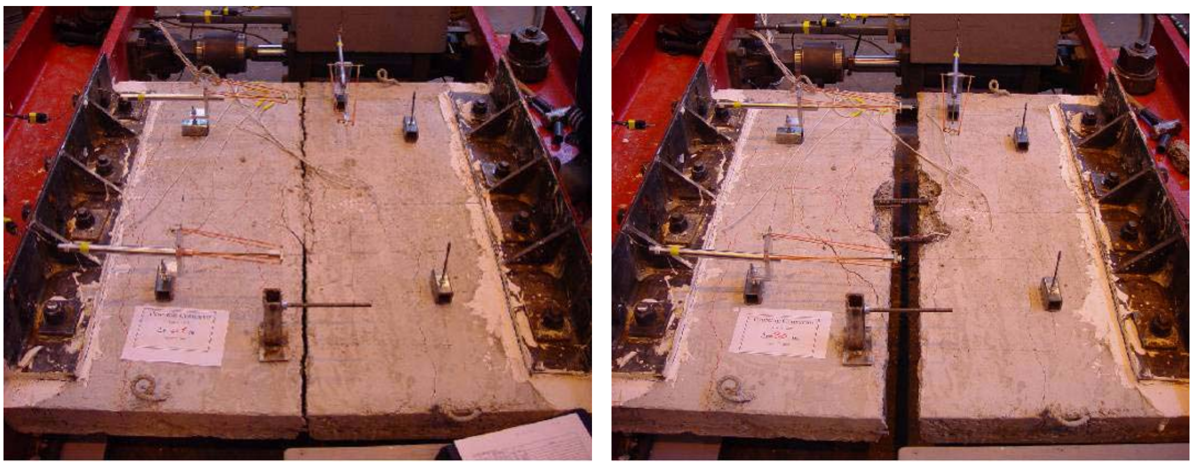

Figure F-1.1: Damage state at 0.5 and 3.0-in. tensile opening

Table F-1.1: Key Test Observations

| Event # | ΔT [in.] | Event Description |
|---|---|---|
| 1 | 0.02 | Centerline crack formed. |
| 2 | 0.04 | Concrete cracking audible. |
| 3 | 0.06 | Cracking visible on the surface, two pops due to wire mesh snapping heard. |
| 4 | 0.08 | 2 wires fractured |
| 5 | 0.1 | 1 fracture heard. Free beam lifts off of the floor at pop. |
| 6 | 0.2 | 4 fractures noises heard, with the 2nd one being considerably louder, and free beam lifted on pops again. |
| 7 | 0.4 | Popping sound heard, beam continues to move, more pronounced. Hydraulic shutdown due to lab system problem. |
| 8 | 0.8 | Crack formation and development at connector interface. |
| 9 | 0.9 | Concrete cracking audible, and minor spalling audible. |
| 10 | 1.2 | Concrete cracking audible. |
| 11 | 1.3 | Small popping noises & spalling heard. |
| 12 | 2.3 | Left connector bar fracture. |
| 13 | 3.5 | End of Test |

| Table F-1.2: Experimental Results Backbone Curve [kip. in.] | | |
|---|---|---|
| Step | Tensile Displacement | Tensile Force |
| 75% Max Load | 0.031 | 46.73 |
| Max Load | 0.137 | 62.31 |
| Fracture of WWR | 0.186 | 48.86 |
| Tensile cracking at connector | 0.772 | 54.23 |
| Tensile cracking & Bar fracture | 1.277 | 43.10 |
| - | 1.339 | 31.73 |
| Bar Fracture | 2.229 | 31.81 |
| - | 2.229 | 3.73 |
| End of test | 3.523 | 2.21 |

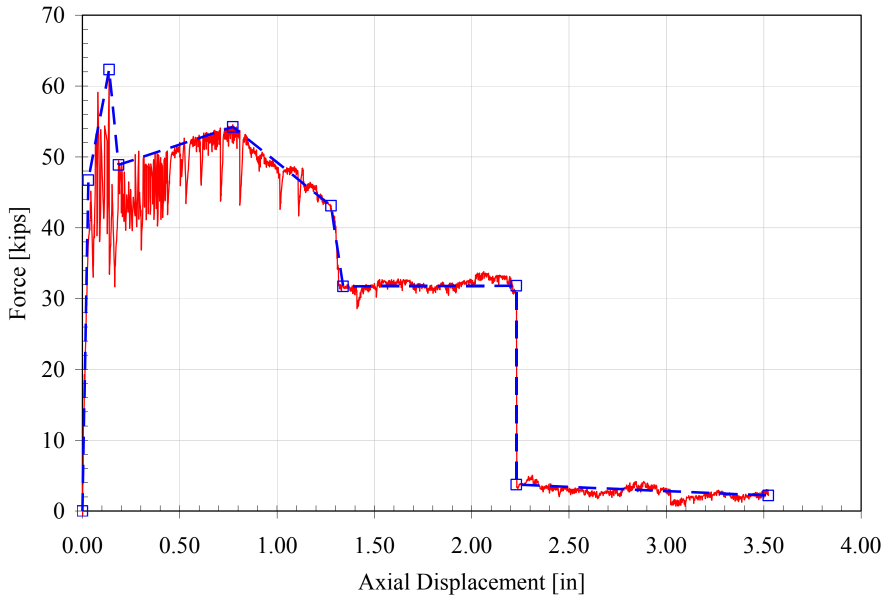


Figure F-1.2: Tensile force and displacement

## TEST F-2: MONOTONIC SHEAR WITH ΔT = 0.1-IN.

The performance of a pour-strip chord connector subjected to monotonic shear is presented in this section. The panel was pre-cracked by applying a tensile opening of 0.1-in. The tension opening was held constant and a monotonically increasing shear displacement was applied. Panel damage consisted of transverse tensile cracking through the topping during the tension step, at approximately the middle of both panels. This cracking did not extend into the base panels, which suggest minimal delamination. No slip between the topping and the panel occurred during the tensile displacement. This was followed by cracking and concrete spalling at the panel interface where the connector legs bared on the concrete, and fracture of the WWR in the topping. The test was stopped at a shear deformation of 3.5-in. due to the limitations of the control system. At this level, the connector shear integrity was maintained at 35.7 kips. To fail the system, the panel was then subjected to a 3in tensile deformation which caused tensile fracture of the main reinforcement bars. The observed events and corresponding displacement cycle is presented in Table F-2.1. The photos of the damage are presented in Figure F-2.1. The global force deformation response and backbone curve is presented in Table F-2.2 and Figure F-2.2.

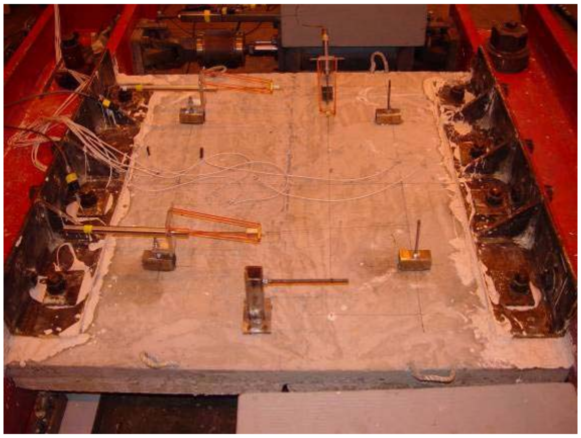
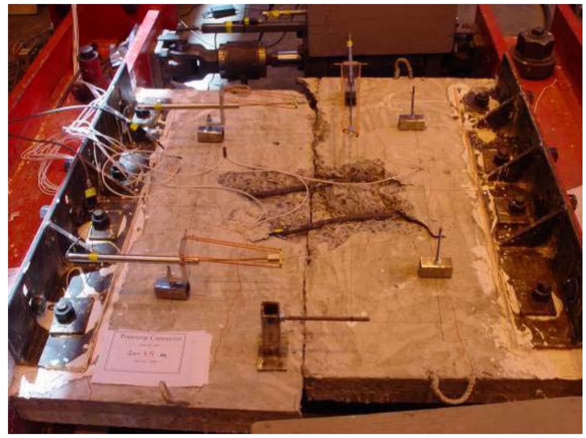


Figure F-2.1: Damage state at 0.5 and 3.5-in. shear opening

| Table F-2.1: Key Test Observations | | | |
|---|---|---|---|
| Event # | ΔV [in.] | ΔT [in.] | Event Description |
| 1 | 0 | 0.01 | Centerline crack formed. |
| 2 | 0 | 0.06 | Tension cracks formed on fixed panel. |
| 3 | 0 | 0.1 | Longitudinal cracks formed over connector bars on both panels. |
| 4 | 0.02 | 0.1 | Small cracking developed around connector. |
| 5 | 0.2 | 0.1 | Concrete cracking audible. Shear crack formation on free panel. |
| 6 | 0.4 | 0.1 | Concrete cracking audible. Two WWR wires fractured. |
| 7 | 0.5 | 0.1 | Two WWR wires fractured. |
| 8 | 1.2 | 0.1 | Concrete cracking audible. One WWR wire fractured. |
| 9 | 1.5 | 0.1 | WWR wire fractured close to connector. |
| 10 | 2.8 | 0.1 | Concrete cracking audible. Left bar exposed ~ 14-in, right bar exposed ~ 12-in. (fixed panel orientation). |
| 11 | 3 | 0.1 | Slip of left bar connector reinforcement over topping. Both bars exposed ~ 14-in. |
| 12 | 3.5 | 0.1 | Both bars exposed ~ 16-in. |
| 13 | 0 | 2.6 | Both connector bars snapped at gage locations 2 & 3 at Ft = 57.21 kip. |
| 14 | 0 | 3 | End of test |

| Table F-2.2: Experimental Results Backbone Curve [kip. in.] | | | | |
|---|---|---|---|---|
| Shear force-deformation | | | Axial force – Shear deformation | |
| Step | Shear Displacement | Shear Force | Shear Displacement | Axial Force |
| 75% Max Load | 0.149 | 27.7 | 0 | 0 |
| Shear crack in free panel | 0.264 | 33.37 | 0.003 | 61.46 |
| Max Load-Fracture of WWR | 0.365 | 34.60 | 0.045 | 49.35 |
| Fracture of WWR | 0.503 | 26.20 | 0.165 | 28.38 |
| - | 0.505 | 21.89 | 0.257 | 21.00 |
| - | 0.803 | 21.52 | 0.403 | 16.59 |
| Fracture of WWR | 1.002 | 18.56 | 0.700 | 18.76 |
| - | 1.002 | 14.75 | 1.002 | 27.91 |
| Fracture of WWR | 1.430 | 11.50 | 1.002 | 34.50 |
| - | 2.587 | 13.70 | 3.499 | 35.73 |
| End of test | 3.5 | 8.87 | | |

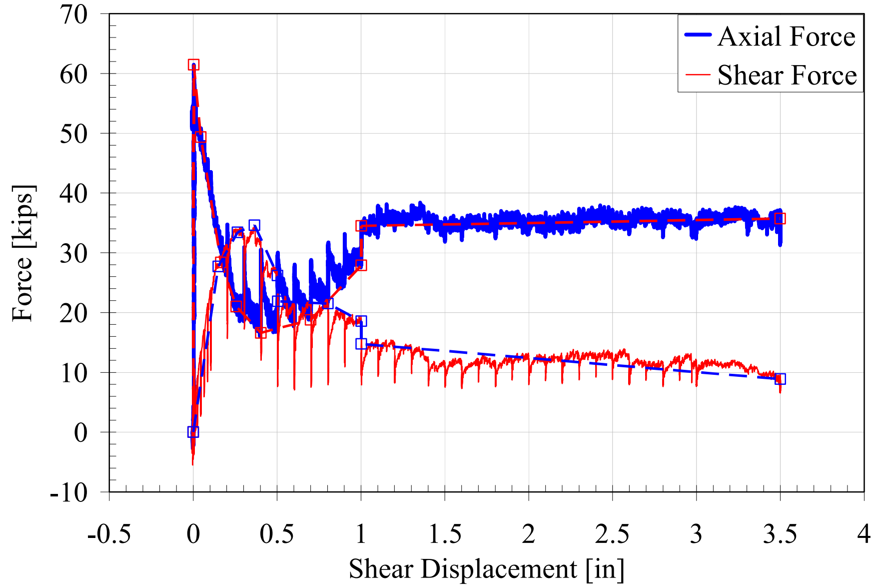


Figure F-2.2: Force and shear displacement

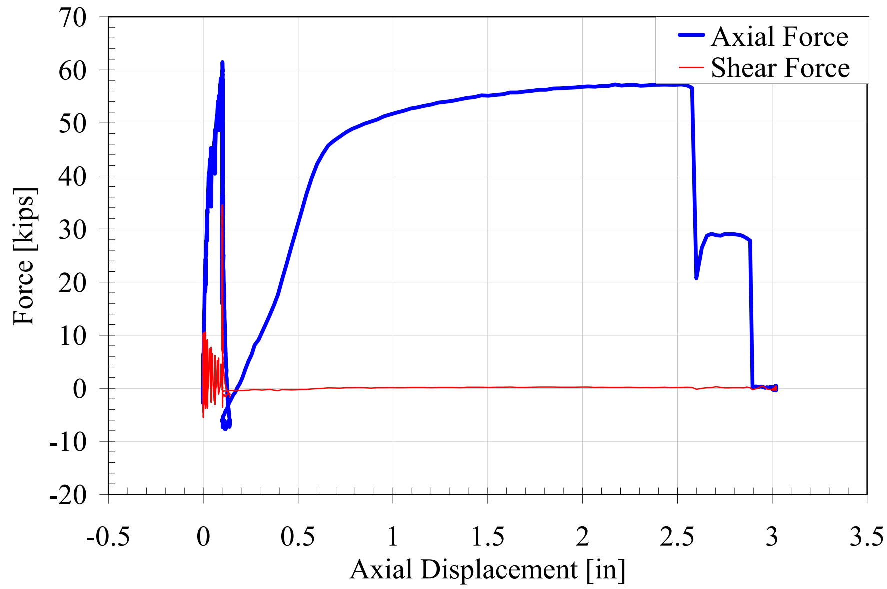


Figure F-2.3: Force and axial displacement

## TEST F-3: MONOTONIC TENSION & SHEAR WITH ΔT/ΔV = 2.0

The performance of a pour-strip chord connector subjected to monotonic tension & shear is presented in this section. Tension deformation to shear deformation was applied at a constant ratio of ΔT/ΔV = 2.0. Panel damage initiated with tensile cracking at approximately the middle of both panels. This cracking did not extend into the panels, which suggest minimal delaminating. No slip between the topping and the panel occurred during early tensile-shear displacement. This was followed by tensile cracking near the connector and by cracking and concrete spalling at the panel interface where the connector legs were bared on the concrete in compression. Finally there was fracture of the WWR in the topping and reinforcement de-bonding and spalling over the connector legs. The connector failed due to fracture of the two #5 connector bars at the center crack interface. The observed events and corresponding displacement cycle is presented in Table F-3.1. The photos of the damage are presented in Figure F-3.1. The global force deformation response and backbone curve is presented in Table F-3.2, Figure F-3.2 and Figure F-3.3.

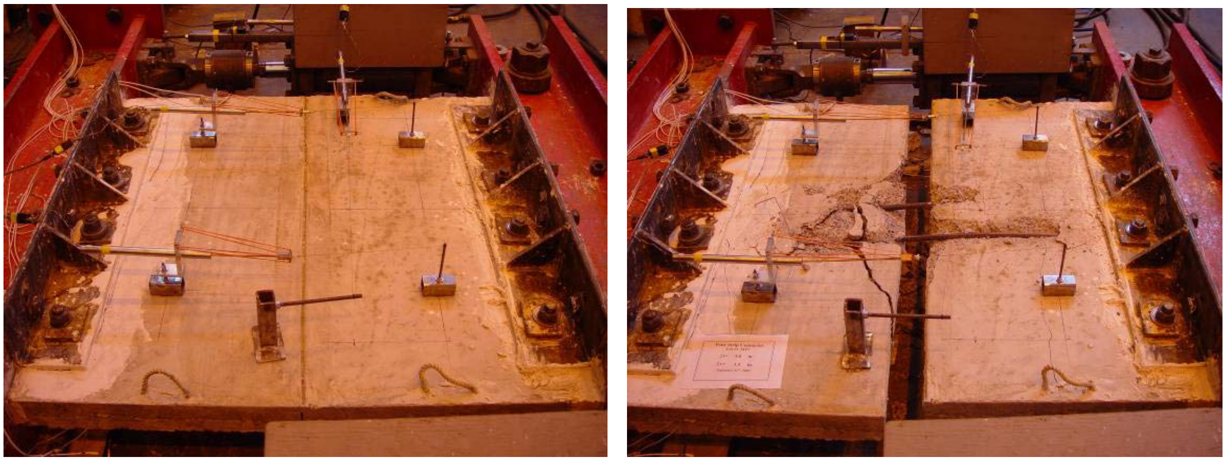

Figure F-3.1:  Damage state at 0 and 3.0-in. tensile opening

| Table F-3.1:  Key Test Observations | | | |
|---|---|---|---|
| Event # | ΔV [in.] | ΔT [in.] | Event Description |
| 1 | 0.03 | 0.06 | Tension, shear & connector legs cracking seen. Tension cracks only in topping. |
| 2 | 0.04 | 0.08 | Concrete cracking audible. More tension cracks developed. |
| 3 | 0.05 | 0.1 | Concrete cracking audible. |
| 4 | 0.1 | 0.2 | Concrete cracking audible. Multiple fracture of WWR wires. |
| 5 | 0.15 | 0.3 | Concrete cracking audible. 2 WWR wires fractured. |
| 6 | 0.2 | 0.4 | Concrete cracking audible. Surface spalling exposing left connector bar. |
| 7 | 0.25 | 0.5 | Concrete cracking audible. Surface spalling exposing right connector bar. |
| 8 | 0.35 | 0.7 | Concrete cracking audible. Surface spalling on fixed panel between connector leg bars. |
| 9 | 0.4 | 0.8 | Concrete cracking audible. Surface spalling on free panel between connector leg bars. |
| 10 | 0.45 | 0.9 | Concrete cracking audible. Surface spalling. |
| 11 | 0.6 | 1.2 | Concrete cracking audible. Exposed leg lengths: left bar: 7.5-in. ; right bar: 5.5-in |
| 12 | 0.65 | 1.3 | Concrete cracking audible. Exposed leg length: left bar: 15-in |
| 13 | 0.95 | 1.9 | Concrete cracking audible. Surface spalling exposing bars on free panel. |
| 14 | 1 | 2 | Concrete cracking audible. Surface spalling. |
| 15 | 1.05 | 2.1 | Right connector bar fracture. |
| 16 | 1.35 | 2.7 | Left connector bar fracture. |

| Table F-3.2: Experimental Results Backbone Curve [kip. in.] | | | | | | |
|---|---|---|---|---|---|---|
| Axial force-deformation | | | | Shear force - Shear deformation | | |
| Step | Axial Δ | Shear Δ | Axial Force | Axial Δ | Shear Δ | Shear Force |
| Tension cracking | 0.040 | 0.020 | 34.88 | 0.019 | 0.010 | 3.22 |
| Max Load-Fracture of WWR | 0.121 | 0.061 | 61.08 | 0.082 | 0.041 | 9.40 |
| - | 0.177 | 0.089 | 46.94 | 0.156 | 0.078 | 5.53 |
| - | 0.293 | 0.147 | 44.95 | 0.182 | 0.091 | 3.21 |
| Steel de-bond from concrete | 0.534 | 0.267 | 50.96 | 0.532 | 0.266 | 2.90 |
| Steel de-bond from concrete | 2.053 | 1.027 | 57.01 | 2.170 | 1.075 | 4.80 |
| Fracture of Connector bar | 2.166 | 1.083 | 54.77 | 2.180 | 1.090 | 1.38 |
| - | 2.171 | 1.086 | 17.03 | 2.246 | 1.123 | 2.25 |
| - | 2.251 | 1.110 | 28.57 | 2.619 | 1.310 | 2.43 |
| Fracture of Connector bar | 2.705 | 1.290 | 28.00 | 2.705 | | 1.37 |
| End of test | 2.717 | | 0 | 2.717 | | 0 |

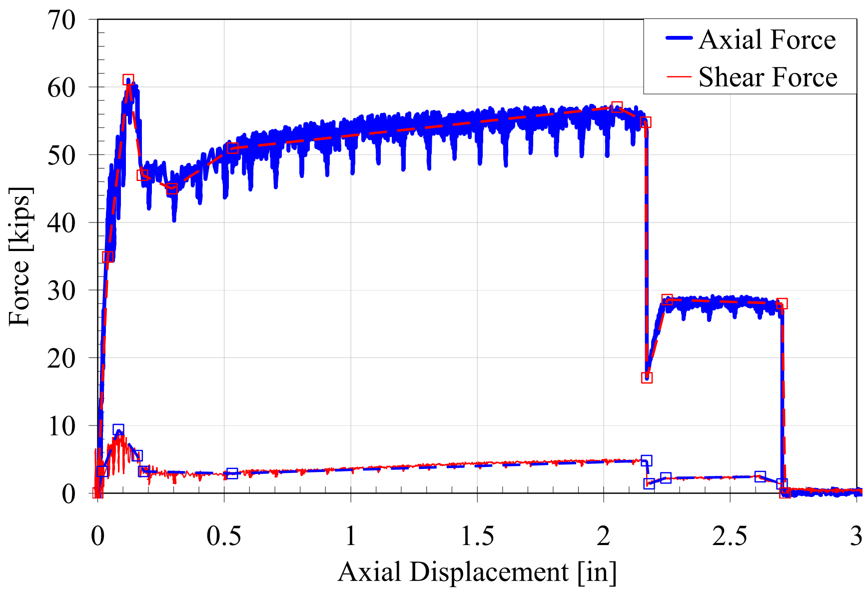


Figure F-3.2: Force and Axial displacement

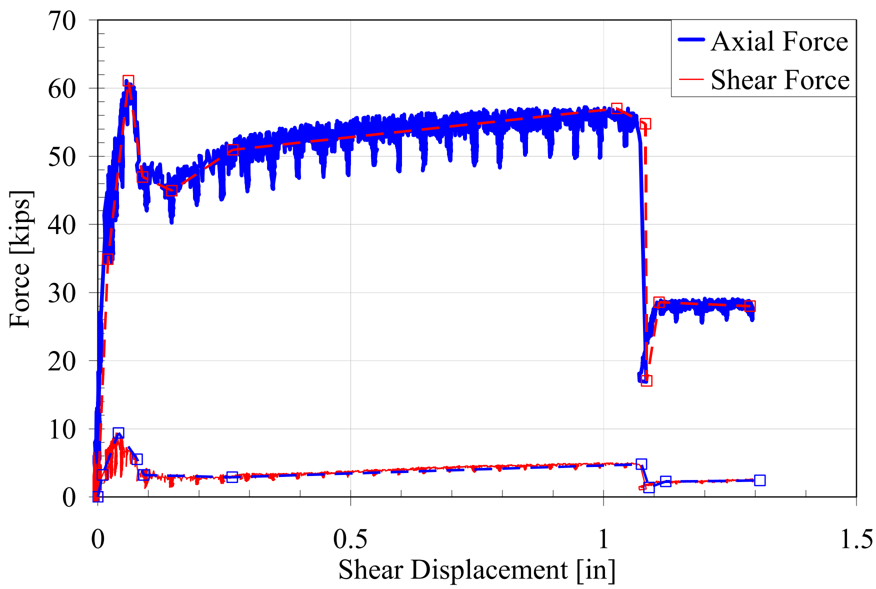


Figure F-3.3: Force and Shear displacement

## TEST F-4: CYCLIC SHEAR WITH ΔT = 0.1-IN.

The performance of a pour-strip chord connector subjected to cyclic shear is presented in this section. The panel was pre-cracked by applying a tensile opening of 0.1-in. A cyclic shear displacement was the applied with the tensile displacement restrained at the 0.1-in. opening. Panel damage initiated with tensile cracking at approximately the middle of both panels, which suggest minimal delaminating, however no slip between the topping and the panel occurred during the tension displacement step. This was followed by cracking near the connector, and fracture of the WWR in the topping, and reinforcement de-bonding and spalling over the connector legs over 0.186-in. – 2.604-in. shear deformation. A max shear deformation of 2.604-in. was applied due to the limitation of the control system. At this level, the connector shear integrity was maintained. To fail the system, the panel was then subjected to a 3-in. tensile deformation, which caused fracture of one of the main reinforcement bars. The observed events and corresponding displacement cycle is presented in Table F-4.1. The photos of the damage are presented in Figure F-4.1. The global force deformation response and backbone curve is presented in Table F-4.2, Figure F-4.2 and Figure F-4.3.

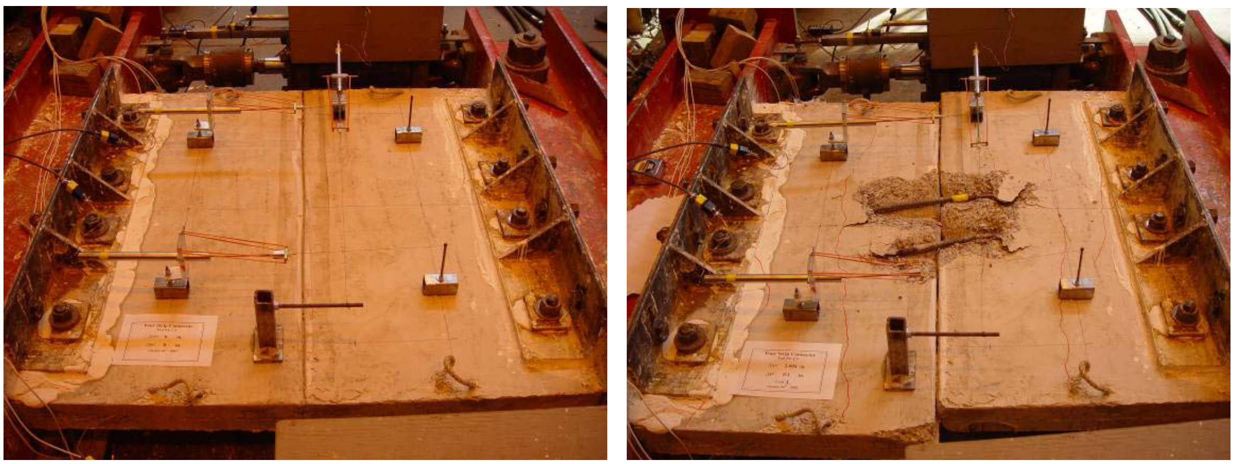

Figure F-4.1: Damage state at 0 and 2.604-in. shear opening

Table F-4.1: Key Test Observations

| Event # | ΔV [in.] | ΔT [in.] | Event Description |
|---|---|---|---|
| 1 | 0 | 0.01 | Centerline cracked. |
| 2 | 0 | 0.04 | Tension cracks formed on free panel (due to topping delaminating). |
| 3 | 0 | 0.06 | Tension cracks formed on fixed panel (due to topping delaminating). |
| 4 | 0 | 0.08 | Tension cracks on both panels. Longitudinal cracks over connector legs. |
| 5 | 0 | 0.1 | Concrete cracking audible. More tension cracks formed on both panels. |
| 6 | 0.0465 | 0.1 | Longitudinal cracks extended. |
| 7 | 0.093 | 0.1 | Longitudinal cracks extended on fixed panel. |
| 8 | 0.1395 | 0.1 | Cracking formed close to the connector on both panels. |
| 9 | -0.1395 | 0.1 | Cracking close to connector developed further. |
| 10 | 0.186 | 0.1 | Cracking extended in free panel. |
| 11 | -0.186 | 0.1 | Cracking extended in fixed panel. Minor surface spalling. |
| 12 | 0.186 (3$^{rd}$ cycle) | 0.1 | Surface spalling exposes right connector bar (from fixed beam perspective) |
| 13 | 0.279 | 0.1 | More surface spalling. |
| 14 | 0 | 0.1 | Small pops heard. |
| 15 | -0.279 | 0.1 | Small pops heard. |
| 16 | 0.372 | 0.1 | Surface spalling exposes connector bar. |

| | | | |
|---|---|---|---|
| 17 | 0.372 (3rd cycle) | 0.1 | Multiple popping noises heard (WWR wire fractures). Surface spalling on fixed panel. |
| 18 | 0.558 | 0.1 | Surface spalling on fixed panel. |
| 19 | -0.558 | 0.1 | Multiple popping noises heard (WWR wire fractures). |
| 20 | 0.558 (2nd cycle) | 0.1 | Popping noises heard. |
| 21 | 0.744 | 0.1 | Surface spalling. Connector bars exposed: left ~ 5-in; right ~ 7.5-in |
| 22 | 1.116 | 0.1 | Surface spalling. Left bar exposed ~ 7-in |
| 23 | 1.488 | 0.1 | Surface spalling. Right bar exposed ~ 12-in |
| 24 | -1.488 | 0.1 | Surface spalling. Left bar exposed ~ 9-in |
| 25 | 2.232 | 0.1 | Surface spalling. Connector bars exposed: left ~ 13-in; right ~ 18-in |
| 26 | -2.604 | 0.1 | Surface spalling. Connector bars exposed: left ~ 20-in; right ~ 16-in |

Table F-4.2: Experimental Results Backbone Curve [kip. in.]

| Shear force-deformation | | | Axial force – Shear deformation | |
|---|---|---|---|---|
| Step | Shear Displacement | Shear Force | Shear Displacement | Axial Force |
| - | -2.597 | -5.03 | -2.597 | 18.85 |
| Steel de-bond from concrete | -1.461 | -8.21 | -1.461 | 17.09 |
| WWR wires fracture | -0.742 | -7.11 | -0.743 | 7.45 |
| Max Reverse Shear Load | -0.138 | -16.06 | -0.138 | 20.83 |
| - | -0.046 | -9.52 | -0.046 | 42.09 |
| - | 0 | 0 | 0 | 0 |
| ~0.75% Max Load | 0.040 | 12.26 | 0.040 | 48.49 |
| Max Load | 0.091 | 17.06 | 0.091 | 35.49 |
| WWR wires fracture | 0.736 | 9.06 | 0.736 | 9.49 |
| Steel de-bond from concrete | 1.032 | 9.70 | 1.032 | 15.05 |
| End of test | 2.583 | 6.24 | 2.583 | 23.74 |

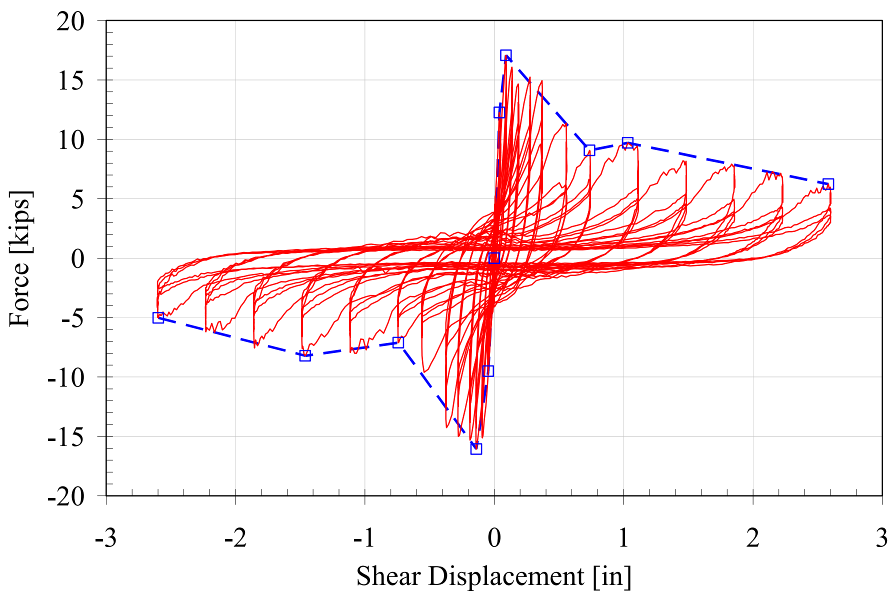


Figure F-4.2: Shear force and displacement

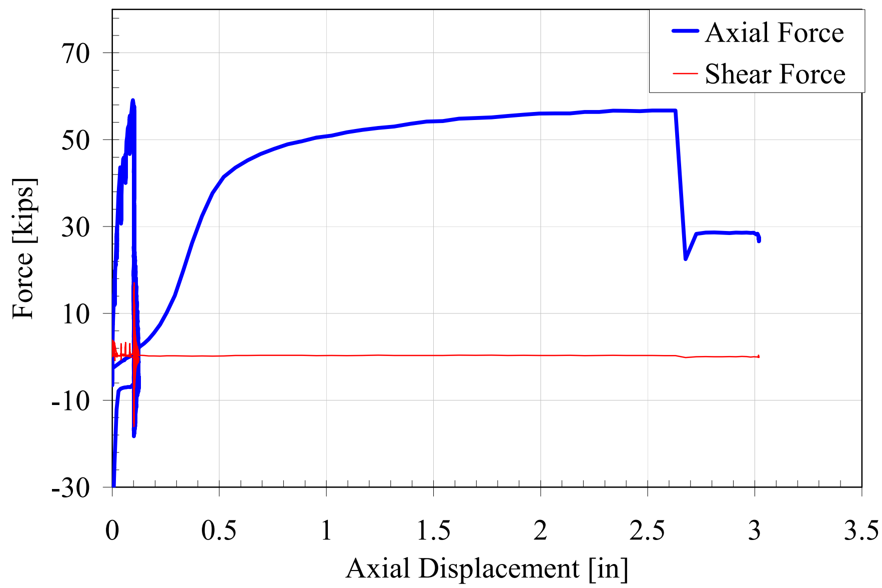

Figure F-4.5: Force and Axial displacement

## TEST F-5: CYCLIC TENSION & COMPRESSION WITH FV = 0

The performance of a pour-strip chord connector subjected to cyclic tension and compression is presented in this section. The panel was subjected to axial displacement with the shear displacement unrestrained, Fv=0. Panel damage initiated with tensile cracking at approximately the middle of both panels. This cracking did not extend into the panels, which suggest minimal delaminating; however no slip between the topping and the panel occurred during early tensile displacement steps. This was followed by cracking near the connector, and fracture of the WWR in the topping. Out of plane upward motion of the free beam then occurred as a result of moments generate due to the connector bars being in the topping and not at the center of the panel. Approximately 900lbs of steel was added to the free beam to prevent this motion at 0.124in. Panel cracking was observed at the right end of the free panel adjacent to the panel to beam connection at a displacement of 0.248in. This damage progressed and at a tensile displacement of 0.826-in the test was terminated due to loss of the boundary support. From the 0.62-in. to the 0.826-in. tensile deformation cycle actuator 3 was unable to achieve its compressive displacement command due to the actuator force capacity being exceeded. Consequently, the compression cycles do not return to the same deformation. The elevated force in actuator 3 can be attributed to the confinement of the left connector bar, which was released when it lost concrete cover at the 2$^{nd}$ 0.826-in. displacement cycle. The other bar was release from its confinement at the 0.62-in. deformation cycle, and hence did not contribute to this inability to achieve compressive displacement demand. The observed events and corresponding displacement cycle is presented in Table F-5.1. The photos of the damage are presented in Figure F-5.1. The global force deformation response and backbone curve is presented in Table F-5.2 and Figure F-5.2.

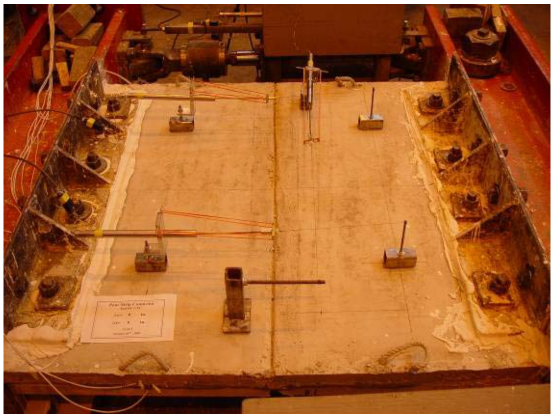 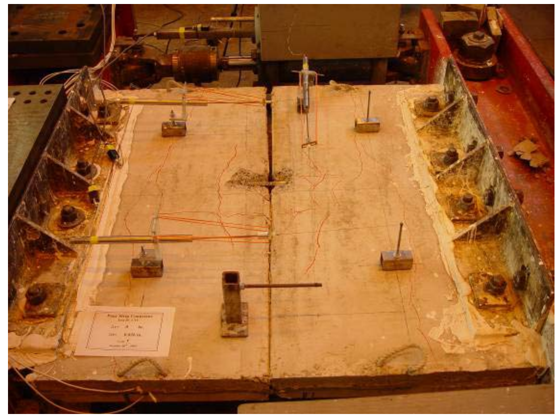

Figure F-5.1: Damage state at 0 and 0.826-in. tensile opening

| Table F-5.1: Key Test Observations | | |
|---|---|---|
| Event # | ΔT [in.] | Event Description |
| 1 | 0 | Prior to test right half of the panel topping has a gap (i.e. pre-cracked), with other half intact. |
| 2 | 0.01 | Centerline cracked through entire center. |
| 3 | 0.031 | Tension cracking on free panel. |
| 4 | 0.0413 | Concrete cracking audible. Present cracks extended & tension crack on fixed panel caused by delaminating. |
| 5 | 0.062 | Concrete cracking audible. Slight pop heard. Tension crack on free panel caused by delaminating. |
| 6 | 0.083 | Tension crack on fixed panel. Longitudinal cracks over bars. Free beam jumped up out of plane. |
| 7 | 0 | Added~300 lbs to free beam to prevent upward motion. |
| 8 | 0.124 | Tension cracks on fixed panel. Free beam still jumps up out of plane. |
| 9 | 0 | Added ~ 600 lbs more to free beam. Concrete cracking audible. |
| 10 | 0.165 | Concrete cracking audible. Out of plane motion no longer occurs. Cracking developed. |
| 11 | 0.165 (3rd cycle) | Pop heard (WWR wire fracture). |
| 12 | 0.248 | Concrete cracking audible. Pop heard. Cracking developed. |
| 13 | 0.330 | Concrete cracking audible. WWR fracture heard. |
| 14 | 0.413 (2nd cycle) | Concrete cracking audible. Pop heard. |
| 15 | 0.413 (3rd cycle) | Concrete cracking audible. Pop heard. |
| 16 | 0.62 | Cracking by connector at panel interface. Support slip on left side of free beam noticed. |
| 17 | 0.826 | Surface spalling exposes connector. |
| 18 | -0.01 | Connector bent upwards. |
| 19 | 0.826 (2nd cycle) | Loud noise heard. Right side of panel opened up, left side in compression due to panel rotation. |
| 20 | -0.01 | Connector bent upward. Concrete spalling exposes connector bars: left ~ 9-in. ; right bar ~ 11-in |
| 21 | 1.033 | Concrete cracking audible. Pop heard. |
| 22 | 0 | Connector bent upwards, spalling exposes the connector bars more. |
| 23 | 1.033 (2nd cycle) | Popping noises heard (WWR wire fractures). |
| 24 | 1.239 | ~ Zero loads - Panel completely slipped out of free beam support. |

| Table F-5.2: Experimental Results Backbone Curve [kip. in.] | | |
|---|---|---|
| Step | Tensile Displacement | Tensile Force |
| - | 0.012 | 17.68 |
| Tensile cracking | 0.042 | 48.36 |
| Cracking around connector | 0.081 | 57.52 |
| Max Load | 0.119 | 62.58 |
| WWR wires fracture | 0.163 | 62.49 |
| WWR wires fracture | 0.304 | 52.43 |
| - | 0.408 | 51.46 |
| - | 0.607 | 56.00 |
| End of test | 0.803 | 53.30 |

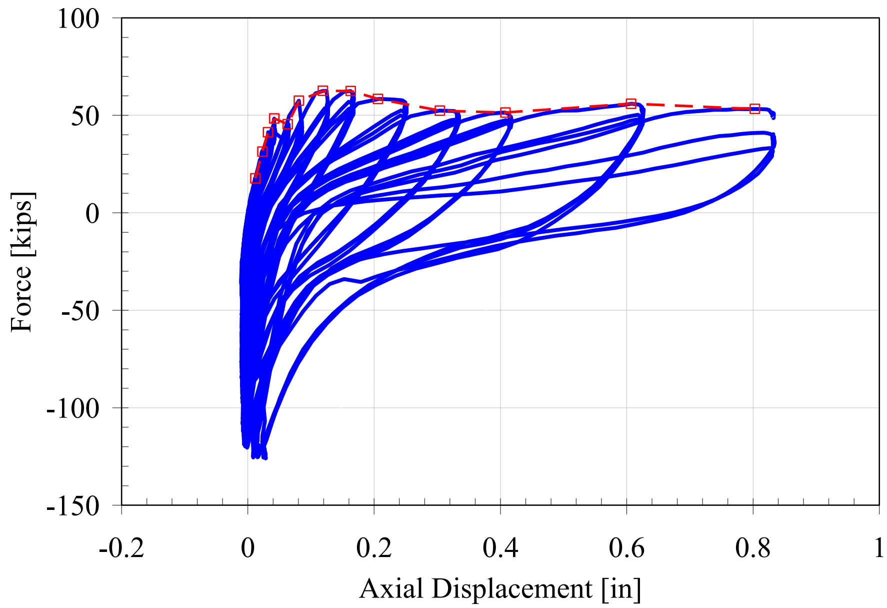


Figure F-5.2: Axial force and displacement

## Subassembly G: Topping Connector

### Subassembly Details G

The specimen tested represents a topping connection without a mechanical connector. The topping reinforcement consists of W2.9XW4.0 6-inx10-in. WWR. This level of reinforcement corresponds to the minimum temperature and shrinkage reinforcement required by ACI. A 10-in. spacing is used across the joint to provide ductility against opening of the joint. Details of the specimen are shown in Figure G.

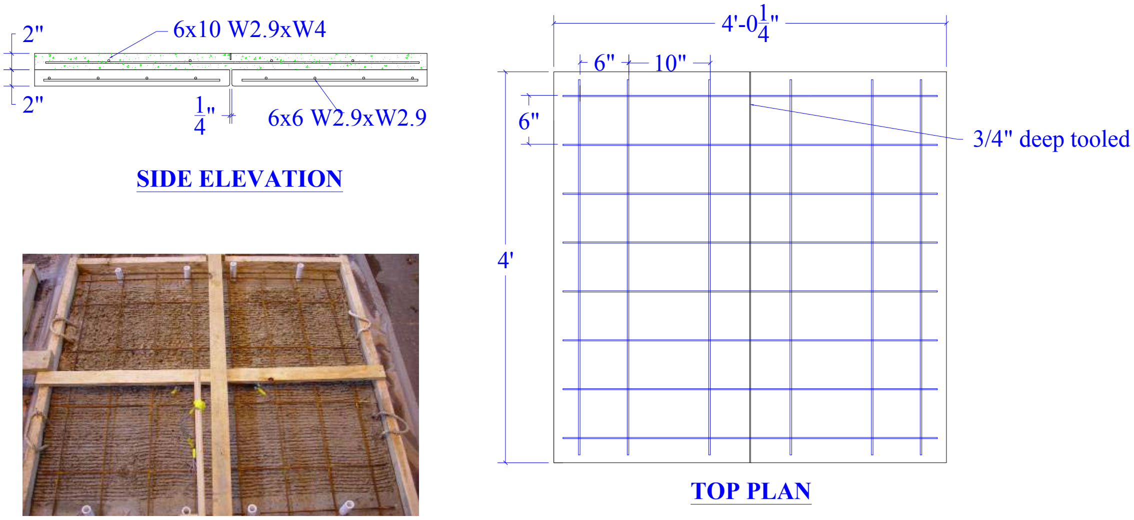


Figure G: Subassembly G

### Material Properties G

The base 2-in. pre-cast panel was fabricated using high early strength self consolidating concrete with a design strength of 7000 psi. A ready mix topping was used to simulate field topped conditions. The design strength of the topping was 4000 psi. The WWR used in the topping and base panel met the requirements of ASTM A185 grade 65 steel. The measured concrete strengths and mill certified steel properties are presented in Table G.

Table G: Material Properties Capacity

| Test | Location in Subassembly | Compressive Strength, f'c [psi] |
|---|---|---|
| G-1 | Topping (T2) | 4032 ± 600 |
| | Base Panels (P3) | 6410 ± 1190 |
| G-2 | Topping (T2) | 4032 ± 600 |
| | Base Panels (P3) | 7406 ± 156 |
| G-3 | Topping (T2) | 4032 ± 600 |
| | Base Panels (P3) | 6410 ± 1190 |
| G-4 | Topping (T2) | 4032 ± 600 |
| | Base Panels (P3) | 6410 ± 1190 |
| G-5 | Topping (T2) | 4032 ± 600 |
| | Fixed Panel (P3) | 6410 ± 1190 |
| | Free Panel (P3) | 7406 ± 156 |

| Size | Reinforcement Usage | Grade | Yield Stress [ksi] | Ultimate Strength [ksi] |
|---|---|---|---|---|
| #4 | Reinforcing Bars | A706 | 65.79 | 91.39 |
| W2.9XW4 6X10 | Topping Mesh | A185 Gr.65 | 65.00* | 103.3 |
| W2.9XW2.9 6X6 | Pre-cast Panel Mesh | A185 Gr.65 | 65.00* | 108.5 |
| * Data unavailable, value assumed | | | | |

### TEST G-1: MONOTONIC TENSION WITH FV = 0

The performance of the topping subjected to monotonic tension is presented in this section. The panel was subjected to tensile displacement with the shear displacement unrestrained, Fv=0. The panel failed due to fracture of the WWR at the joint interface, no other damage was observed. Fracture of all eight wires across the joint did not occur simultaneously but was spread over a displacement of approximately 0.1 to 0.2-in. The observed events and corresponding displacement cycle is presented in Table G-1.1. The photos of the damage are presented in Figure G-1.1. The global force deformation response and backbone curve is presented in Table G-1.2 and Figure G-1.2.

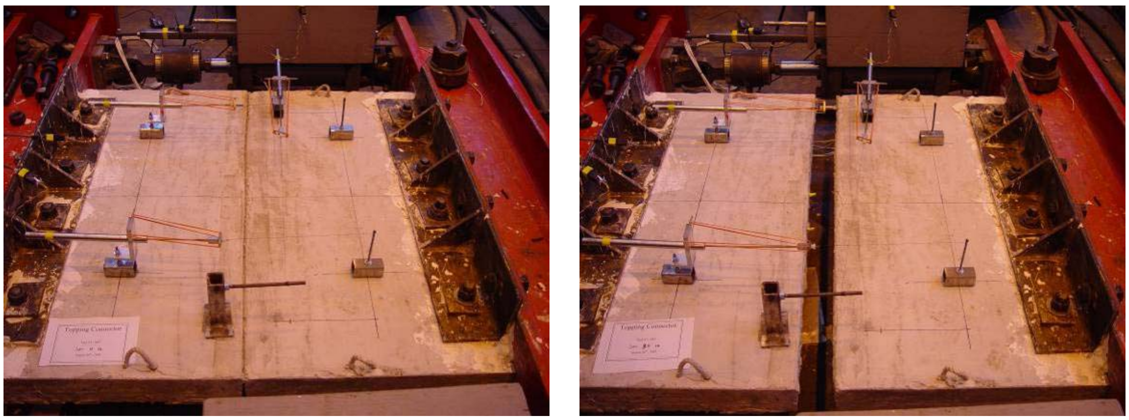

Figure G-1.1: Damage state at 0 and 3.0-in. tensile opening

| Table G-1.1: Key Test Observations | | |
|---|---|---|
| Event # | Tension Δ [in.] | Event Description |
| 1 | 0 | Centerline crack formed. |
| 2 | 0.2 | Eight WWR wires fractured. |
| 3 | 3.5 | End of Test |

| Table G-1.2: Experimental Results Backbone Curve [kip. in.] | | |
|---|---|---|
| Step | Tensile Displacement | Tensile Force |
| ~ 75% Max Load | 0.035 | 19.42 |
| - | 0.053 | 23.37 |
| Max Load | 0.083 | 24.86 |
| Fracture of WWR | 0.130 | 21.94 |
| - | 0.137 | 18.23 |
| Fracture of WWR | 0.157 | 17.96 |
| - | 0.177 | 2.19 |
| Fracture of WWR | 0.201 | 2.07 |
| End of test | 0.201 | 0 |

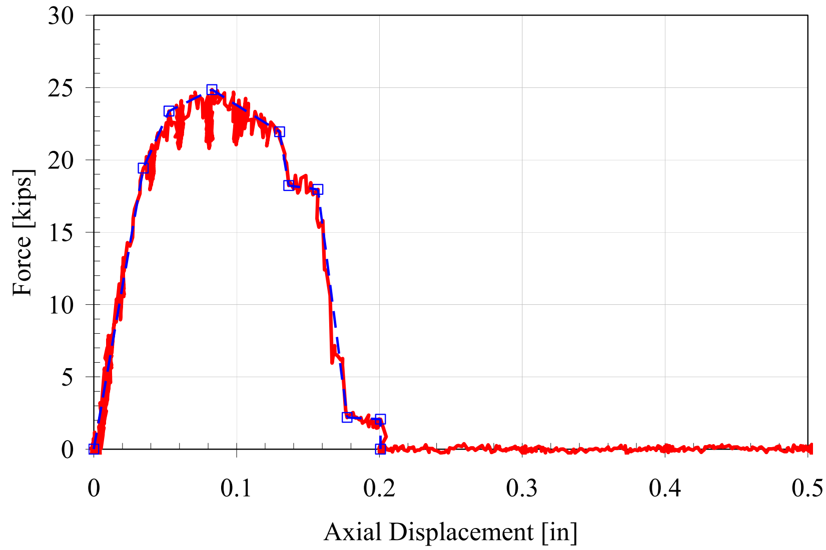


Figure G-1.2:  Tensile force and displacement

### TEST G-2: MONOTONIC SHEAR WITH ΔT = 0.1

The performance of the topping subjected to monotonic shear is presented in this section. The panel was pre-cracked by applying a tensile opening of 0.1-in. A shear displacement was then applied with the tensile displacement restrained at the 0.1-in. opening. The panel failed due to progressive fracture of the WWR from 0.4 to 0.5-in. of joint shear deformation.  The observed events and corresponding displacement cycle is presented in Table G-2.1.  The photos of the damage are presented in Figure G-2.1.  The global force deformation response and backbone curve is presented in Table G-2.2 and Figure G-2.2.

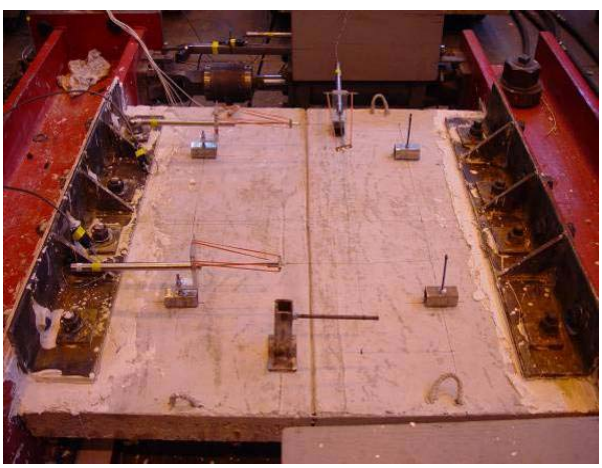

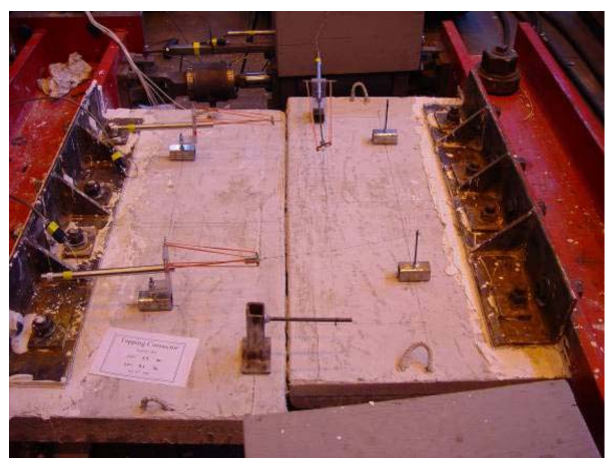

Figure G-2.1:  Damage state at 0 and 3.5-in. shear opening

Table G-2.1:  Key Test Observations

| Event # | ΔV [in.] | ΔT [in.] | Event Description |
|---|---|---|---|
| 1 | 0 | 0.01 | Centerline crack formed. |
| 2 | 0.4 | 0.1 | One WWR wire fractured. One WWR wire fractured after cycle. |
| 3 | 0.5 | 0.1 | Six WWR wires fractured. |
| 4 | 0.6 | 0.1 | Concrete bearing in shear at interface audible. |
| 5 | 3.5 | 0.1 | End of Test |

| Table G-2.2: Experimental Results Backbone Curve [kip. in.] | | | | |
|---|---|---|---|---|
| Shear force-deformation | | | Axial force – Shear deformation | |
| Step | Shear Displacement | Shear Force | Shear Displacement | Axial Force |
| - | 0.047 | 3.27 | 0.002 | 24.90 |
| - | 0.295 | 10.33 | 0.065 | 20.40 |
| Max Load – Fracture of WWR | 0.372 | 11.00 | 0.227 | 15.50 |
| Fracture of WWR | 0.400 | 4.56 | 0.364 | 14.14 |
| Concrete friction at interface | 1.323 | 1.76 | 0.473 | -2.64 |
| Concrete friction at interface | 1.527 | 2.72 | 0.771 | -3.98 |
| Concrete friction at interface | 1.825 | 1.59 | 2.420 | -1.08 |
| Concrete friction at interface | 3.000 | 1.81 | 2.959 | -1.67 |
| End of test | 3.493 | 0.76 | 3.491 | -0.07 |

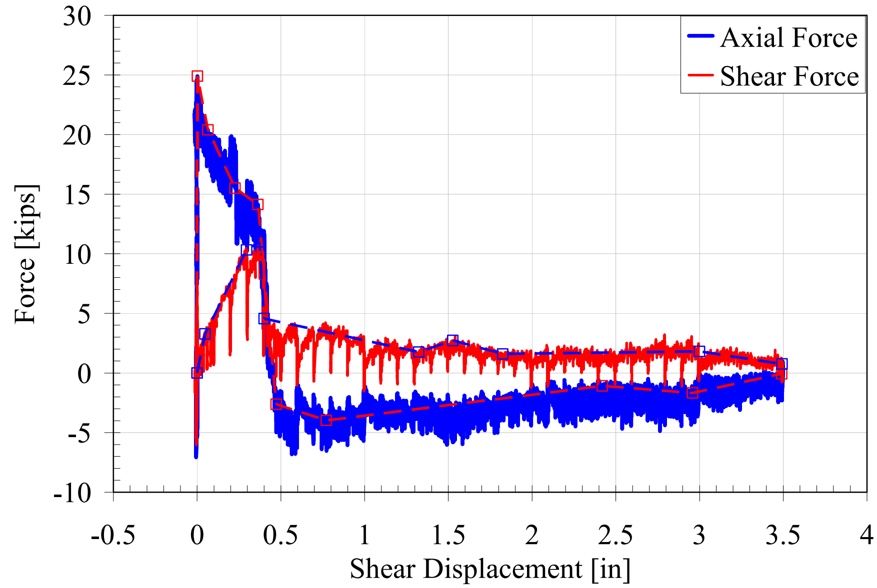


Figure G-2.2: Shear force and displacement

## TEST G-3: MONOTONIC SHEAR WITH ΔT = 0

The performance of the topping subjected to monotonic shear was repeated without a 0.1-in. gap, instead the original panel spacing was maintained. The panel was pre-cracked by applying a tensile opening of 0.03-in. after which the specimen was returned to zero axial displacement. A shear displacement was applied with the tensile displacement restrained to zero opening. The panel failed due to progressive fracture of the WWR from 0.4 to 1.5-in. of joint shear deformation. Shear friction at the front edge of the panel resulted in diagonal crack formation at about 8-in. from the end of the fixed panel. The observed events and corresponding displacement cycle is presented in Table G-3.1. The photos of the damage are presented in Figure G-3.1. The global force deformation response and backbone curve is presented in Table G-3.2, Figure G-3.2 and Figure G-3.3.

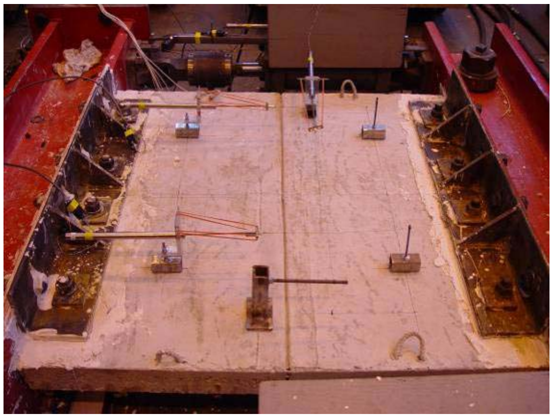

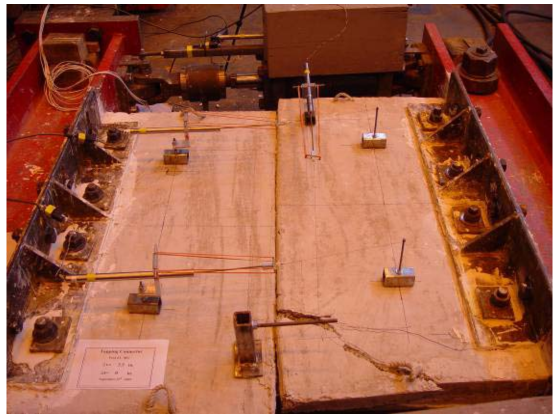

Figure G-3.1: Damage state at 0 and 3.5-in. shear opening

| Table G-3.1: Key Test Observations | | | |
|---|---|---|---|
| Event # | Shear Δ [in.] | Tension Δ [in.] | Event Description |
| 1 | 0 | 0 | Center pre-cracked. |
| 2 | 0.2 | 0 | Concrete cracking audible. Cracking on fixed panel. |
| 3 | 0.3 | 0 | Concrete cracking audible. Crack opening. |
| 4 | 0.4 | 0 | Concrete cracking audible. More cracking developed. |
| 5 | 0.5 | 0 | Concrete cracking audible. 1 WWR wire fracture. |
| 6 | 0.6 | 0 | Concrete cracking audible. 2 WWR wire fracture. |
| 7 | 0.7 | 0 | Concrete cracking audible. 2 WWR wire fracture. |
| 8 | 0.8 | 0 | Concrete cracking audible. 1 WWR wire fracture. |
| 9 | 1.4 | 0 | 1 WWR wire fracture. |

| Table G-3.2: Experimental Results Backbone Curve [kip. in.] | | | | |
|---|---|---|---|---|
| Shear force-deformation | | | Axial force – Shear deformation | |
| Step | Shear Displacement | Shear Force | Shear Displacement | Axial Force |
| ~0.75% Max load | 0.104 | 36.60 | 0.077 | -26.46 |
| Max load-panel cracking | 0.250 | 43.79 | 0.274 | -46.90 |
| Fracture of WWR | 0.479 | 31.87 | 0.35 | -27.43 |
| Fracture of WWR | 0.571 | 14.02 | 0.561 | -9.19 |
| Fracture of WWR | 1.031 | 8.48 | 0.801 | -12.86 |
| Fracture of WWR | 1.488 | 7.71 | 1.089 | -7.18 |
| Concrete friction at interface | 1.518 | 3.60 | 1.410 | -10.60 |
| Concrete friction at interface | 3.489 | 1.21 | 1.630 | -4.76 |
| End of test | | | 3.489 | -2.38 |

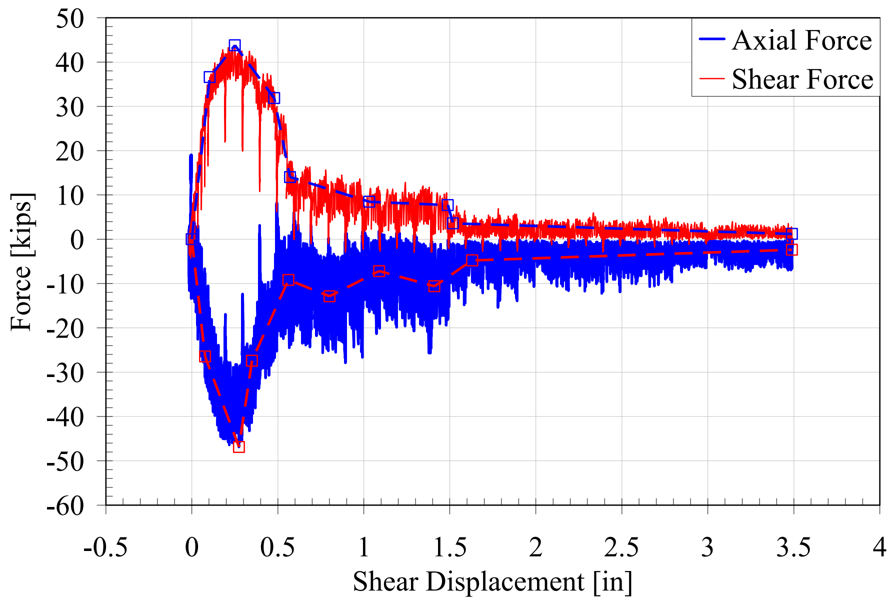


Figure G-3.2: Shear force and displacement

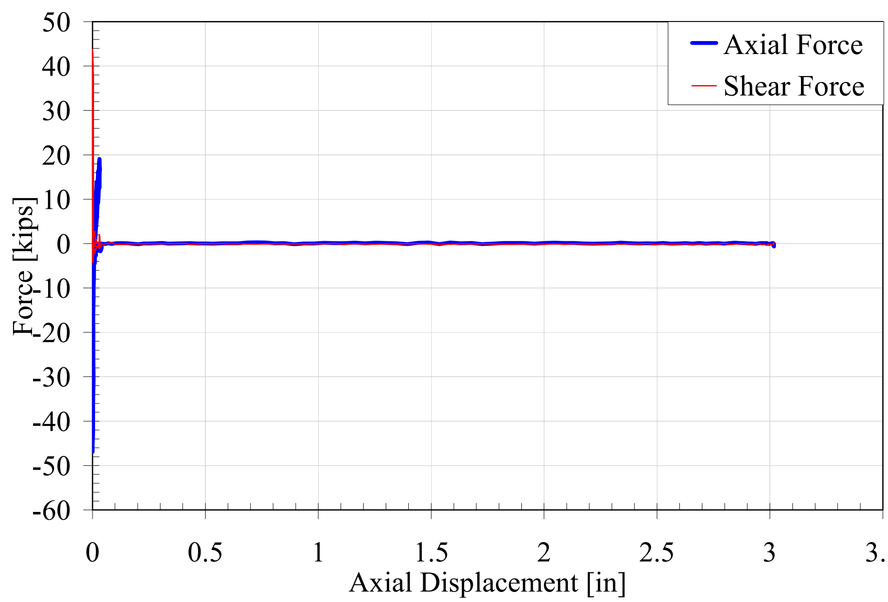


Figure G-3.3: Force and Axial displacement

## TEST G-4: MONOTONIC TENSION & SHEAR WITH $\Delta T/\Delta V = 0.5$

The performance of the topping subjected to monotonic tension and shear is presented in this section. Tension deformation to shear deformation was applied at a constant ratio of $\Delta T/\Delta V = 0.5$. The panel failed due to progressive fracture of the WWR from 0.2 to 0.3-in. of joint shear deformation. The observed events and corresponding displacement cycle is presented in Table G-4.1. The photos of the damage are presented in Figure G-4.1. The global force deformation response and backbone curve is presented in Table G-4.2 and Figure G-4.2 and Figure G-4.3.

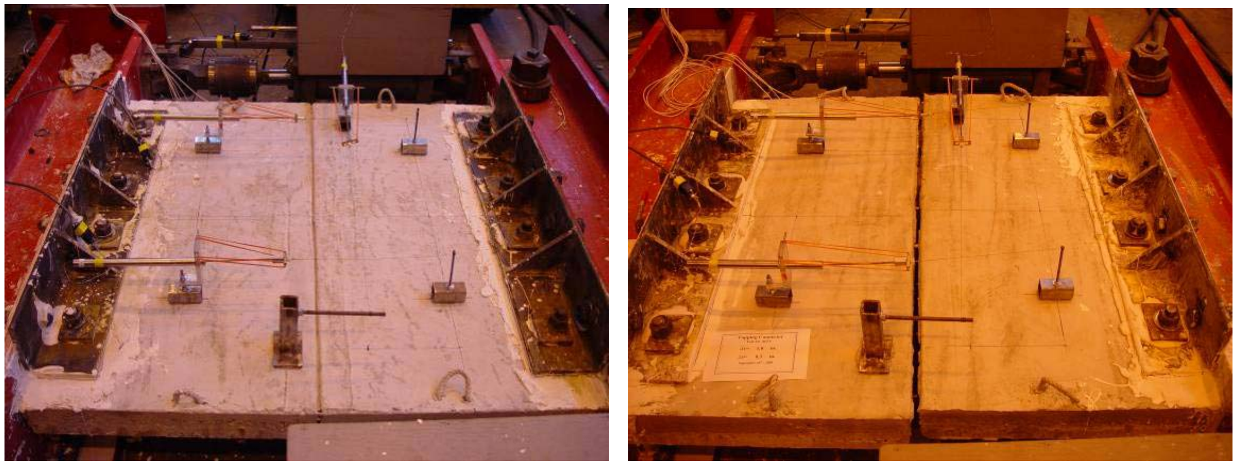

Figure G-4.1: Damage state at 0 and 1.0-in. shear opening

| Table G-4.1: Key Test Observations | | | |
|---|---|---|---|
| Event # | Shear Δ [in.] | Tension Δ [in.] | Event Description |
| 1 | 0 | 0 | Centerline crack prior to test. |
| 2 | 0.3 | 0.15 | WWR wires fractured. |

| Table G-4.2: Experimental Results Backbone Curve [kip. in.] | | | | | | |
|---|---|---|---|---|---|---|
| Shear force-deformation | | | | Axial force – Shear deformation | | |
| Step | Axial Δ | Shear Δ | Shear Force | Axial Δ | Shear Δ | Axial Force |
| - | 0.053 | 0.106 | 0.117 | 0.005 | 0.010 | 5.04 |
| - | 0.104 | 0.208 | 1.458 | 0.064 | 0.128 | 19.04 |
| Max Load – Fracture of WWR | 0.116 | 0.231 | 2.239 | 0.0835 | 0.167 | 21.89 |
| Fracture of WWR | 0.139 | 0.278 | 0.495 | 0.1145 | 0.229 | 15.83 |
| - | 0.153 | 0.306 | 0 | 0.144 | 0.288 | 1.60 |
| End of test | 0.5 | 1 | 0 | 0.151 | 0.302 | 1.48 |
| | | | | 0.1545 | 0.309 | 0 |
| | | | | 0.5 | 1 | 0 |

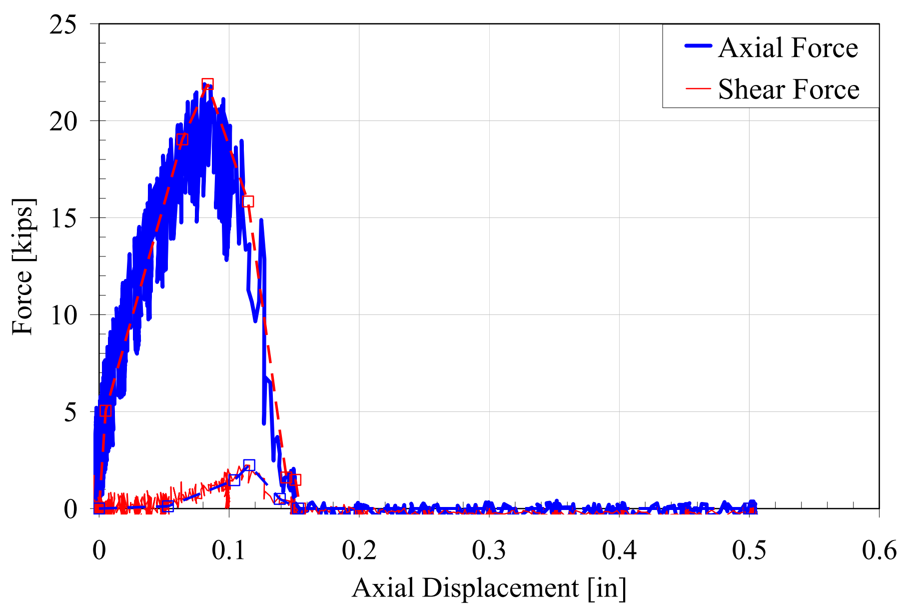


Figure G-4.2: Force and Axial displacement

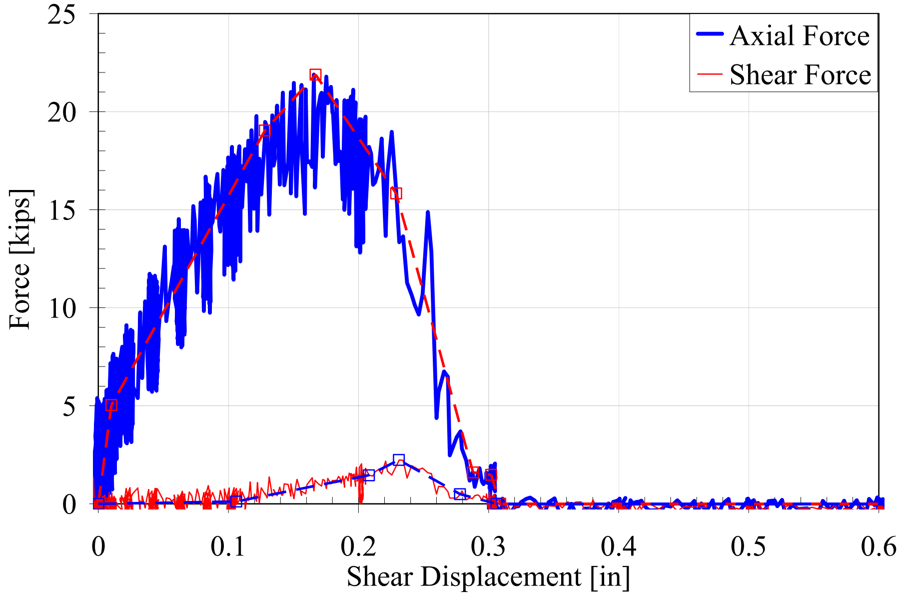


Figure G-4.3: Force and Shear displacement

### TEST G-5: CYCLIC SHEAR WITH ΔT = 0

The performance of the topping subjected to cyclic shear is presented in this section. The panel was pre-cracked by applying a tensile opening of 0.03-in. after which the specimen was returned to zero axial displacement. A shear displacement was applied with the axial displacement restrained to zero opening. The panel failed due to progressive fracture of the WWR from 0.15 to 0.7-in. of joint shear deformation. To ensure failure of the system, the panel was then subjected to a 3-in. tensile deformation which ensured fracture of the WWR wires. The observed events and corresponding displacement cycle is presented in Table G-5.1. The photos of the damage are presented in Figure G-5.1. The global force deformation response and backbone curve is presented in Table G-5.2, Figure G-5.2 and Figure G-5.3.

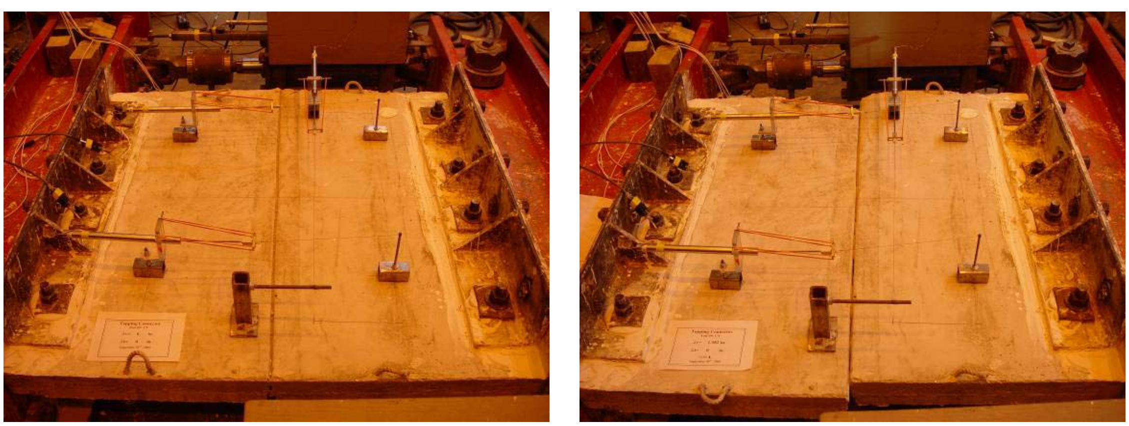

Figure G-5.1: Damage state at 0 and 1.582-in. shear opening

| Table G-5.1: Key Test Observations | | | |
|---|---|---|---|
| Event # | Shear Δ [in.] | Tension Δ [in.] | Event Description |
| 1 | 0 | 0 | Centerline cracked prior to test. |
| 2 | 0.08475 | 0 | Longitudinal crack at the end of the free panel formed. |
| 3 | -0.08475 | 0 | Longitudinal crack at the end of the fixed panel formed. |
| 4 | 0.113 | 0 | Crack opening leading to block shear on both panels. |
| 5 | -0.113 | 0 | Block shear results in spalling at the end of both panels. |
| 6 | 0.1695 | 0 | WWR wire fracture heard. |
| 7 | -0.1695 | 0 | WWR wire fracture heard. |
| 8 | 0.226 | 0 | Concrete cracking audible. |
| 9 | 0.339 (3rd cycle) | 0 | WWR wire fracture heard. |
| 10 | -0.339 (3rd cycle) | 0 | WWR wire fracture heard. |
| 11 | 0.452 | 0 | WWR wire fracture heard. |
| 12 | -0.452 | 0 | 2 WWR wire fractures heard. |
| 13 | 0.452 (2nd cycle) | 0 | WWR wire fracture heard. |
| 14 | -0.452 (3rd cycle) | 0 | Slight popping noises heard. |
| 15 | 0.678 | 0 | Concrete cracking audible. WWR wire fracture heard. |
| 16 | -0.678 | 0 | 2 WWR wires fracture. |
| 17 | 0.678 (3rd cycle) | 0 | Popping noises heard. |

| Table G-5.2: Experimental Results Backbone Curve [kip. in.] | | | | |
|---|---|---|---|---|
| Shear force-deformation | | | Axial force – Shear deformation | |
| Step | Shear Displacement | Shear Force | Shear Displacement | Axial Force |
| - | -1.55 | -3.89 | -1.55 | -4.33 |
| WWR wire fractures | -0.663 | -5.75 | -0.663 | -6.48 |
| WWR wire fractures | -0.339 | -16.52 | -0.339 | -2.61 |
| Max Reverse Shear Load | -0.085 | -17.46 | -0.085 | -11.88 |
| - | -0.055 | -15.57 | -0.055 | -7.47 |
| - | 0 | 0 | 0 | 0 |
| - | 0.056 | 17.54 | 0.056 | -8.15 |
| Max Load | 0.084 | 19.04 | 0.084 | -11.20 |
| WWR wire fractures | 0.327 | 15.97 | 0.327 | -1.71 |
| WWR wire fractures | 0.673 | 7.68 | 0.673 | -1.68 |
| End of test | 0.901 | 5.03 | 0.901 | -6.64 |

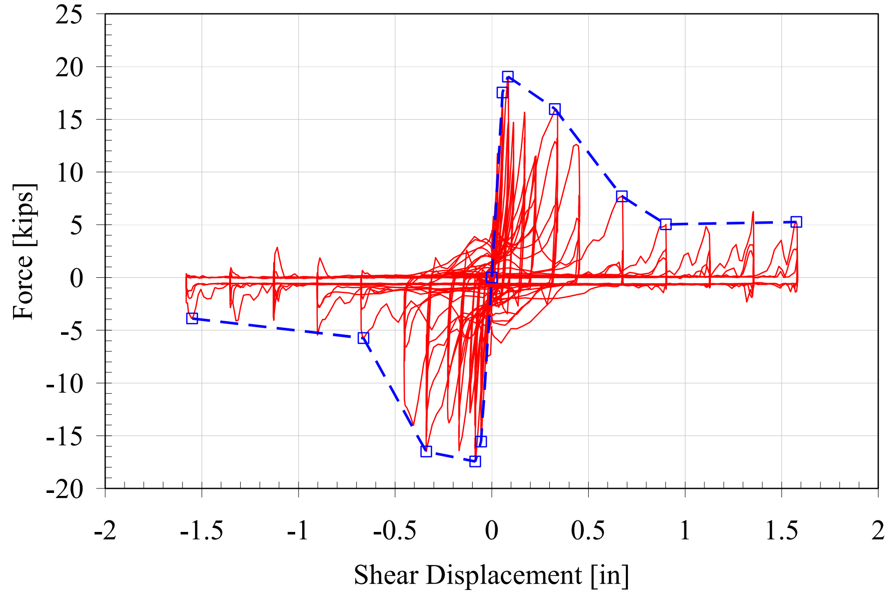

Figure G-5.2: Shear force and displacement

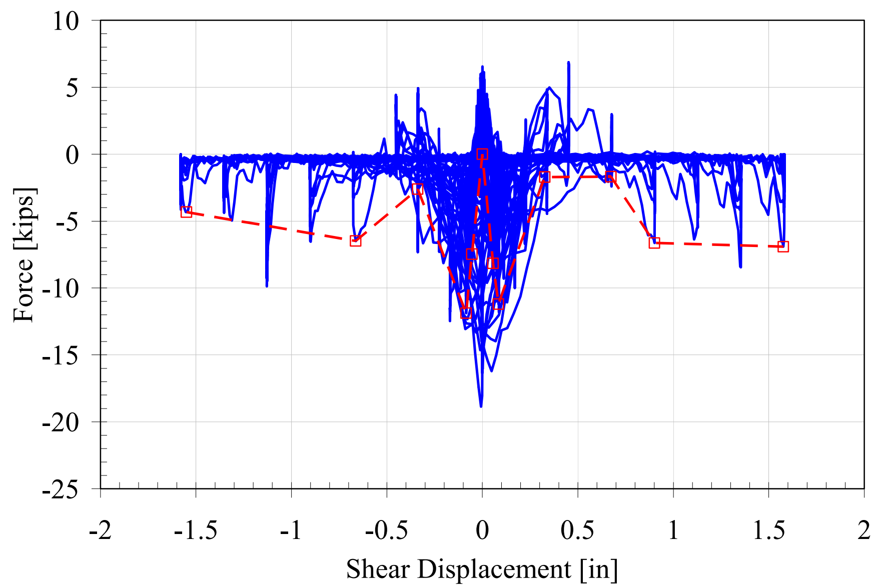

Figure G-5.3: Axial force and shear displacement

## DISCUSSION

In the following sections we will look at tension and shear comparisons between the tested specimens and accepted industry design standards found in the PCI Design Handbook 5$^{th}$ edition and the ACI 318-05.

## COMPARATIVE TENSION BEHAVIOR

The experimental data was compared to the design strength and the expected ultimate tension strength. The design strengths were based on the expected yield stress of the material. All ultimate strength estimates were computed using the tensile strengths of the connectors based on mill certified properties. The formulations were computed based on a simplified truss analogy in accordance with the PCI Design Handbook Section 3.6.2. This force-based method estimates the available capacities due to a ductile failure in the connector leg. It is assumed that the welds were adequately proportioned to resist the bar fracture strength and that forces are applied uniformly and concentrically to the connector.

For the splayed leg connectors (JVI & hairpin connectors), the capacity is estimated with the truss model to determine the PCI design strength. For the perpendicular leg connectors (chord, pour-strip, cover plate connectors & topping) the capacity of the connector is based on the bar strength. In computing the design capacity of the topped connectors, it was assumed that the WWR mesh and connector were both at yield; however, for the ultimate capacity the assumption was made that the wires were already fractured. Hence the topping WWR mesh ultimate strength was not added to connector strength. The following terminology is used: cross-sectional area of one leg: $A_s$, bar yield or tensile strength: $f$, total cross-sectional area of WWR: $A_{s\_wwr}$, WWR yield or ultimate tensile strength: $f_{wwr}$. The formulations used for design capacity and ultimate strength are summarized in Table 3

| Table 3: Capacity Formulation Estimates | | |
|---|---|---|
| Connector | Design Capacity, Pn | Ultimate Capacity, Pu |
| A: JVI | $2 \cdot (f_y \cdot A_s \cdot \cos 45°)$ | $2 \cdot (f_u \cdot A_s \cdot \cos 45°)$ |
| B: Chord | $2 \cdot (f_y \cdot A_s)$ | $2 \cdot (f_u \cdot A_s)$ |
| C: Un-topped Hairpin | $2 \cdot (f_y \cdot A_s \cdot \cos 45°)$ | $2 \cdot (f_u \cdot A_s \cdot \cos 45°)$ |
| D: Topped Hairpin | $2 \cdot (f_y \cdot A_s \cdot \cos 45°) + f_{wwr-y} \cdot A_{s\_wwr}$ | $2 \cdot (f_u \cdot A_s \cdot \cos 45°)$ |
| E: Topped Cover Plate | $2 \cdot (f_y \cdot A_s) + f_{wwr-y} \cdot A_{s\_wwr}$ | $2 \cdot (f_u \cdot A_s)$ |
| F: Pour-strip | $2 \cdot (f_y \cdot A_s) + f_{wwr-y} \cdot A_{s\_wwr}$ | $2 \cdot (f_u \cdot A_s)$ |
| G: Topping | $f_{wwr-y} \cdot A_{s\_wwr}$ | $f_{wwr-u} \cdot A_{s\_wwr}$ |

The calculated strengths are compared to the measured responses in Table 4. The results from the monotonic tension, MT, monotonic tension and shear, MTV, and the cyclic tension-compression, CTC, are presented. The mill certified material properties, presented in Table A-G, were used for ultimate strength calculations when available.

| Table 4: Connector Ultimate Tensile Strength | | | | | |
|---|---|---|---|---|---|
| Connector | Design Capacity, $P_n$ [kips] | Ultimate Capacity, $P_u$ [kips] | MT [kips] | MTV [kips] | CTC [kips] |
| A: JVI | 16.50 | 32.00 | 9.69 | 1.48* | 5.90 |
| B: Chord | 37.20 | 59.25 | 36.37 | 33.78 | - |
| C: Un-topped Hairpin | 17.00 | 25.80 | 7.71 | - | - |
| D: Topped Hairpin | 32.10 | 25.80 | 25.00 | 22.65 | - |
| E: Cover Plate | 39.08 | 36.56 | 43.42 | 28.17 | - |
| F: Pour-strip | 52.28 | 59.25 | 62.31 | 61.08 | 62.58 |
| G: Topping | 15.08 | 23.97 | 24.86 | 21.89 | - |
| *Note, failure controlled by shear | | | | | |

The topped connectors: topped hairpin, cover plate, pour strip and the topping connector, all met or exceeded their estimated design and ultimate capacities. The pre-topped and un-topped connections such as the JVI, hairpin, and dry chord did not achieve their expected design or ultimate capacities due to premature failures at the welded regions.

In general, the splayed leg connectors exhibited a flexible tensile response. The connectors achieved large deformations prior to strength loss due to bending of the un-welded portion of the connector front face; however, they were not able to achieve their design strength capacity. The straight leg connectors in comparison exhibited a high initial tensile stiffness, and were capable of only limited ductility. Nevertheless, in most cases the straight leg connectors were able to achieve their tensile design strength. An in-depth evaluation of each connection follows.

## JVI CONNECTOR

**MT**: The measured capacity of the connector in pure tension was 30% of the ultimate capacity and 59% of the design capacity according to PCI design standards. This was due to the fact that the connector did not fail from fracture of the connector legs as desired, but failed due to connector-to-slug weld failure. This occurred despite design of the weld to resist the bar fracture strength and also proper welding techniques with L309 electrodes for stainless steel. This might have been caused by observed eccentricity in the placement of the connector slug and between the connectors themselves, which may have resulted in undesired moments generated at the connector and stress concentration at the end of the welds. This in turn would have caused tearing of the weld resulting in the observed weld fracture (see Figure 6). Hence the connector was not able to attain the ultimate strength or even the design strength of the connector legs. The connector performance is displayed in Figure 8.

Figure 6: JVI-MT: Damage state at 2-in tensile opening

**CTC**: The measured tensile capacity of the connector was 18% of the ultimate capacity and 36% of the design capacity according to PCI design standards. This was due to the fact that the connector did not fail from the fracture of the connector legs as desired, but failed due to connector-to-slug failure, which was also exacerbated by low cycle fatigue of the weld metal. The failure was similar to monotonic test, with the connectors having the same observed eccentricity in the placement of the connector slug and between the connectors themselves. This may have resulted in undesired moments generated at the connector and stress concentration at the end of the welds, and would have caused tearing of the weld resulting in the observed weld fracture (see Figure 7). The maximum capacity of the connector under cyclic deformations was slightly lower than in the monotonic test. Also, the connector was considerably less ductile, failing at only 0.773-in. compared to 2.01-in. in the monotonic test. These differences can be attributed to low cycle fatigue of the weld stemming from pseudo-static cyclic deformation of the connector, which would cause early fracture of the weld with reduced capacity. Hence the connector was not able to attain the ultimate strength or design strength of the connector legs. The connector performance is displayed in Figure 8.

Figure 7: JVI-CTC: Damage state at 0.68-in tensile opening

**SUMMARY**: The previously developed backbone axial force-deformation curves of the connectors are presented in Figure 8. The axial portion of the MTV test is included for comparison although the connector failed in a shear mode and its discussion is presented in the shear comparison section. Due to weld failures the connector is not capable of achieving the predicted ultimate or design strength. The connector, however, is capable of maintaining a moderate tensile resistance under significant joint openings. This moderate level of resistance can contribute significantly to the overall joint flexural strength. With improved predictive models for estimating the strength of existing designs or enhanced details that allow the connector to achieve the expected PCI strength the JVI connector can improve the flexural behavior of a diaphragm joint.

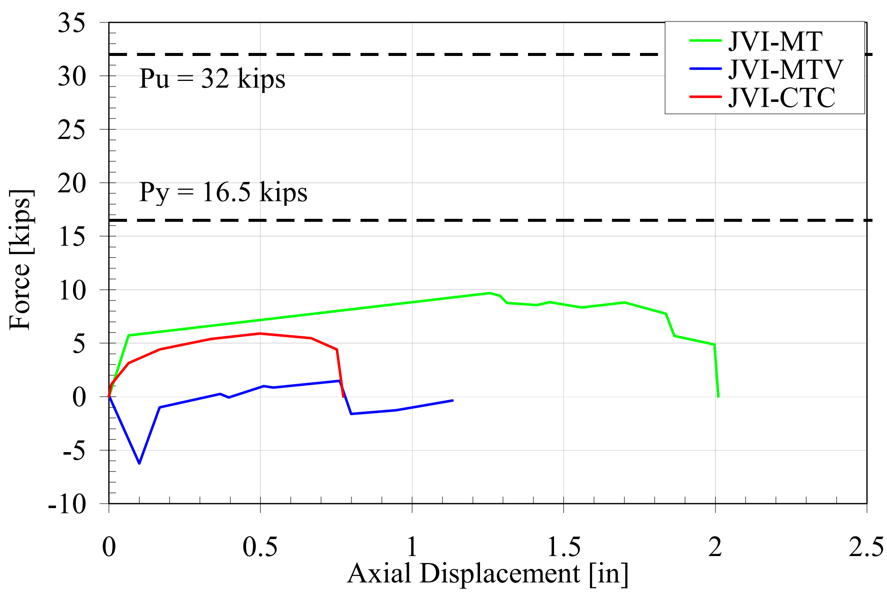


Figure 8: JVI Tensile Data

### PRE-TOPPED CHORD CONNECTOR

**MT**: The measured capacity of the connector in pure tension was 57% of the ultimate capacity and 98% of the design capacity according to PCI design standards. This was due to the fact that the connector bars did not fracture from pure tension as desired, but failed due to connector-to-slug weld tearing, despite design of the weld to resist the bar fracture strength. Weld tearing might have been caused by minor eccentricity in the placement of the connector slug, both horizontally and vertically, and between the connectors themselves, which may have resulted in undesired moments generated at the connector and stress concentration at the end of the welds. Once the weld began to tear, it caused the connector plate to deform, introducing bending in the connector bars (see Figure 9). This resulted in the anchorage bars fracturing at the weld toe prematurely. Hence the connector was not able to attain the ultimate or design strength of the connector bars. The connector performance is displayed in Figure 10.

Figure 9: Chord-MT: Damage state at 1.0-in tensile opening

**SUMMARY**: The previously developed backbone axial force-deformation curves of the connectors are presented in Figure 10. The axial portion of the MTV test is included and its discussion is presented in the shear comparison section. The chord exhibited a stiff initial response followed by tearing and a rapid softening. The addition of shear marginally reduced the load resistance but significantly decreased the ductility of the connection. The MTV force deformation curve exhibited a shift of approximately 0.1-in. after its first initial 14.41 kip peak at 0.071-in. This was due to a minor reduction in axial force to 11.38 kips at 0.129-in. tensile deformation that coincided with the peak shear capacity. Once local cracking at the tension leg occurred causing a decrease in the shear capacity, the tensile resistance in the connector resumed its normal load path. In either case, the connector was not able to attain its design or ultimate capacity and the deformation capacity was minimal.

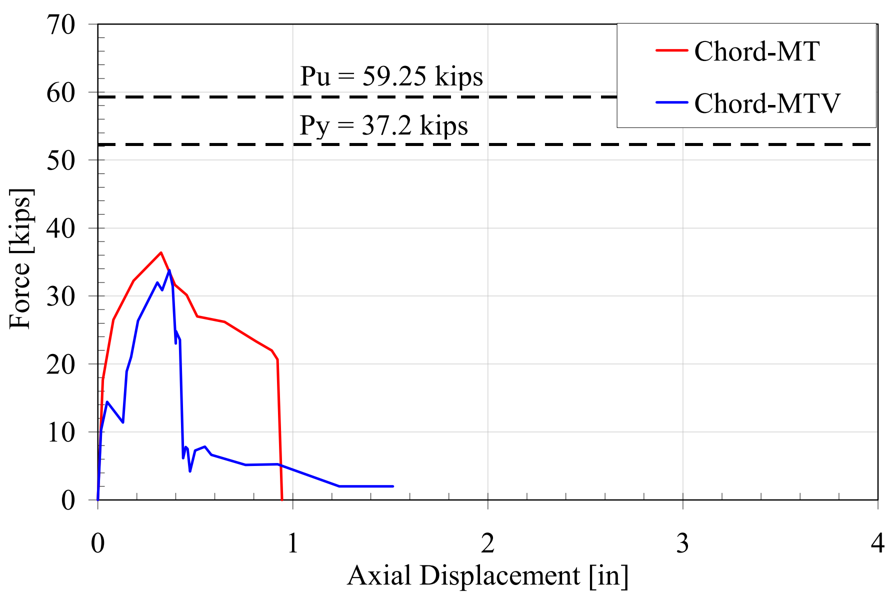


Figure 10: Chord & Tensile Data

### HAIRPIN CONNECTOR

**Un-topped MT**: The measured capacity of the un-topped connector in pure tension was 30% of the ultimate capacity and 45% of the design capacity according to PCI design standards. This was due to the fact that the connector bars did not fracture from pure tension as desired, but failed mainly due to connector-to-slug weld tearing, despite design of the weld to resist the bar fracture strength. Weld tearing was observed at about 0.7-in. coupled with noticeable connector slug rotation, which caused the connector's strength gain to decrease until it peaked at 1.4-in. Bar fracture then occurred in the weld region due to weld tearing propagating into the bar, which is also corroborated by the strain data (see Figure 11). After the bar fractured the connector lost all capacity. Further tensile deformation only increased connector rotation, which resulted in a minimal strength gain. Hence the connector was not able to attain the ultimate design strength of the connector bars. The connector load-deformation response is displayed in Figure 13.

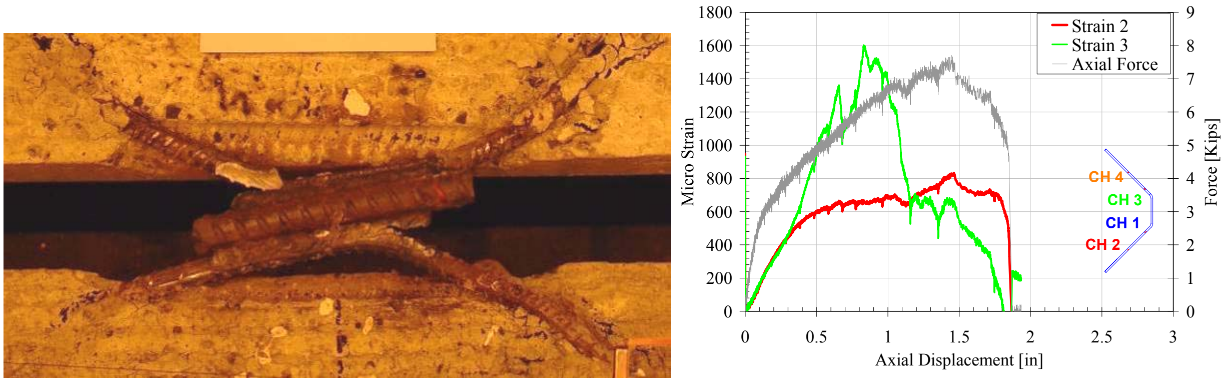

Figure 11: Un-topped Hairpin-MT: Damage state at 2.2-in tensile opening and Strain Data

**Topped MT**: The measured capacity of the topped connector in pure tension was 97% of the ultimate capacity and 78% of the design capacity according to PCI design standards. However, the peak capacity occurs at 0.014-in. tensile deformation, hence it does not only take into account the tensile strength of the connector, but also the strength of the topping with all the WWR wires still intact. If the topping design strength of 22.04 kips is subtracted from the connector's maximum capacity of 25 kips, the resulting 3 kips at 0.014-in. tensile deformation corresponds almost exactly to the un-topped specimen's force deformation curve. When compared to the design strength, which does take into account the mesh's strength, the connector's tensile resistance is still under capacity. In addition to this, once the mesh completely fractured at 0.158-in. the force-deformation curve is almost exactly that of the un-topped connector. The connector's failure progression is also similar, although ultimate failure was due to different mechanism. Weld tearing was observed, however without any appreciable connector rotation, and this caused the connector's strength gain to decrease until a secondary peak of 8.78 kips formed at 1.32-in. Weld tearing also allowed the connector bar connected to the slug to bend, which in turn lead to increased tearing, and eventually to complete fracture of the weld at 1.7-in., which is also corroborated by the strain data (see Figure 12). Hence the connector was not able to attain the ultimate strength or even the design strength of the connector bars. The connector performance is displayed in Figure 13.

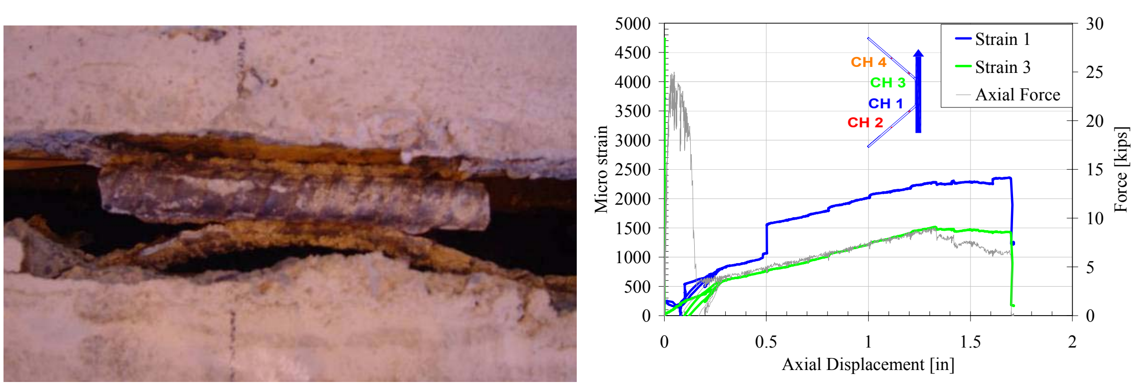

Figure 12: Topped Hairpin-MT: Damage state at 1.6-in tensile opening and Strain Data

**SUMMARY**: The previously developed backbone axial force-deformation curves of the connectors are presented in Figure 13. The axial portion of the MTV test is included for comparison and its discussion is presented in the shear comparison section. Due to weld tearing and failures the connector is not capable of achieving the predicted design strength. The addition of shear marginally reduces the connector resistance but significantly decreased the ductility of the connection. In all cases the connectors were not able to achieve their design or ultimate capacities. The connector, however, is capable of maintaining some tensile resistance under significant joint openings. This moderate level of resistance can contribute significantly to the overall joint flexural strength. With improved predictive models for estimating the strength of existing designs or enhanced details that allow the connector to achieve the expected PCI strength the hairpin connector can improve the flexural behavior of a diaphragm joint.

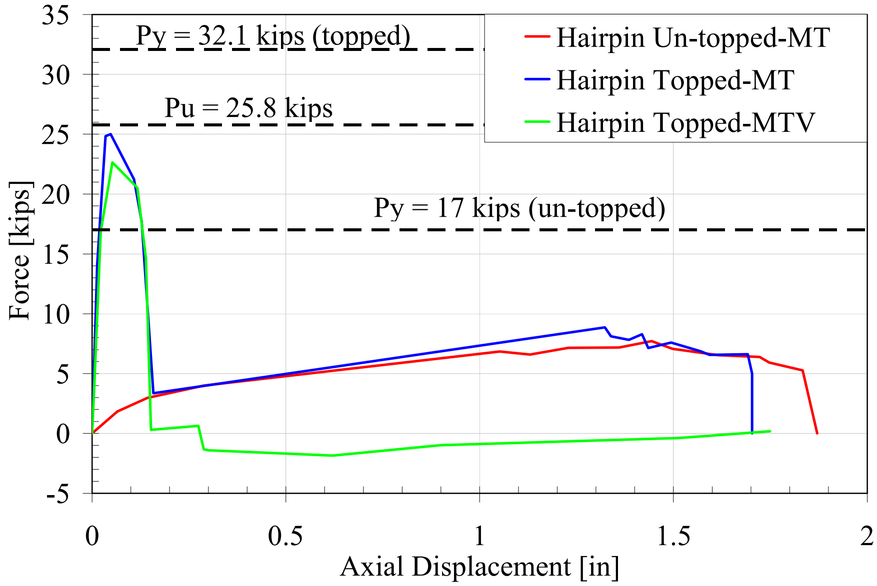


Figure 13: Hairpin Tensile Data

### Cover Plate Connector

**MT**: The measured capacity of the connector in pure tension was 19% over the ultimate capacity and 11% over the design capacity according to PCI design standards. However, this peak capacity occurs at 0.148-in. tensile deformation, hence it does not only take into account the tensile strength of the connector bars, but also the strength of the topping with all the WWR wires still intact. The connector's resistance at this level is also over the design capacity, which does take into account the topping strength. The topping WWR mesh wire fractures occurred over a deformation of 0.148-in. to 0.303-in, which suggest that the mesh's total ultimate design strength of 22.04 kips was not reached at the connectors max capacity. Instead each individual mesh wire reached its individual ultimate strength and fractured at different tensile deformations based on their location in relation to the connector. Also at 0.148-in. the connector bars themselves may not have reached their ultimate design strength. This is further illustrated by the strain data, which shows that high levels of strain in the bar occurred after the WWR had fractured between 0.1-in. and 0.2-in (figure 14). Hence the total ultimate design strength of the WWR mesh and the connector bars' design strength cannot be added to yield the actual capacity. After all the WWR wires fractured, a secondary peak of 29.65 kips at 0.552-in. was observed which is 81% of the design capacity. Hence it can be observed that the connector's ultimate capacity was approximately equal to the actual capacity of the connector and well over the design capacity. The connector performance is displayed in Figure 15.

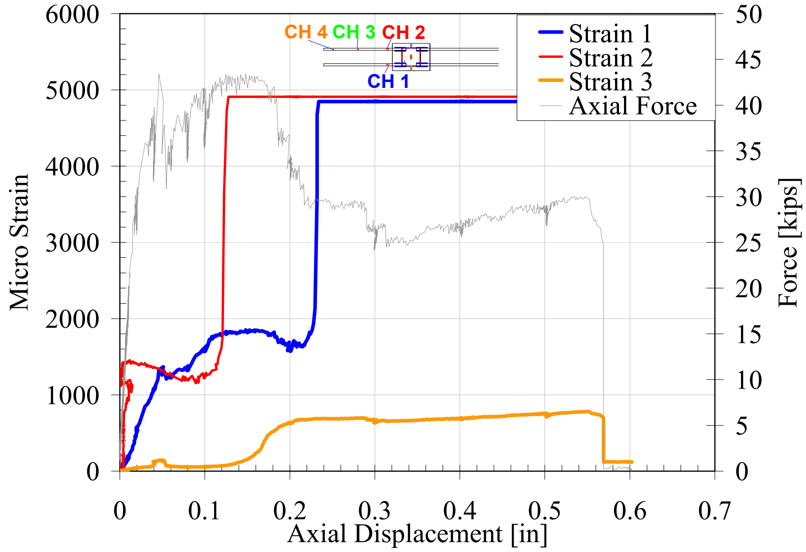


Figure 14: Cover Plate-MT: Strain Data

**SUMMARY**: The previously developed backbone axial force-deformation curves of the connectors are presented in Figure 15. The axial portion of the MTV test is included for comparison although the connector failed in a primarily shear mode and its discussion is presented in the shear comparison section. The connector is able to surpass the predicted design and ultimate strengths and exhibits a stiff initial response but extremely low ductility. The addition of shear changes the failure pattern resulting in a reduction in connector resistance to below the design and ultimate levels, but also allows for increased ductility. The MTV test experiences a significant drop in capacity at the same deformation as the monotonic test. This is probably because this initial drop was due to failure of the two diagonally opposite tensile bars in the MTV test, which should coincide with the same fracture strain for the two tensile bars in the monotonic test. However the remaining undamaged bars still provide tensile resistance at higher deformation levels.

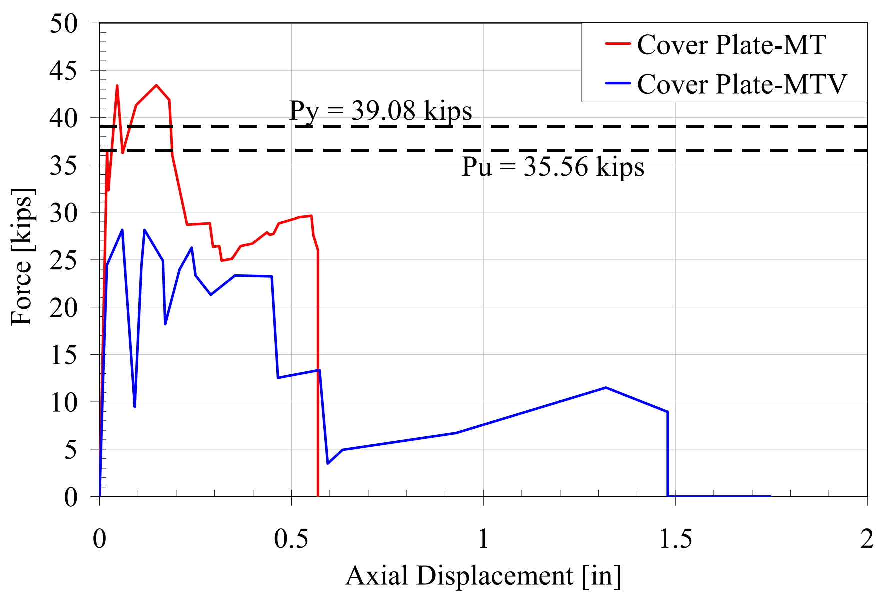


Figure 15: Cover Plate Tensile Data

### POUR-STRIP CONNECTOR

**MT**: The measured capacity of the connector in pure tension was 5% over the ultimate capacity and 19% over the design capacity according to PCI design standards. This peak capacity occurs at 0.148-in. tensile deformation, hence it does not only take into account the tensile strength of the connector bars, but also the strength of the topping with all the WWR wires still intact. However, the capacity is still greater than the design strength, which considers both the bars and WWR wires design strengths. After all the WWR wires fractured, a secondary peak of 54.23 kips (92%Pu) at 0.772-in. was observed. At this point the strain demand on the pour strip reinforcement increases dramatically as illustrated in strain gage 4 of Figure 16. The strain on the bar then rebounds and the load deformation exhibits a softening response. This can be attributed to a failure in one of the pour strip bars. The failure may have occurred in the embedded length of the bar or at the rear of the bar at the welded support. The softening progresses until at 1.277-in. of tensile deformation, there was significant drop in the load capacity corresponding to the fracture of one of the connector bars. The remaining capacity of 31.81 kips is almost exactly the capacity of one connector bar (half the design capacity), 29.63 kips. Complete failure occurred at 2.229-in. with the fracture of the second connector bar, which is also corroborated by the rise in strain after1-in. and sudden drop at 2.229-in., of the second bar (Figure 16). Hence it can be observed that the connector's ultimate capacity was approximately equal to the actual capacity of the connector. The connector performance is displayed in Figure 18.

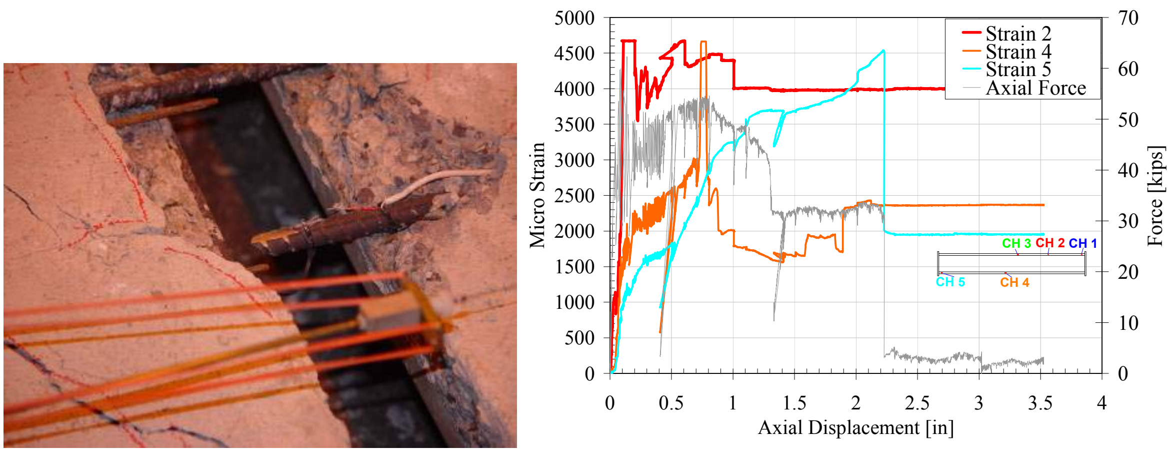


Figure 16: Pour Strip-MT: Damage state at 3.5-in tensile opening and Strain Data

**MTV**: The measured tensile capacity of the connector in combined tension and shear where $\Delta T/\Delta V = 2.0$, was 3% over the ultimate capacity and 17% over the design capacity according to PCI design standards. This peak capacity occurs at 0.121-in. tensile deformation, hence it does not only take into account the tensile strength of the connector bars, but also the strength of the topping with all the WWR wires still intact. However, the capacity is still greater than the design strength, which considers both the bars and WWR wires design strengths. Also at 0.121-in. the connector bars themselves may not have reached their ultimate design strength. Hence the total ultimate design strength of the WWR mesh and the connector bars' ultimate strength should not be added to yield the actual capacity. However, this peak capacity is greater than the design strength, which does consider the WWR wires design strength. After all the WWR wires fractured, a secondary peak of 57.01 kips (or 96% Pu) at 2.053-in. was observed. At 2.166-in. tensile deformation there was a drop in the load capacity corresponding to the fracture of one of the connector bars. The remaining capacity of 28.57 kips is approximately the capacity of one connector bar (half the design capacity), 29.63 kips. The force deformation curve for combined test was similar to the monotonic tensile test with the failure mechanism being exactly the same. However the combined test showed a higher ductility, which was due to local cracking and spalling close to the connector due to shear deformation. This is also corroborated by the strain data which shows that strain close to the center crack is high early in the test, but as the displacement increases beyond 1-in. the strain at the end of the bars also start to gradually increase (see Figure 17). This local concrete damage resulted in a longer un-bonded length of connector requiring a larger strain to fracture the connector bars, which resulted in the bars fracturing at larger deformation levels than in the monotonic test. Hence it can be observed that the connector's actual capacity was approximately equal to the ultimate capacity of the connector and higher than the design capacity. The connector performance is displayed in Figures 18 and 40.

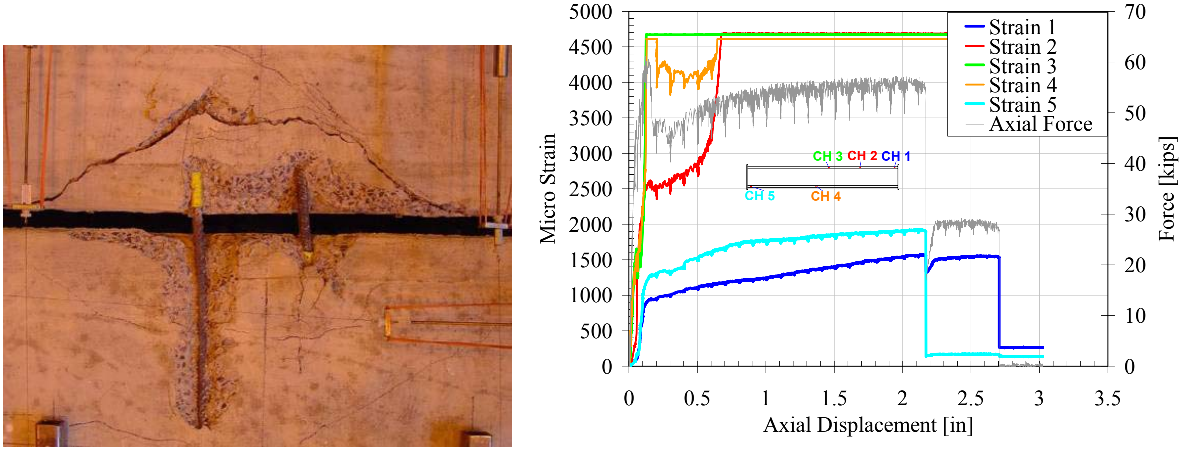


Figure 17: Pour Strip-MTV: Damage state at 1.3-in tensile opening and Strain Data

**CTC**: The measured capacity of the connector in pure tension was 6% over the ultimate capacity and 19% over the design capacity according to PCI design standards. This peak capacity occurs at 0.148-in. tensile deformation, hence it does not only take into account the tensile strength of the connector bars, but also the strength of the topping with all the WWR wires still intact. However, the capacity is still greater than the design strength, which considers both the bars and WWR wires design strengths. At 0.148-in. the connector bars themselves may not have reached their ultimate design strength. Hence the total ultimate design strength of the WWR mesh and the connector bars' design strength should not be added to yield the actual capacity. At the max deformation of 0.826-in. a number of the WWR wires were still intact, so no significant inferences can be made on how WWR failure affected the connector performance, or on the actual failure of the connector. However, it can be observed that early connector data follows the same force deformation curve as the monotonic tensile data, indicating that the cyclic deformation did not have any adverse effects on the load capacity of the connector. Hence it can be observed that for the available data, the connector's actual capacity was approximately equal to the ultimate capacity and higher than the design capacity of the connector. Connector data was not available after 0.826-in. when the test was prematurely stopped due to panel slippage at the boundary conditions. The connector performance is displayed in Figure 18.

**SUMMARY**: The previously developed backbone axial force-deformation curves of the connectors are presented in Figure 18. All load application methods result in a comparable tension response up to the peak capacity. The connector exhibits a stiff initial response up to fracture of the topping mesh. After fracture of the mesh a strength gain occurs most likely attributed to the strain hardening of the pour strip reinforcement. The addition of shear increases the un-bonded length of the bars, which results in a higher ductility and delayed strain hardening and fracture of the bars. Cyclic demands and additional shear actually improve the initial hardening. The connectors are able to maintain high tensile resistances at large deformation levels, with both the design and the ultimate capacities being exceeded. Even after fracture of one bar, the connector is still capable of maintaining moderate tensile resistance under significant joint openings. This level of resistance can contribute significantly to the overall joint flexural strength.

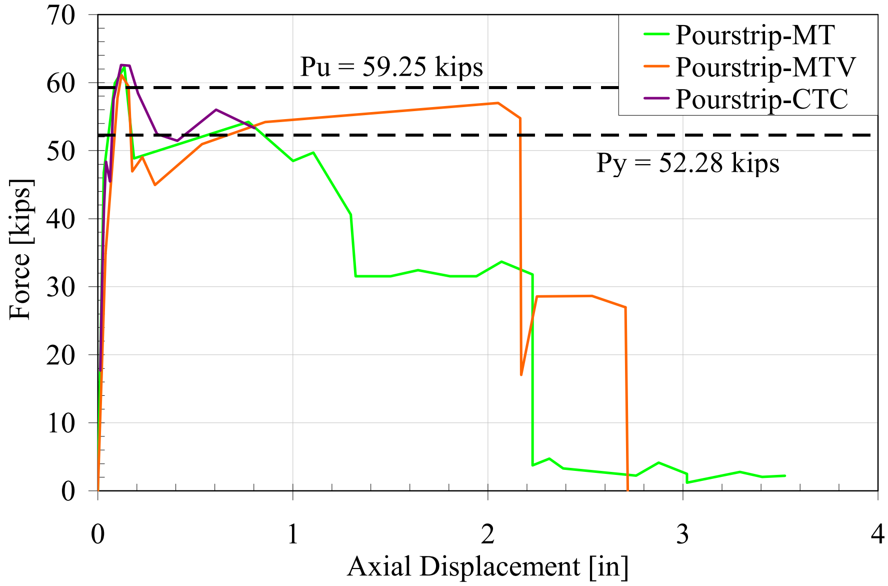


Figure 18: Pour-strip Tensile Data

## WWR Topping

**MT**: The measured capacity of the connector in pure tension was 4% over the ultimate capacity and 65% over the design capacity according to PCI design standards. The PCI estimated capacity of 23.67kips, which was calculated with the mill cert values of $f_u$, was the same as the capacity obtained from the wire test data at Ivy Steel & Wire Inc. (24 kips). The connector failed due to tensile fracture of the wires between 0.1-in. and 0.2-in. of joint opening (see Figure 19). This corresponds to the tensile strain capacity of the wire over a 10-in. gage length which is equivalent to the mesh spacing, which is also corroborated by the strain gage (strain 1) at the cross wire location experiencing a moderate amount of strain(Figure 19). Hence it can be observed that the mesh is fully activated between cross-wires. While the deformation capacity is limited it can be enhanced by using materials with higher ductility or a greater spacing between transverse wires. The load carrying capacity is predictable and also well above the design capacity. The connector performance is displayed in Figure 21.

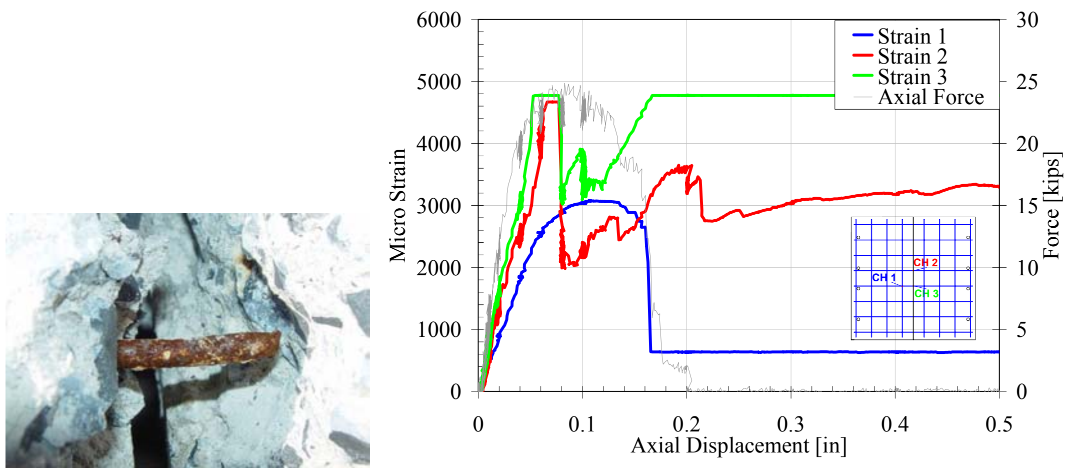


Figure 19: WWR-MT: Fractured Wire and Strain Data

**MTV**: The measured tensile capacity of the connector in combined tension and shear where ΔT/ΔV = 0.5, was 91% of the ultimate capacity and 45% over the design capacity according to PCI design standards. The connector failed due to fracture of the wires between 0.064-in. and 0.15-in, which was the expected failure mechanism (see Figure 20). The force deformation curve for the combined test was similar to the monotonic test, with the capacity and ductility slightly reduced. It is also interesting to note that the shear force in the connector was minimal; maxing out at about 2.24 kips, even though shear deformation was dominant. Hence it can be observed that the connector's design capacity was approximately equal to the ultimate capacity of the connector. Shear deformation caused a slight reduction in resistance and ductility but the capacity was still well above the design capacity. The connector performance is displayed in Figures 21 and 44.

Figure 20: WWR-MTV: Fractured Wire

**SUMMARY**: The previously developed backbone axial force-deformation curves of the connectors are presented in Figure 21. The connectors are able to achieve its ultimate capacity, surpass its design capacity, and it also displayed low ductility as expected. The action of added shear deformation resulted is slightly lower tensile resistance and ductility.

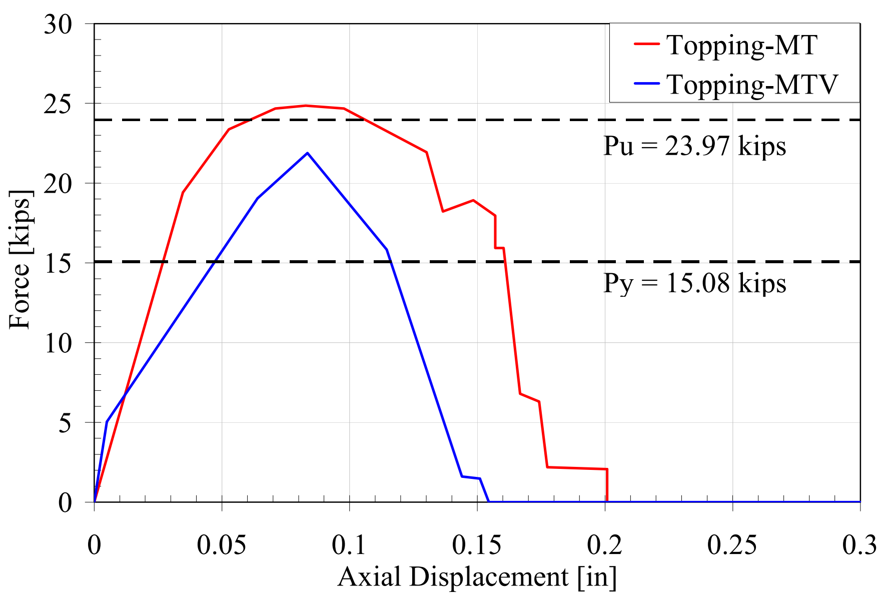


Figure 21: Topping Tensile Data

## COMPARATIVE SHEAR BEHAVIOR

The experimental data was compared to the expected connector ultimate shear strength. The shear strengths of the connectors were computed based on a simplified truss analogy in accordance with the PCI Design Handbook 5$^{th}$ edition Section 3.6.2, and with an ACI shear-friction model (ACI 318 Sec.11.7.4.3). This force-based design is a simple method to estimate the available capacities by ductile failure in the connector leg coupled with shear friction. It is assumed that the weld is adequately proportioned to resist the bar fracture strength and that forces are applied uniformly and concentrically to the connector.

For the splayed leg connectors (JVI & hairpin connectors), the tensile strength of the bar is used in conjunction with the truss model to determine the PCI design shear strength. The JVI connector's unique configuration allowed both the tensile and compressive legs to provide shear resistance, hence the ultimate tensile strength of both bars were used to determine the ultimate strength. The ultimate tensile strengths of both compressive and tensile legs also provided significant resistance in the topped hairpin and were both used in determining the design shear strength. Due to its flexibility and failure modes, the un-topped hairpin connector did not gain significant resistance from its compressive leg, and hence only the tensile leg was used in the design strength calculation.

For the perpendicular leg connectors (chord, pour-strip, cover plate connectors & topping) the tensile strength of the connector bars was used in conjunction with the ACI shear friction model (Section 11.7.4.1). For the topping connector tested in shear with $\Delta t$ = 0-in. two equations were used to determine the design shear strength. The first equation is the general shear friction model with the frictional contribution of the concrete included in the $\mu$ factor. The second equation (ACI 318 C11.7) gives more detailed calculations for the concrete contribution to the shear friction.

The shear friction coefficient, $\mu$ (ACI 11.7.3), was assumed to be 0.6 for un-topped hairpin, the pour-strip, and for the topping for all the topped connectors that had a 0.1-in. tensile gap, which simulating the ACI condition of concrete placed against hardened concrete not intentionally roughened. For the topping test with no tensile gap a value of $\mu$ = 1.4 was used to simulate the ACI condition of concrete placed monolithically, and for the chord connector $\mu$ = 0.7 was used to simulate concrete anchored to as rolled structural steel by reinforcing bars.

The formulation and resulting strengths calculated from the connector material properties are presented in Table 4. The following terminology is used: area of one bar leg: $A_s$, bar yield tensile strength: $f_u$, bar ultimate tensile strength: $f_u$, cross-sectional area of WWR: $A_{s\_wwr}$, WWR tensile yield strength: $f_{ywwr}$, area of concrete: $A_c$, $K_I$=400psi, and shear friction coefficient: $\mu$.

Table 5: Connector Ultimate Shear Strength by Calculation

| Connector | Formulation | Design $P_y$ [kips] | Ultimate $P_u$ [kips] | MV [kips] | MTV [kips] | CV [kips] |
|---|---|---|---|---|---|---|
| A: Pre-topped JVI | $2 \cdot (f_u \cdot A_s \cdot \cos 45°)$ | 16.50 | 32.00 | 35.87 | 27.40 | - |
| B: Pre-topped Chord | $2 \cdot (f_u \cdot A_s \cdot \mu)$ [μ = 0.7] | 36.05 | 41.47 | 56.90 | 34.91 | 63.80 |
| C: Un-topped Hairpin | $(f_u \cdot A_s \cdot \cos 45° \cdot \mu)$ [μ=0.6] | 5.10 | 7.80 | 8.74<br>8.58 | - | - |
| D: Topped Hairpin | $2 \cdot (f_y \cdot A_s \cdot \cos 45°) + f_{ywwr} \cdot A_{s\_wwr} \cdot \mu$ [μ=0.6] | - | 27.70 | 47.62<br>54.94 | 29.80 | 53.81 |
| E: Topped Cover Plate | $(2 \cdot (f_y \cdot A_s) + f_{ywwr} \cdot A_{s\_wwr}) \cdot \mu$ [μ=0.6] | - | 24.84 | 53.89 | 34.12 | 26.47 |
| F: Pour-strip | $(2 \cdot (f_y \cdot A_s) + f_{ywwr} \cdot A_{s\_wwr}) \cdot \mu$ [μ=0.6] | - | 34.20 | 34.60 | 9.40* | 17.06 |
| G: Topping w/ Δt = 0.1-in. | $f_{ywwr} \cdot A_{s\_wwr} \cdot \mu$ [μ=0.6] | - | 9.05 | 11.00 | 2.239* | - |
| G: Topping with Δt = 0 (equation 1) | $f_{ywwr} \cdot A_{s\_wwr} \cdot \mu$ [μ=1.4] | - | 21.11 | 43.79 | - | 19.04 |
| G: Topping with Δt = 0 (equation 2) | $0.8 \cdot f_{ywwr} \cdot A_{s\_wwr} + A_c \cdot K_1$ | - | 36.06 | | | |

*Note, failure controlled by tension

### JVI CONNECTOR

**MV**: The measured capacity of the connector in pure shear was 12% over the ultimate capacity according to PCI design standards. The connector's max load capacity was achieved at 0.767-in. where diagonal cracking occurred from the tension leg of the fixed panel to the supports (see Figure 22). It was also noted at this point that the compressive force in the connector reached its maximum value of 24.66 kips (see Figure A-2.2). As the compression forces in the connector decreased, so did the shear force, with the connector eventually failing due to concrete pullout failure cone at the connector's tensile leg. Therefore it can be inferred that the increase in the connector's shear capacity was directly related to its compressive force, which was a result of friction between the concrete and the connector. The PCI model that was used to obtain the ultimate capacity, however does not take into account the effects of the friction due to concrete-connector interaction, nor does it account for the concrete contribution to the shear stiffness. This results in a conservative estimate of the shear capacity of the connector, and hence the connector was able to exceed its ultimate strength. The connector performance is displayed in Figure 24.

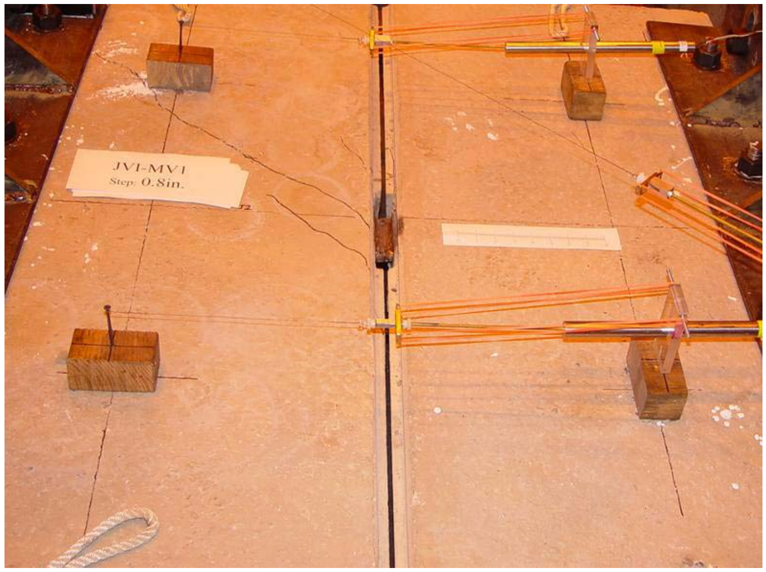

Figure 22: JVI-MV: Damage state at 0.8-in shear opening

**MTV**: The measured shear capacity of the connector in combined tension and shear where ΔT/ΔV = 0.5, was 86% of the ultimate capacity according to PCI design standards. The connector's max load capacity was achieved at 0.209-in. where local connector cracking occurred at the tension leg of the fixed panel (see Figure 23). It was also noted at this point that the compressive force in the connector reached its maximum value of 6.26 kips (see Figure A-3.3). This was followed by a drop in the shear about 18.90 kips, approximately 15% over the ultimate capacity, with the compressive force near zero. The shear force gained a second and third peak of 22.66 and 24.51 kips respectively, which were both followed by a drop in force due to tension leg pullout. The peaks were also accompanied by minimal axial forces between 2 kips tension and compression. The connector eventually failed due to concrete pullout failure cone at the connector's tensile leg. The combined test failed due to the same tension pullout mechanism as the pure shear test with almost the exact same ductility. However tensile pullout in this case occurred in smaller finite steps, rather than one big pullout failure, due to the combined tensile force with shear. Hence the connector had a smaller shear load peak, which was reached its peak earlier. Therefore it can be inferred that the increase in the connector's shear capacity was directly related to its compressive force, which was a result of friction between the concrete and the connector. The PCI model that was used to obtain the ultimate capacity does not take into account the effects of the friction due to concrete-connector interaction, nor does it account for the concrete contribution to the shear stiffness. However the combined tensile action was enough to reduce the capacity to just below the calculated ultimate capacity. The connector performance is displayed in Figures 8 and Figure 24.


Figure 23: JVI-MTV: Damage state at 0.4-in shear opening

**SUMMARY**: The previously developed backbone axial force-deformation curves of the connectors are presented in Figure 24. Due to high compressive forces at the joint and the associated friction the connector was able to surpass its predicted ultimate strength. The connector is capable of maintaining a high level of shear resistance under significant joint shear deformation; however an abrupt pullout failure of the tension leg occurred resulting in a loss in capacity under both pure shear and shear with combined tension conditions. The action of combined tensile deformation serves to reduce the compressive forces in the connector, hence reducing the resistance capacity. The connector's resistance is just below the calculated ultimate capacity, but the ductility and failure mode remains the same.

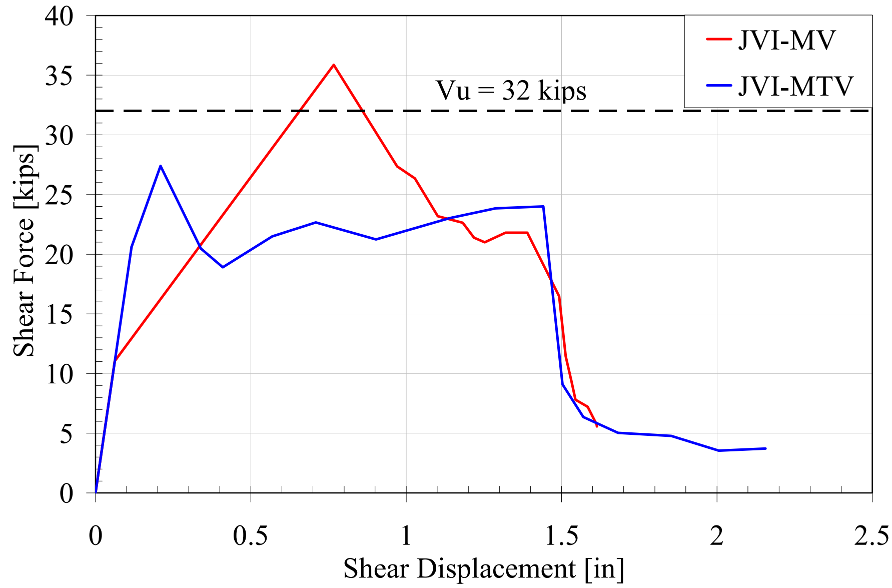


Figure 24: JVI Shear Data

## CHORD CONNECTOR

**MV**: The measured capacity of the connector in pure shear was 37% over the ultimate capacity according to PCI design standards. The connector's max load capacity was achieved at 0.131-in. where diagonal cracking occurred from the tension leg of the both panels to their respective supports (see Figure 25). It was also noted at this point that the compressive force in the connector reached its maximum value of 49.86 kips (see Figure B-2.2). Post peak behavior was characterized by a steep decline in both the shear and compressive forces in the connector. Both the axial and shear forces eventually leveled off at low load levels. Failure of the bars was not achieve due to deformation limits of the actuators. Therefore it can be inferred that the increase in the connector's shear capacity was directly related to its compressive force which was a result of friction between the concrete and the connector. The PCI model that was used to obtain the ultimate capacity, however does not take into account the effects of the friction due to concrete-connector interaction, nor does it account for the concrete contribution to the shear stiffness. This results in a conservative estimate of the shear capacity of the connector, and hence the connector was able to exceed its ultimate strength. The connector performance is displayed in Figure 28.

Figure 25: Chord-MV: Damage state at 0.3-in shear opening

**MTV**: The measured shear capacity of the connector in combined tension and shear where ΔT/ΔV = 0.5, was 84% of the ultimate capacity according to PCI design standards. The measured tensile capacity of the connector was about 57% of the ultimate capacity according to PCI ultimate standards. The connector's max shear load capacity was achieved at a shear deformation of 0.27-in. where diagonal cracking occurred from the tension leg of the both panels to their respective supports (see Figure 24). It was also noted that throughout the test, the connector was always in tension (see Figure B-3.2 and B-3.3). Post shear peak behavior was characterized by a steep decline in the shear force accompanied by a steep increase in the tensile force in the connector (see Figure 26-Combined Data). At a shear deformation of 0.89-in. the tensile connector bar in the free panel fractured after gaining a peak tensile force of 33.78 kips and was followed by a steep decline. Both the tensile and shear force eventually leveled off at low load levels of about 5 kips as a result of weld tearing and connector plate bending (see Figure 26). Failure of the second connector bar was not achieve due to deformation limits of the actuators. It can be observed that even though shear deformation was dominant, most of the shear resistance was due to steel concrete interaction prior to concrete cracking. Once concrete cracking at the tension legs occurred, the connector itself actually displayed more tensile resistance, which was characterized by the tensile peak at 0.89-in shear deformation. and its steep decline when the connector bar fractured. However, shear deformation did influence the post peak behavior, causing plate bending and weld tearing, which prohibited fracture of the second connector bar at maximum deformation levels. Both tensile and shear load deformation curves were similar to their respective monotonic tests, with both having smaller peak capacities at the same deformations as the monotonic tests, and the combined test showing less ductility compared to the monotonic tension test. The mechanisms that caused peak load behavior were also the same as the monotonic test. It can be inferred that even though there exists a complex interaction between the shear and tensile forces in the combined monotonic test, generally the action of combined forces tend to reduce the force magnitude in the force deformation curves of the connector when compared to their respective monotonic test. The connector performance is displayed in Figures 10 and Figure 28.

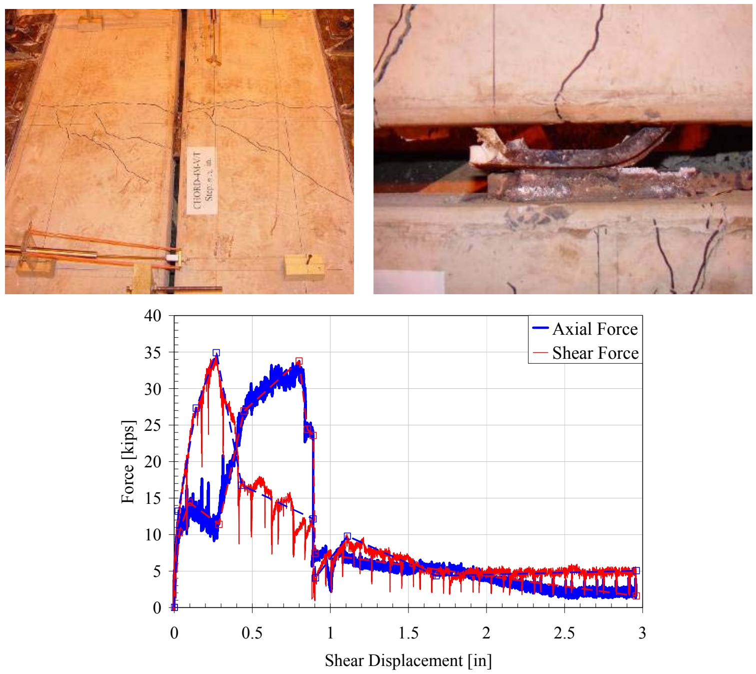

Figure 26: Chord-MTV: Damage state at 0.2-in and 3.0-in shear openings and Combined Data

**CV**: The measured capacity of the connector in cyclic shear was 54% over the ultimate capacity according to PCI design standards. The connector's max load capacity was achieved at 0.235-in. where diagonal cracking occurred on both panels to their respective supports (see Figure 27). It was also noted at this point that the compressive force in the connector reached its maximum value of 60.52 kips (see Table B-4.2). The max shear performance of the connector was higher than the monotonic test most likely due to a higher concrete strength of the cyclic specimen. Failure of one the connector bar occurred during the 0.96-in. deformation cycle, but the other bar could not be failed due to deformation limits of the actuators. The force deformation curve for the cyclic test was almost exactly the same as the monotonic test with post peak behavior characterized by a steep decline in both the shear and compressive forces in the connector and both eventually leveling off at low load levels. The connector was once again able to exceed its ultimate strength. The connector performance is displayed in Figure 28.

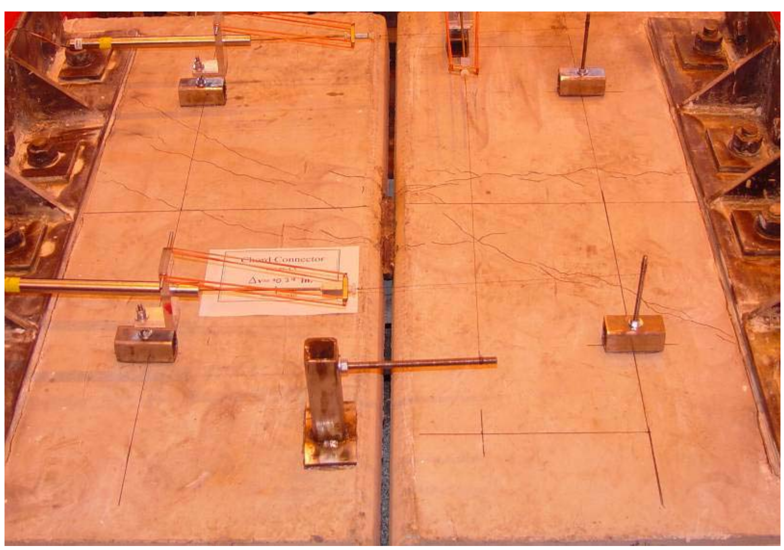
Figure 27: Chord-CV: Damage state at 0.24-in tensile opening

**SUMMARY**: The previously developed backbone axial force-deformation curves of the connectors are presented in Figure 28. Due to high compressive forces at the joint and the associated friction the connector was able to surpass its predicted ultimate strength. The chord exhibited a stiff initial response followed by diagonal cracking causing a reduction in compressive forces and a rapid softening. The addition of tension placed the connector in tension and reduced the load resistance to just below the calculated level, but had almost no effect on the ductility of the connection. Cyclic action seemed to have little effect on the connector's shear response. In all cases, the deformation capacity was minimal with a loss in capacity prior to 1-inch. The measured shear strengths were generally higher than the estimated ultimate strength.

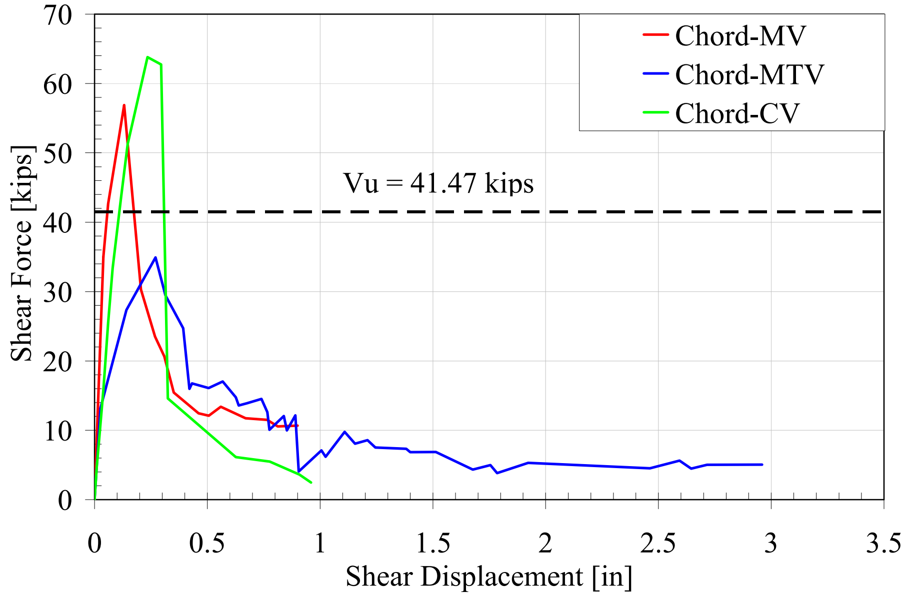


Figure 28: Chord Shear Data

**HAIRPIN CONNECTOR**

**Un-topped MV**: The measured capacities of the connectors tested in pure shear were 12% and 10% over the ultimate capacity according to PCI design standards. Both connectors had almost the exact same load-deformation curves and failure modes, which indicate that the tests had near perfect repeatability. The connectors' max load capacities were achieved at 0.127-in. and 1.298-in. where pullout of the tension leg in the fixed panel occurred (see Figure 29). Pullout occurred due to the short anchorage length of the connector bars in the panels of approximately 14-in. This anchorage length was due to the placement of the connector in the 2-in. thick panel, which left 4-in. of the 18-in. leg close to the bend being exposed. The shear resistance by the compression leg was observed to be minimal, further corroborated by the strain data (Figure 25), and was not included in the ultimate strength calculation. The resulting ultimate capacity hence correctly assumes almost no concrete contribution ($\mu$ = 0.6) and that shear resistance is basically provided by dowel action of the connector's tensile bar. Hence the connector shear resistance was approximately equal to its ultimate strength. The connector performance is displayed in Figure 33.

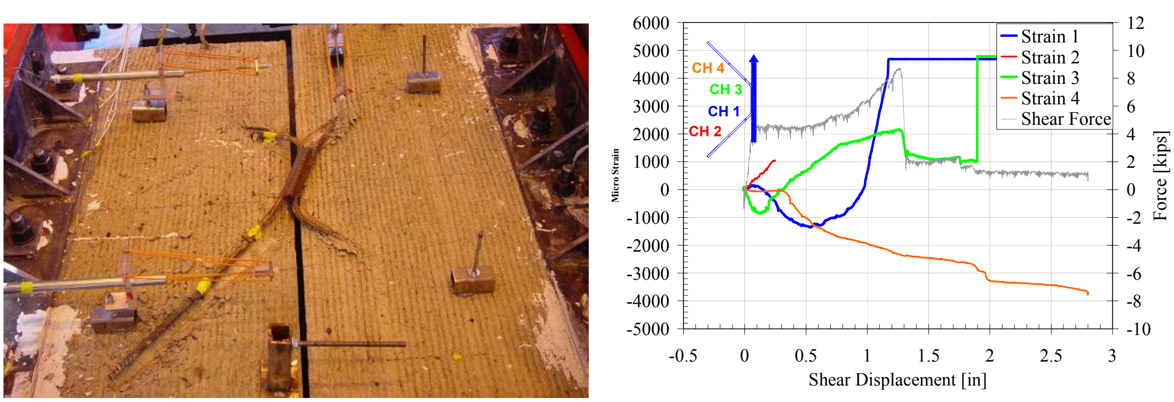


Figure 29: Un-topped Hairpin-MV: Damage state at 1.4-in shear opening & Strain Data

**Topped MV**: The measured capacities of the connectors tested in pure shear were 71% and 98% over the ultimate capacity according to PCI design standards. Both connectors had almost the exact same load-deformation curves and failure modes, which indicate that the tests had near perfect repeatability. The connectors' max load capacities were achieved at 0.206-in. and 0.342-in. where diagonal cracking occurred from the connectors' tensile legs to both supports (see Figure 30). Unlike the un-topped case, the topping produced a consistent force demand in the connector legs. The strain measurements (Figure 30) indicate that the compression leg yielded in compression and the tension leg yielded in tension. The tension yield of the bar progressed along the embedded length, reaching yield at approximately 1-in. of shear deformation. It was also noted at this point that the compressive force in the connector reached its maximum value of 17.84 kips and 24.87 kips respectively (see Figures D-2.2 & D-3.2). Post peak behavior was characterized by a steep decline in both the shear and compressive forces in the connector, with both the shear force leveling off about 6 kips below the ultimate capacity of 27.70 kips, and the axial forces actually going into low tension of about 2-3 kips. Failure was as a result of fracture of the connector's tensile bar at approximately 2.83-in. Therefore it can be inferred that the increase in the connector's shear capacity was directly related to its compressive force, which was a result of friction between the concrete and the connector. This is also corroborated by the fact that at low axial forces the connector's capacity is slightly less than the ultimate strength. The ACI model that was used to obtain the ultimate capacity does not take into account the effects of the friction due to concrete-connector interaction. This results in a conservative estimate of the shear capacity of the connector, and hence the connector was able to exceed its ultimate strength. The connector performance is displayed in Figure 33.

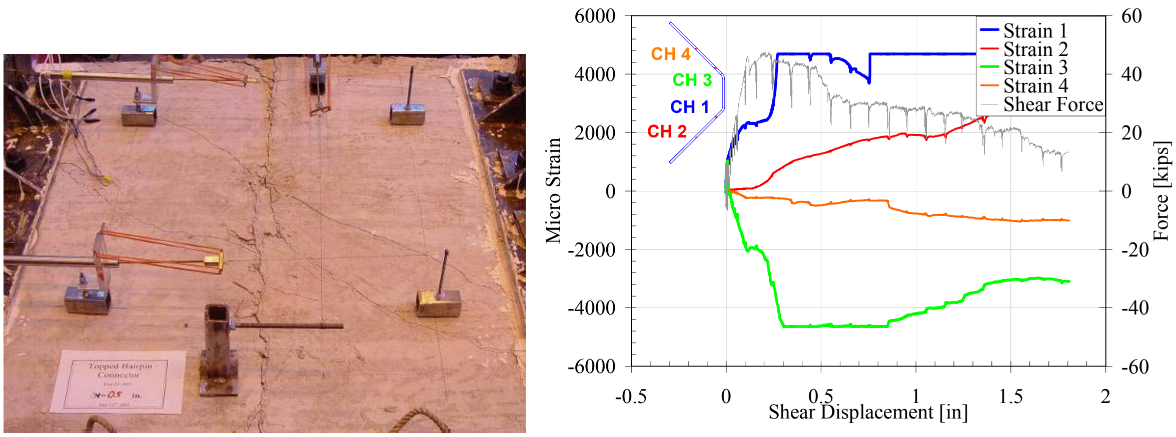

Figure 30: Topped Hairpin-MV: Damage state at 0.5-in shear opening and Strain Data

**Topped MTV**: The measured shear capacity of the connector in combined tension and shear where $\Delta T/\Delta V = 0.5$, was 8% over the ultimate capacity according to PCI design standards. The measured tensile capacity of the connector was about 88% of the ultimate capacity according to PCI design standards. The connector's max shear capacity was achieved at 0.206-in. shear deformation where complete fracture of the WWR wires occurred. It was also noted at this point that the axial force in the connector reached its maximum value of 22.65 kips and 24.87 (see Figures D-4.2 & D-4.3). Post peak behavior was characterized by a steep decline in the shear by about 9 kips, and also a total loss in tensile capacity of the connector. The connector's tensile bar in the free panel fractured at 0.273-in. resulting in another sharp decline in the connector's tensile capacity to about 5 kips (see Figure 31). Post fracture behavior was characterized by a gradual reduction in shear force to about 1.5 kips due to tearing of the weld. It can be inferred that the initial 9-kip drop in the shear force was solely due to loss of the WWR wires' shear capacity, which was approximately equal to the observed topping shear strength of 11 kips (see Table 5). This is also reinforced by the tensile force deformation curve following the exact same peak data as the monotonic topped test. The failure mechanism for the test was the same as for the monotonic shear topped tests and this was reflected by post bar fracture data following the monotonic shear force deformation curves. The connector's shear force deformation curve is similar to the monotonic shear test, with peak capacities significantly lower (about 50%) and a reduced ductility, due to earlier tensile bar failure. With the absence of compressive forces, it can be observed that this reduction in the capacity results in the shear resistance almost equaling the calculated ultimate strength. It can be inferred that even though there exists a complex interaction between the shear and tensile forces in the combined monotonic test, generally the action of combined forces tend to reduce the force magnitude in the force deformation curves of the connector when compared to their respective monotonic test. However, the shear capacity of the connector is approximately equal to the calculated ultimate strength. The connector performance is displayed in Figures 13 and 33.

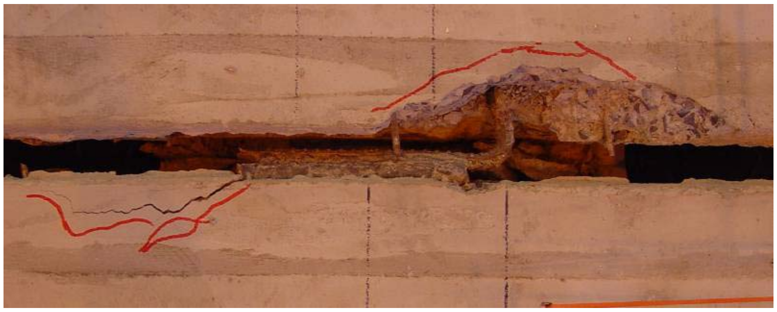

Figure 31: Topped Hairpin-MTV: Damage state at 2.0-in tensile opening

**Topped CV**: The measured capacity of the connector in cyclic shear was 94% over the ultimate capacity according to PCI design standards. The connector's max load capacity was achieved at 0.476-in. where diagonal cracking from the connector to the supports and fracture of the WWR wires occurred (see Figure 32). It was also noted at this point that the compressive force in the connector reached its maximum value of 18.75 kips (see Table D-5.2). Post peak behavior was characterized by a steep decline in both the shear and compressive forces in the connector, with failure occurring soon after as a result of fracture of the connector's tensile bars at the 0.683-in. shear deformation cycle. The force deformation curve for the cyclic test was almost exactly the same as the monotonic test except that failure occurred much earlier, reducing the connector's ductility significantly to approximately 1-in., as opposed to 2.8-in. for the monotonic test. The failure mechanism was also similar with fracture of the tensile bar occurring at a much smaller deformation, and with both bars fracturing in tension at the opposite phases of the shear cycle. The connector was again able to exceed its ultimate strength. The connector performance is displayed in Figure 33.

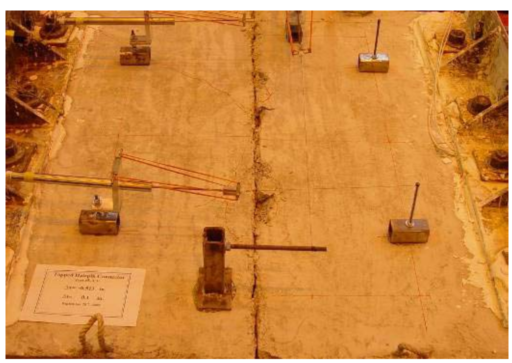

Figure 32: Topped Hairpin-CV: Damage state at 0.513-in shear opening

**SUMMARY**: The previously developed backbone axial force-deformation curves of the connectors are presented in Figure 33. The un-topped connectors displayed very low shear capacities as expected, as well as low levels shear resistance under significant joint shearing. Due to high compressive forces in the connector the topped connectors were able to surpass its predicted ultimate strength. The topped connectors are capable of maintaining a high level of shear resistance under significant joint opening, but connector failure is very abrupt with almost all load capacity lost. The action of combined tensile deformation serves to reduce the shear resistance capacity and the ductility of the connector. The connector's resistance is now approximately equal to the calculated ultimate capacity, but the failure mode remains the same. Cyclic action did not affect peak capacity but it did cause a reduction in the ductility due to early failure.

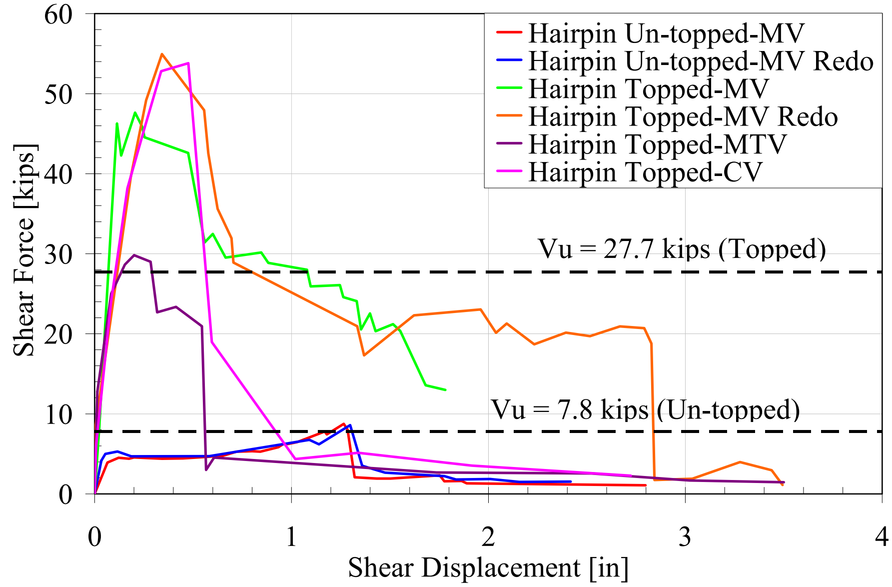


Figure 33: Hairpin Shear Data

### COVER PLATE CONNECTOR

**MV**: The measured capacity of the connector in pure shear was 117% over the ultimate capacity according to ACI design standards. The connector's max load capacity was achieved at 0.338-in. where diagonal cracking occurred from the tension leg of the both panels to their respective supports (see Figure 34). It was also noted at this point that the compressive force in the connector reached its maximum value of 31.96 kips (see Figure E-2.2). Post peak behavior was characterized by a steep decline in both the shear and compressive forces in the connector, with the shear force approximately 17 kips, and the axial forces actually going into low tension of about 13-15 kips. Therefore it can be inferred that the increase in the connector's shear capacity was directly related to its compressive force, which was a result of friction between the concrete and the connector. Once diagonal cracking occurred there was a release in this concrete-connector frictional interaction, resulting in the drastic drop in connector performance. This is also evident in the strain data, which shows that after this concrete contribution has been lost at 0.338-in. the strain in the connector bars start to increase drastically from a prior moderate level of strain. The ACI model that was used to obtain the ultimate capacity does not take into account the effects of friction due to concrete-connector interaction, only the dowel action of the connector legs and the shear friction of the topping. Failure was as a result of fracture of the connector's tensile bar at approximately 0.897-in. and compressive bar at 2.84-in. This results in a conservative estimate of the shear capacity of the connector, and hence the connector was able to exceed its ultimate strength. The connector performance is displayed in Figure 37.

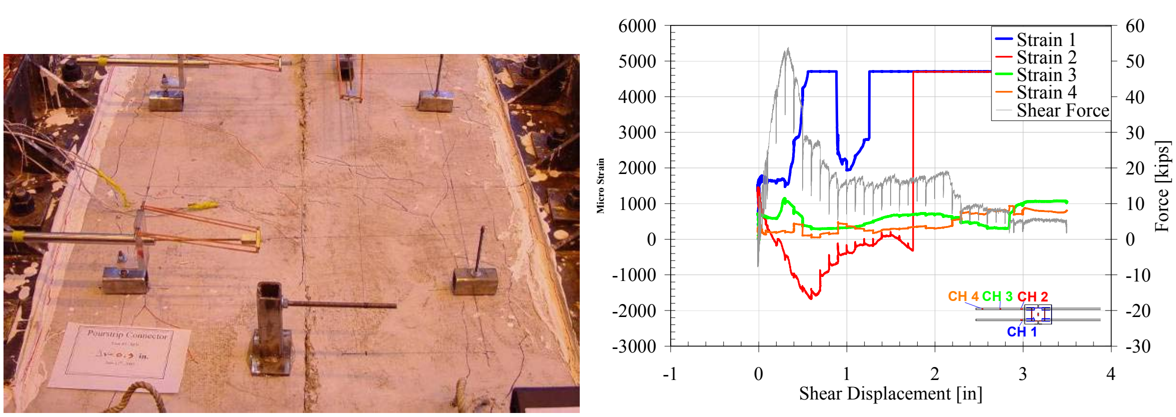


Figure 34: Cover Plate-MV: Damage state at 0.3-in shear opening and Strain Data

**MTV**: The measured shear capacity of the connector in combined tension and shear where $\Delta T/\Delta V = 0.5$, was 38% over the ultimate capacity according to ACI design standards. The measured tensile capacity of the connector was about 77% of the ultimate capacity according to PCI design standards. The connector's max load capacity was achieved at 0.179-in. where diagonal cracking occurred from the tension leg of the both panels to their respective supports (see Figure 35). It was also noted at this point that there was a temporary decline in the tensile force from 28.17 kips to 9.47 kips (see Figures E-3.2 and E-3.3). Post peak behavior was characterized by a steep decline in the shear force to approximately 7 kips and a steep increase in the tensile force to 24.22 kips. Loads were maintained at these levels until fracture of the tensile connector bar in the fixed panel occurred, which dropped the tensile load capacity to about half (12.5 kips) and the shear force to about 2.5 kips. Loads were again maintained at these levels until fracture of then tensile connector bar in the free panel occurred, dropping the compressive force to 3.5 kips and the shear force to 0 kips. Complete failure and total loss of load was as a result of fracture of the connector compressive bar in the fixed panel at approximately 3-in. The shear load deformation curve was similar to the monotonic shear curve with the connector exhibiting less ductility and a lower capacity, which was closer to the ultimate strength and most likely due to the absence of compressive forces in the connector. It can also be noted this sudden peak in shear force was accompanied by a complementary dip in the tensile force, reconfirming the idea that the shear capacity is directly related to compression in the panel/connector. The tensile load deformation curve was also similar to the monotonic tension test, with the tensile capacity significantly reduced, and fracture of the second tensile bar occurring at the same fracture deformation in the monotonic test. The failure mechanism was different from either monotonic test, with fracture first occurring in the tension legs in each panel, which allowed for rotation of the connector slug. This rotation then led to severe bending of the remaining leg, which coupled with increasing tensile deformation, caused tensile fracture. This allowed for a final low load ductile phase in the tension curve, after the monotonic fracture deformation level. It can be inferred that even though there exists a complex interaction between the shear and tensile forces in the combined monotonic test, generally the action of combined forces tend to reduce the force magnitude in the force deformation curves of the connector when compared to their respective monotonic test. Hence it can be inferred that the connector was slightly higher than its ultimate strength. The connector performance is displayed in Figures 15 and 37.

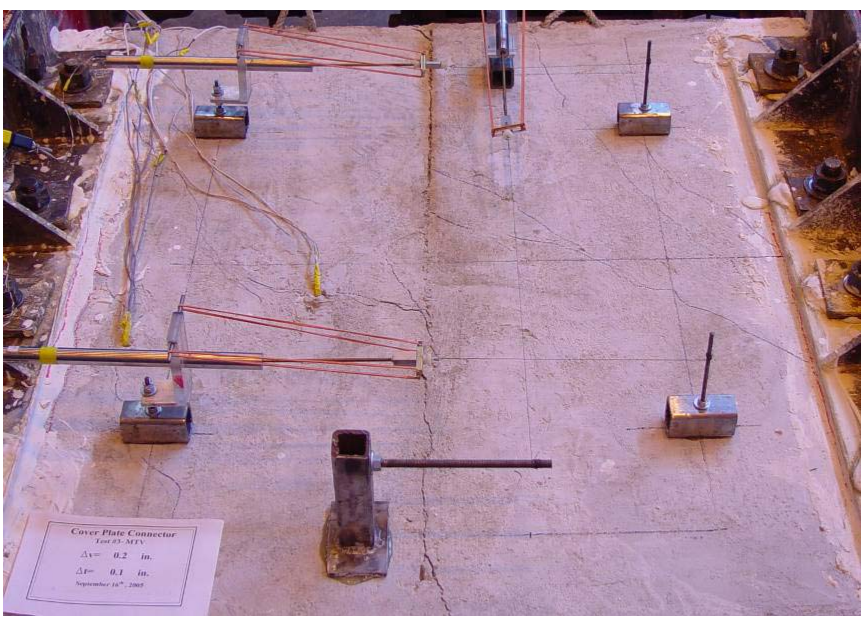


Figure 35: Cover Plate-MTV: Damage state at 0.2-in shear opening

**CV**: The measured capacity of the connector in cyclic shear was 7% over the ultimate capacity according to ACI design standards. The cyclic shear application resulted in a significant reduction in the shear strength of the connection in comparison to the monotonic load application. The connector's max load capacity was achieved at 0.162-in. where local cracking occurred around the connector plates (see Figure 36). It was also noted at this point that the connector was in tension (see Table E-4.2). Post peak behavior was characterized by a decline in the shear force until it leveled out at less than 4 kips. Failure was as a result of tensile fracture of the connector bars at the 0.507-in. shear deformation step with the load levels at approximately 20 kips prior to fracture, which is approximately 80% of the ultimate capacity. The load deformation curve was similar to the monotonic shear curve, with the connector exhibiting less ductility and a lower load level due to the absence of compressive forces in the connector. If you compare the axial force generated on the monotonic and the cyclic shear cases (Fig. E.2.2 with E.4.3) it can be observed that under cyclic load application the connection does not accumulate elevated compression forces. This can probably be attributed to cyclic action causing cracking around the connector, hence reducing the friction between the connector and the panel. This cyclic action also serves to reduce the topping shear friction component of the shear force, since the repeated cycles would increase the smoothness of the interface by repeated shearing of concrete protrusions. The maximum shear force resistance was lower than the monition and the combined test. Hence it can be inferred that the connector was approximately equal to its ultimate strength. The connector performance is displayed in Figure 37.

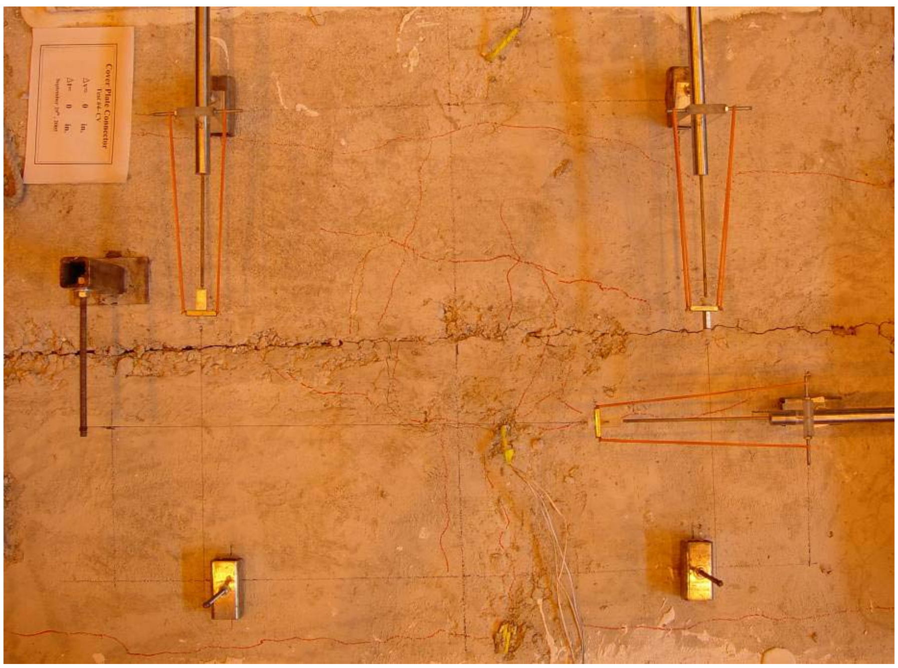

Figure 36: Cover Plate-CV: Damage state at 0.196-in shear deformation cycle

**SUMMARY**: The previously developed backbone axial force-deformation curves of the connectors are presented in Figure 37. Due to high compressive forces in the connector that indicates high levels of friction between the concrete and the connector, the connector tested under monotonic shear was able to surpass its predicted ultimate strength. In all cases the connector exhibited a stiff initial response followed by concrete cracking causing a reduction in compressive forces and a rapid softening. The connector is still capable of maintaining a moderate level of shear resistance under significant joint shearing; even after single bar failure occurs. When tested in combined tension, it produced a decrease in the connection capacity from that of the pure shear loading as a result of a lack of compressive demand. Additional tension also changed the ultimate failure mode from fracture of the two bars in the free panel, to fracture of the two diagonally opposite tensile bars, with complete failure from fracture of one of the remaining bars. Cyclic loading resulted in a minimal amount of axial demand on the connection, as well as a reduction in the shear friction of the topping, which led to a lower capacity and ductility. In all cases the load capacities was in excess of the calculated ultimate strength.

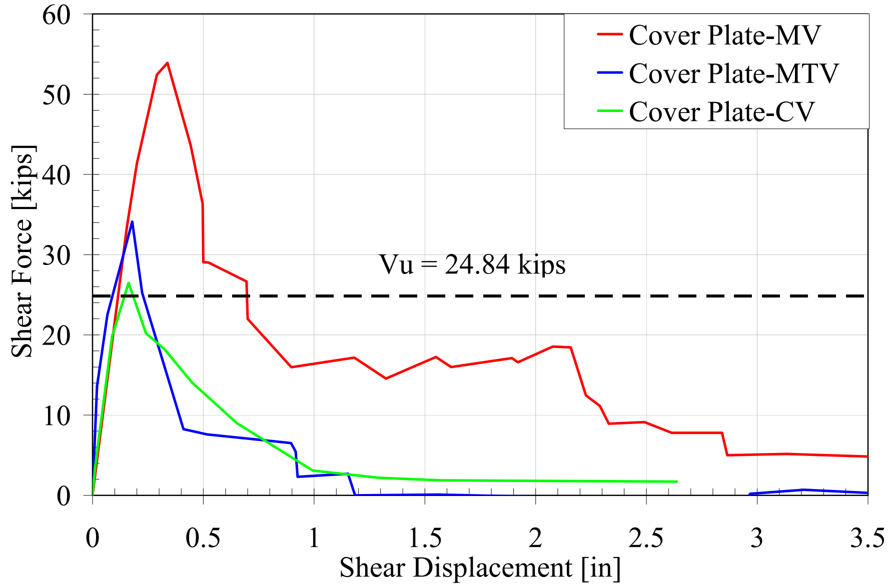


Figure 37: Cover Plate Shear Data

### POUR-STRIP CONNECTOR

**MV**: The measured capacity of the connector in pure shear was about 1% over the ultimate capacity according to ACI design standards. The connector's max load capacity was achieved at 0.365-in. where local connector cracking and fracture of the WWR wires occurred. It was also noted at this point that the connector is in tension (see Figure F-2.2). Fracture of the WWR wires continued from 0.3-in. to 1.5-in. Post peak damage also included local cracking and spalling at the connector bar locations at the panel center crack location. Fracture of the connector bars did not occur, and the test was limited by the deformation capacity of the actuators. The shear capacity of the specimen was close to its ultimate capacity just before fracture of the WWR wires. Post wire fracture load levels reduced to about 15 kips at which point significant concrete cracking had occurred. Once the concrete spalling exposed the connectors at 0.5-in, it was noticed that the bars were actually deforming laterally based on its free un-bonded length (see Figure 38). As the shear deformation increase, further cracking and spalling increased this un-bonded length. It can be inferred that there was a certain amount of un-seen, but audible, concrete cracking around the connector bars location. With the fracture of the WWR wires this cracking became more severe, which increased the un-bonded length of the connector. Since this length continually increased the bars were never able to achieve the strain required to increase their shear capacity or even attain fracture. This is further corroborated by the strain data which display only moderate levels of strain at the interface, and almost no strain at the end of the connector bars (figure 36). The max load that was achieved was in part due to the shear capacity of the topping, but still mainly due to the capacity of the bars, which had minimal un-bonded length at this shear deformation. Hence the connector was equal to its ultimate strength. The connector performance is displayed in Figure 40.

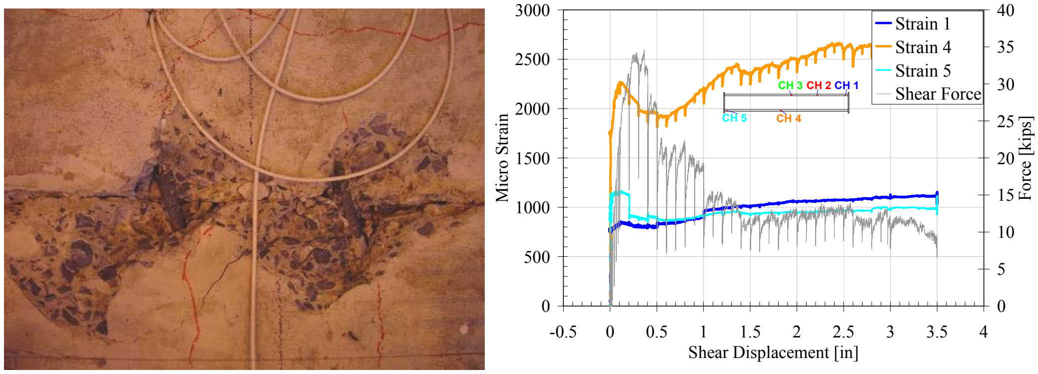

Figure 38: Pour Strip-MV: Damage state at 1.0-in shear opening and Strain Data

**CV**: The measured capacity of the connector in cyclic shear was 50% of the ultimate capacity according to ACI design standards. The connector's max load capacity was achieved at 0.091-in. where local connector cracking occurred. It was also noted at this point that the connector is in tension (see Table F-4.2). Post peak behavior included fracture of the WWR wires from 0.3-ib to 0.6-in. and extensive local cracking and spalling over the connector bars. Fracture of the connector bars did not occur, and the test was limited by the deformation capacity of the actuators. Post wire fracture levels dropped to about 10 kips at which point significant concrete cracking had occurred. Once the concrete spalling exposed the connectors at 0.186-in, it was noticed that the bars were actually deforming laterally based on its free un-bonded length (see Figure 39). As the shear deformation increase, further cracking and spalling increased this un-bonded length, which was significantly exacerbated by cyclic action. Basically the same series of events can be inferred as in the monotonic shear test, but with the cyclic action, the mechanisms formed at lower deformations and with increased effect. Hence the connector was not able to achieve its ultimate strength. The connector performance is displayed in Figure 40.


Figure 39: Pour Strip-CV:  Damage state at 1.16-in shear deformation cycle

**SUMMARY**: The previously developed backbone axial force-deformation curves of the connectors are presented in Figure 40.  The shear portion of the MTV test is included for comparison although the connector failed in a tensile mode and its discussion is presented in the tensile comparison section. The estimated shear capacity of the connection assumes that both the chord reinforcement and topping wires are active in transferring the shear from panel to panel.  The model provides an accurate estimate of the capacity of the monotonic response.  During cyclic loading however, damage is progressively incurred on both sides of the chord reinforcement creating a de-bonded region. This loss in bond results in a decrease in the peak shear capacity of the connection. While the initial stiffness is still comparable to that of the monotonic response the strength can be more accurately approximated by the calculated ultimate capacity of the topping WWR of 9.05 kips, which gives a lower bound estimate for conservative behavior.

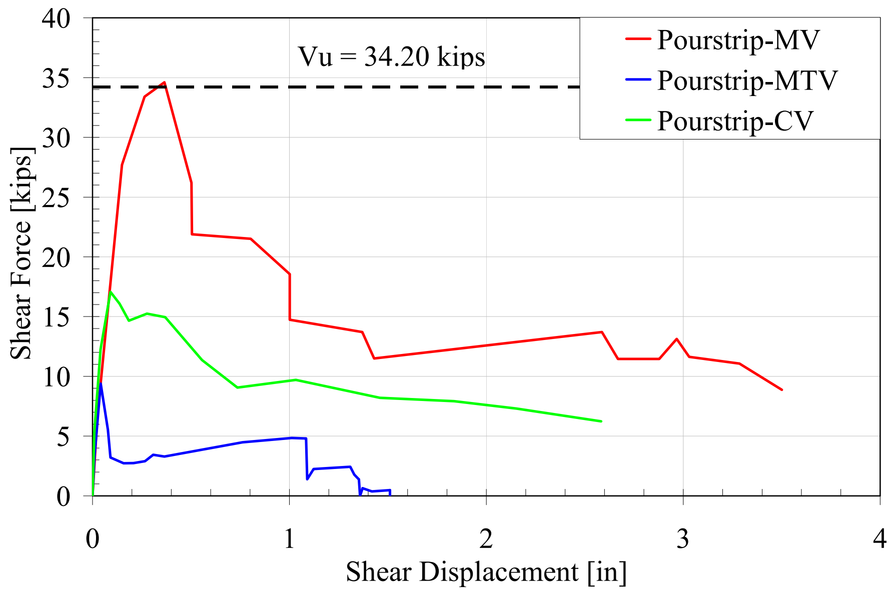


Figure 40: Pour-strip Shear Data

## TOPPING

**MV (Δt = 0.01-in)**: The measured capacity of the connector in pure shear was approximately 22% over the ultimate capacity according to ACI design standards. The connector's max load capacity was achieved at 0.372-in. where fracture of the WWR wires began. It was also noted at this point that the connector is in tension, so there was no increase in shear force due to compression in the connector (see Figure G-2.2). Resistance is provided by dowel action of the WWR with almost no concrete contribution, which can be inferred from the high early levels of strain in the WWR at the connector interface (figure 41). The connector failed due to fracture of the WWR wires between 0.3-in. and 0.4-in, which was the expected failure mechanism. Hence it can be observed that the connector's ultimate capacity was approximately equal to the measured capacity of the connector. The connector performance is displayed in Figure 44.

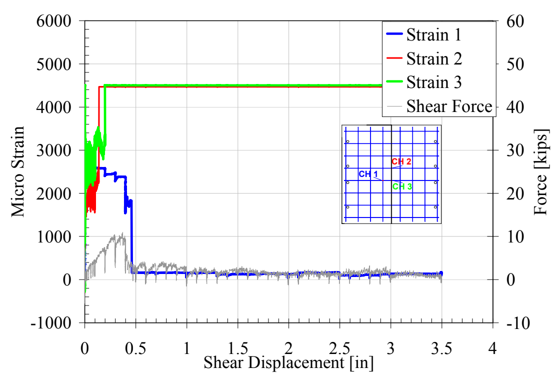


Figure 41: Topping-MV (Δt = 0.01-in): Strain Data

**MV (Δt = 0-in)**: The measured capacity of the connector in pure shear was approximately 107% over the ultimate capacity when using equation 1 in Table 4, and 21% over the ultimate capacity when using equation 2 according to ACI design standards. The connector's max load capacity was achieved at 0.25-in. where some diagonal panel cracking at the end of the panel occurred (see Figure 42). It was also noted at this point that the compressive force in the connector reached its maximum value of 46.90 kips (see Figure G-3.2). Therefore it can be inferred that the increase in the connector's shear capacity was directly related to its compressive force. Theses high force was mainly due to resistance to the shearing off of protrusions on the center crack face, which was released once cracking occurred. Some resistance is provided by dowel action of the WWR but the concrete contribution is considerable which can be inferred from the lower early levels of strain in the WWR at the connector interface in comparison to the monotonic test with Δt = 0.1-in (figure 41 & 42). Connector failure was as a result of fracture of the WWR wires between 0.4-in. and 1.5-in, which was the expected failure mechanism. The equation 1 ACI shear friction model that was used to obtain the ultimate capacity does not accurately account for the concrete bearing contribution to the shear stiffness. The equation 2 ACI shear friction model has a separate component that more accurately calculates the shear resistance provided by the concrete, and does a better job in capturing the concrete contribution. This results in a conservative estimate of the shear capacity of the topping utilizing equation 1, and a more accurate, although still conservative, estimate of the shear capacity of the topping utilizing equation 2. The connector performance is displayed in Figure 44.

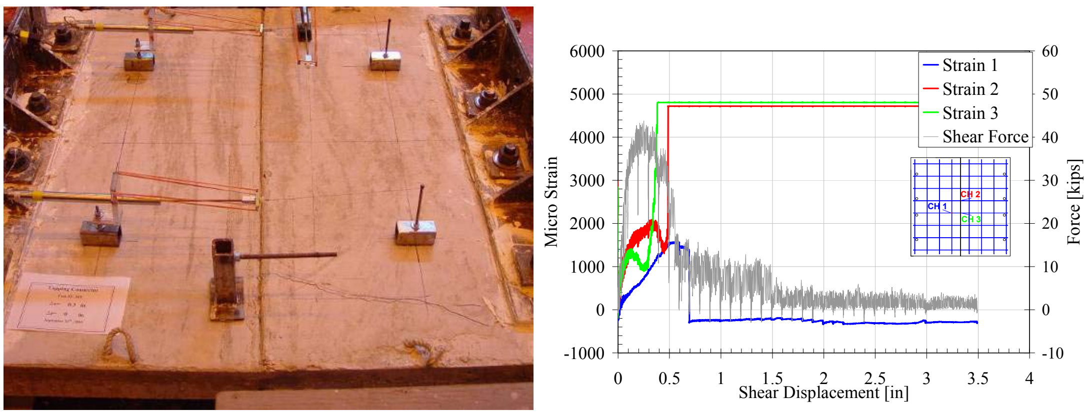


Figure 42: Topping-MV (Δt = 0-in): Damage state at 0.3-in shear opening & Strain Data

**CV**: The measured capacity of the connector in cyclic shear was approximately 90% of the ultimate capacity when using equation 1 in Table 4, and 53% of the ultimate capacity when using equation 2 according to ACI design standards. The connector's max load capacity was achieved at 0.084-in. where diagonal cracking at the end of the panel occurred. It was also noted at this point that the connector achieves its maximum compression of 11.88 kips at this displacement level (see Table G-5.2). There was a considerably smaller compressive force generated at the crack interface, since the diagonal cracking at the end of the panel was much less severe than in the monotonic test with no gap at the center. The cracking also resulted in early block shear/spalling of the concrete at the diagonal crack at 0.113-in. (see Figure 43). This resulted in a complementary reduction of shear force when compared to the monotonic test. It can be assumed that the panel center crack interface was too smooth to generate shear forces as high as the equation 1 or equation 2 ultimate capacities, which assumes a much rougher interface, but still rougher than when there is a 0.1-in. gap between panels. Connector failure was as a result of fracture of the WWR wires between 0.1-in. and 0.7-in, which was the expected failure mechanism. The connector was not able to achieve its ultimate strength. The connector performance is displayed in Figure 44.

Figure 43: Topping-CV (Δt = 0-in): Damage state at 0.113-in shear deformation cycle

**SUMMARY**: The previously developed backbone axial force-deformation curves of the connectors are presented in Figure 44. The shear portion of the MTV test is included for comparison although the connector failed in a tensile mode and its discussion is presented in the tensile comparison section. The connectors' peak performance was based heavily on the assumed center crack interface conditions. For the monotonic test with a 0-in. gap, the interface conditions assumed as monolithically placed concrete was also accurate enough so that the shear resistance was slightly higher than the ultimate strength (when utilizing the more accurate equation 2 method). Pre-cracking of the connection to a 0.1-in. gap results in a significant decrease in stiffness and the shear strength of the connection, allowing the capacity be accurately approximated using ACI formulations with μ of 0.6. For the cyclic shear test with 0-in. gap, the interface was observed to be much smoother than the assumed monolithically placed concrete, and still slightly rougher than an un-roughened surface, so the peak shear resistance lies in between ultimate strength for the two assumed conditions. Cyclic loading produces an initial stiffness equal to that of the monotonic condition even though the capacity of the connection is significantly reduced. All connectors displace very low ductility with loss of significant capacity prior to 1-in. and almost no shear resistance after failure. For floor diaphragms with relatively stiff flange to flange connections (i.e., cover plate) the mesh will most likely remain undamaged under normal service loads. For this case it would be appropriate to account for the mesh using the ACI formulation with μ of 0.6.

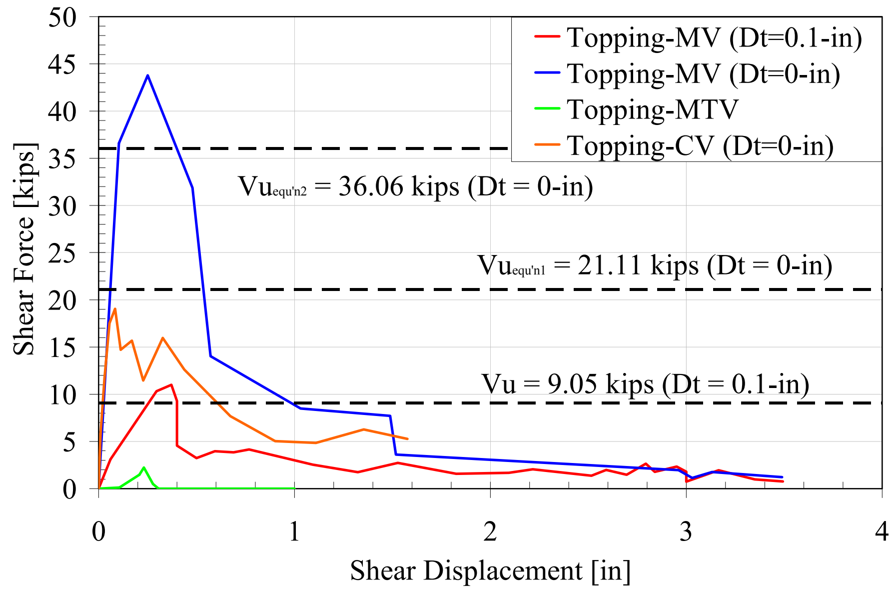


Figure 44: Topping Shear Data

## CONCLUSIONS

From the experimental study of double tee flange to flange connectors the following conclusions can be made:

### GENERAL CONCLUSIONS

**Tension**

- The splayed leg connectors such as a hairpin and JVI exhibited a flexible tensile response. The connectors achieved large tensile openings in excess of 1-in. prior to strength loss; however, they were not able to achieve their design strength capacity. This was due mainly to weld damage as a result of stress concentrations cause by flexibly plate or bar deformations.
- The straight leg connectors in comparison exhibited a high initial tensile stiffness, but were capable of only limited ductility, except for the pour strip connector which exhibited ductility closer to that of the steel connector bars. Nevertheless, in most cases the straight leg connectors were able to achieve or exceed their tensile design strength, when the full tensile strength of the connector bars was properly engaged. The chord connector, however, was subject to the same weld damage as in the splayed connectors and subsequently did not achieve its design capacity.
- The cast-in-place topping conforms to the expected capacity of the wires in strength and deformation according to the WWR material properties. The concrete has no contribution to the tensile strength, with the full 10-in. length between cross wires being engaged. The strength of the topping is additive between un-topped and topped test.

**Shear**

- The splayed leg connectors such as a hairpin and JVI exhibited a flexible shear response. The connectors achieved large tensile openings in excess of 1-in. prior to strength loss and they were able to achieve or exceed their design strength capacity. Max shear performance was accompanied by high compressive forces in the connector prior to diagonal concrete shear cracking, which was due concrete connector friction interaction.
- The straight leg connectors in comparison exhibited a high initial tensile stiffness, and were still able to achieve large tensile opening around 1-in. or more, prior to significant strength loss. In most cases the straight leg connectors were easily able to surpass their design strengths. Max shear performance was accompanied by high compressive forces in the connector prior to diagonal concrete shear cracking, which was due concrete connector friction interaction.
- The cast-in-place topping conforms to the expected capacity of the wires in strength based on accurate assumption of the interface conditions. Concrete has no significant contribution under 0.1-in. gap conditions but under zero gap conditions its contribution is significant.

### CONNECTOR SPECIFIC CONCLUSIONS

**JVI**

- The JVI splayed leg proprietary connection provides a tensile strength well below the calculated design capacity but a high ductility with tensile deformations surpassing 2-in. The tensile capacity was limited by weld fracture due to stress concentrations from eccentric weld placement. Cyclic tension and compression elevates the demand and produces a 39% decrease in the force and a 61% decrease in the deformation capacity.
- The JVI splayed leg proprietary connection provides shear strengths well above the calculated ultimate capacity and a high ductility with shear deformations surpassing 1.5-in. The high shear capacity was as a result of

concrete-connector interaction not accounted for in the design equations. Combined tension elevates the demand and produces a 24% decrease in the force and no appreciable change in ductility.

**Chord**

- The chord straight leg connector provides a tensile strength well below the calculated design capacity and low ductility with tensile deformations less than 1-in. The tensile capacity was reduced by stress concentrations in the bar due to weld tearing resulting from eccentric weld placement and connector plate flexibility. Combined shear elevates the demand and produces a 7% decrease in the force and 42% decrease in the deformation capacity.
- The chord straight leg connector provides shear strengths well above the calculated ultimate capacity, but a low ductility with shear deformations less than 1.0-in. The high shear capacity was as a result of concrete-connector interaction not accounted for in the design equations. Combined tension elevates the demand and produces a 39% decrease in the force and no appreciable change in ductility. Cyclic action had little effect on the capacity and ductility, with the 12% increase in the shear capacity due to higher material properties.

**Hairpin**

- The un-topped hairpin splayed leg connector provides a tensile strength well below the calculated design capacity but with a high ductility of over 1.7-in tensile deformation. The tensile capacity was reduced by stress concentrations in the bar due to weld tearing resulting from connector bar flexibility. The topped hairpin provides a tensile strength in accordance with design standards. Combined shear elevates the demand and produces a 9% decrease in the tensile force and a 91% decrease in the deformation capacity.
- The un-topped hairpin splayed leg connector provides shear strengths at approximately the calculated ultimate capacity and a high ductility with shear deformations about 1.3-in. The topped hairpin provides a tensile strength well above calculated ultimate capacity, and high ductility with shear deformations of over 2.9-in. The high shear capacity was as a result of concrete-connector interaction not accounted for in the design equations. Combined tension elevates the demand and produces a 42% decrease in the force and 79% decrease in ductility. Cyclic action also elevated the demand with no appreciable change in the force, but resulted in a 64% decrease in ductility.

**Cover Plate**

- The cover plate straight leg connector provides a tensile strength above the calculated design capacity and low ductility with tensile deformations less than 0.6-in. The connector displayed stiff initial response with the failure occurring in the connector bars. Combined shear elevates the demand and produces a 35% decrease in the tensile force, but due to a change in the failure pattern increased the ductility by150%.
- The cover plate straight leg connector provides shear strengths well above the calculated ultimate capacity and high ductility with shear deformations less than 2.9-in. The high shear capacity was as a result of concrete-connector interaction not accounted for in the design equations. Combined tension elevates the demand and produces a 37% decrease in the force and a 59% decrease in ductility. Cyclic action also elevates the demand and produces a 51% decrease in the force and a 66% decrease in ductility.

**Pour Strip**

- The pour strip straight leg connector provides a tensile strength at the calculated design capacity and a high ductility with tensile deformations over 2.2-in. Connector failure was attributed to bar fracture which corresponds to the tensile strength of the bars. Combined shear had little effect on the tensile demand producing a 2% decrease in the force, but due to shear deformation lengthening the un-bonded bar lengths, increased the ductility by 23%. Cyclic action also had no appreciable effect on the demand with less than 0.5% difference in tensile force (maximum deformation was limited to 0.826-in. well before failure).

- The pour strip straight leg connector provides shear strengths approximately equal to the calculated ultimate capacity and high ductility with shear deformations over 3.5-in. Cyclic action elevates the demand and produces a 51% decrease in the force and also displayed high ductility over 2.6-in. In both test connector bar failure did not occur, and test data was limited by the maximum actuator deformations.

**Topping**

- Welded wire reinforcement in a cast-in-place topping provides a tensile strength and deformation in accordance with WWR material properties. The deformation capacity is approximately equal to the fracture strain of 0.01 multiplied by the transverse wire spacing of 10-in. giving a joint opening capacity of 0.1-inch. Combined shear and tension deformations elevate the demand on the wire crossing the joint. The combined deformation cases used in this program produced a 22% decrease in the force and 22% decrease in the deformation capacity over a pure tension demand.
- Welded wire reinforcement in a cast-in-place topping provides shear strength in accordance with ACI shear friction models. When the joint is pre-cracked and separated a $\mu$=0.6 was found to be conservative. When the joint is closed the shear friction model is very conservative. Accounting for the compressive demands in the concrete using the alternate ACI shear friction model provides an improved estimation of capacity. Cyclic shear elevates the demand and produces a 57% decrease in the force with no significant change in the deformation capacity.

## REFERENCES


1. ACI 318, Building Code Requirements for Structural Concrete and Commentary. American Concrete Institute, 2005
2. AWS Structural Welding Committee, “AWS D1.4-92 Structural Welding Code,” American Welding Society, Miami, FL, 1992.
3. Cao, L., Naito, C., Sause, C., “Phase 1 Experimental Evaluation of Diaphragm Connections: Program Overview,” PCI-NSF Project Development of Seismic Design Methodology for Precast Diaphragms, Internal Report, November 2004, p.16.
4. Load and Resistance Factor Design (LRFD) 3rd Edition, 2001. American Institute of Steel Construction, Chicago
5. Naito, C., Cao, L., Peter, W., Sause, C., “Phase 1 Experimental Evaluation of Diaphragm Connections: Loading Protocol,” PCI-NSF Project Development of Seismic Design Methodology for Precast Diaphragms, Internal Report, December 2004, p.6.
6. PCI Design Handbook, Precast and Pre-stressed Concrete, Fifth Edition, Chicago, IL, 1999
7. Priestley, M.J.N., “The U.S. –PRESSS Program Progress Report,” Third Meeting of the U.S. –Japan Joint Technical Coordinating Committee on Precast Seismic Structural Systems (JTCC-PRESSS), San Diego, CA, November 18-20, 1992.